©2012

Sayantani Das

ALL RIGHTS RESERVED

Multifunctional Mesoporous and Nanostructured Catalysts: Exploring Novel Synthetic Methods, Properties and Applications

by

SAYANTANI DAS

A Dissertation submitted to the

Graduate School-New Brunswick

Rutgers, The State University of New Jersey

In Partial fulfillment of the requirements

For the degree of

Doctor of Philosophy

Graduate Program in Chemistry

Written under the direction of

Professor Tewodros Asefa

And approved by

____

____

____

____

New Brunswick, New Jersey

October 2012

ABSTRACT OF THE DISSERTATION

Multifunctional Mesoporous and Nanostructured Catalysts: Exploring Novel Synthetic Methods, Properties and Applications

By: SAYANTANI DAS

Dissertation Director: Professor Tewodros Asefa

Novel multifunctional mesoporous and nanostructured catalysts containing two or more different types of judiciously chosen functional / catalytic groups were developed and their unique and cooperative catalytic activities in various useful organic reactions were explored. First, mesoporous silica material containing tertiary amine/silanol groups was synthesized by simple postgrafting synthetic method. The material was found to exhibit efficient cooperative acid/base bifunctional catalytic activity towards Michael addition reactions between *trans-β*-nitrostyrene and various active methylene compounds such as malononitrile, acetylacetone and dimethylmalonate. Besides serving as a solid base catalyst, such organoamine-functionalized mesoporous silica materials can be utilized as effective support materials for catalytically active organometallic complexes. This was demonstrated by immobilizing ethylenediamine onto mesoporous silica via postgrafting synthetic method and then complexing Fe(III) onto the supported ethylenediamine groups. This yielded a bifunctional Fe(III)/silanol-based heterogeneous catalyst that showed efficient catalytic activity towards epoxide ring opening reactions. Next, the potential of these types of organic-functionalized mesoporous silicas for immobilization of metallic nanoparticle catalysts was investigated. Specifically, mercaptopropyl-functionalized mesoporous silica was synthesized and the material was then supported with ultrasmall Au_n nanoclusters. The catalytic properties of the resulting materials in styrene oxidation were studied. Furthermore, the effect of the removal of the thiol groups from around the surfaces of the gold nanoclusters on catalytic activities of the mesoporous silica-supported nanoparticles was investigated. As mesoporous silica have some limitations of crowding in their pores and poor mass transport for reactants when they are functionalized with larger groups such as nanoparticles, a new strategy was developed, where such catalytic groups were immobilized on the outer surface of silica microspheres. These supported nanoparticle catalytic groups on the silica nanospheres were further coated with a porous silica shell in order to overcome their possible aggregation, sintering and loss of catalytic activities. The resulting nanomaterials, dubbed produced SiO_2-Au-pSiO_2 core-shell-shell microspheres, were then used as efficient and recyclable nanocatalysts for styrene epoxidation. This strategy was further extended to core-shell-shell microspheres containing the metal (*e.g.*, Pd) nanoparticles within G4 PAMAM dendrimers that are supported on silica nanosphere cores and coated by nanoporous silica shells. These nanomaterials, denoted as SiO_2-Pd/PAMAM-pSiO_2 core-shell-shell microspheres, were shown to serve not only as efficient and recyclable catalysts but also as selective catalysts for specific functional groups in hydrogenation reaction of various substrates.

Dedicated to my family.

ACKNOWLEDGEMENTS

First I would like to thank Almighty God for enabling me to reach the milestone in my life and helping me with all the abilities and opportunities I have always needed to succeed.

I would like to take this opportunity to convey my sincere thanks to my advisor Professor Tewodros Asefa for his invaluable guidance and support throughout my Ph.D work. It was a very pleasant experience to have him as my advisor.

I would also like to convey my thanks to my committee members for their valuable time, suggestion and cooperation: Dr. Eric Garfunkel, Dr. Alan Goldman and Dr. Michal Kruk for serving as my external member.

I am thankful to the members of the Asefa group for all their support, help and all good times both in and outside the lab. A special thanks to Dr. Anandarup Goswami for his help in catalysis and invaluable discussion during the preparation of the thesis.

I want to thank our collaborators Dr. Jing Li (Rutgers University) to use the TGA machine. Dr. Flavio Maran (University of Padova) for providing me with the ultrasmall gold nanoclusters and his suggestions on the supported ultrasmall gold nanocluster work. Dr. Manish Chhowalla (Rutgers University) for providing me with grapheme oxide samples.

I am very much indebted to Dr. Thomas Emge for his valuable time and patience with my good and bad samples. Many thanks to Dr. Fred Cosandy for training me on TEM and Dr. Sylvie Rangan for training me on XPS. I would like to thank Dr. Damien Voiry for synthesizing the grapheme oxide samples and helping me with the SEM, AFM and Raman studies and Dr. Saquib Ahmed for aiding me in TEM.

I am grateful to my parents for their continuous support and encouragement. It is for them I have reached so far. I owe them everything for coming this far in my life.

A big thanks to my husband Dr. Chandra kanta De for his mental support and encouragement from the very beginning of my career. Words are not enough to express my indebtedness to his great moral support.

I am thankful to all my friends who have directly or indirectly supported me during my Ph.D thesis work.

ABBREVIATIONS, SYMBOLS AND UNITS

a.u	Absorbance unit
δ	Chemical shift
λ	Wavelength
λ_{max}	Wavelength of maximum absorbance
°	Degree
°C	Degree Celsius
%	Percent
Å	Angstrom
^{13}C	Carbon-13
cc	Cubic centimeter
$CDCl_3$	Dueterated chloroform
$CHCl_3$	Chloroform
cm^{-1}	inverse centimeter
CP-MAS	Cross Polarization Magic Angle Spinning
DATS	(N,N-Dimethylaminopropyl)trimethoxy silane
DMSO	Dimethyl Sulfoxide
dr	diastereoselectivity
ee	enantiomeric excess
EDC	1-Ethyl-3-(3-dimethylaminopropyl) carbodiimide
Et_2O	Diethyl ether
EtOH	Ethanol
FT-IR	Fourier Transorm Infared Spectroscopy
g	gram
GC	Gas Chromatography
GC-MS	Gas Chromatography Mass Spectra
h	hour
h^{-1}	inverse hour
H	Hydrogen, Proton
HMDS	Hexamethyldisilazane
^{1}H NMR	Proton Nuclear Magnetic Resonance
H_2O	Water
Hz	Hertz
IPA	Isopropanol
J	Coupling constant
KBr	Potassium Bromide
m	multiplet
M	molar
m^2/g	meter square per gram
mg	Miligram
MHz	Megahertz
MAS	Magic Angle Spinning
min	minute

mL	Mililiter
mmol	Milimolar
NMR	Nuclear Magnetic Resonance
nm	Nanometer
TMS	Trimethylsilyl
PAMAM	Poly(amidoamine)
PhMe	Toluene
ppm	parts per million
rt	Room Temperature
s	Singlet
^{29}Si	Silicon-29
t	Triplet
θ	Theta
TEM	Transmission Electron Microscopy
TEOS	Tetraethyl Orthosilicate
THF	Tetrahydrofuran
TLC	Thin Layer Chromatography
TOF	Turn Over Frequency
TON	Turn Over Number
μL	Microliter
UV	Ultraviolet
wt	Weight
XRD	X-ray diffraction

TABLE OF CONTENTS

ABSTRACT OF THE DISSERTATION ii

DEDICATION iv

ACKNOWLEDGEMENTS v

ABBREVIATIONS, SYMBOLS AND UNITS vii

TABLE OF CONTENTS ix

LIST OF TABLES xv

LIST OF FIGURES xviii

LIST OF SCHEMES xxix

1. Chapter-I Introduction 1
    - 1.1 Heterogeneous Catalysis 2
    - 1.2 Mesoporous Silica Materials 3
        - 1.2.1 Functionalization of Mesoporous Silicas 6
        - 1.2.2 Literature Review on Functionalized Mesoporous Silica Materials for Heterogeneous Catalysis 9
            - 1.2.2.1 Mesoporous Materials Acid Catalyst 9
            - 1.2.2.2 Mesoporous Materials Base Catalyst 12
            - 1.2.2.3 Cinchona Alkaloid-Immobilized Mesoporous Silica Catalysts for Asymmetric Catalysis 19
            - 1.2.2.4 Enzyme-Immobilized Mesoporous Catalyst (Heterogeneous Bio-Catalysts) 23

1.3 Core-Shell Nanostructured Materials for Synthesis of Heterogeneous Catalysts 25
    1.3.1 Metal Nanoparticles Embedded in Sol-Gel Synthesized Metal Oxide Matrices for Catalysis 26
    1.3.2 Metal@Core-Shell Catalyst 28
    1.3.3 Metal@Core-Shell-Shell Catalyst 30
1.4 Objective 32
Reference 34

2. Chapter-II Amine/Silanol Bifunctionalized Mesoporous Silica Catalysts for Michael Addition Reactions between Active Methylene Compounds and Nitroolefin 36
2.1 Michael Addition Reaction 36
    2.1.1 Homogeneous Michael Addition Reaction 36
    2.1.2 Bifunctional Catalyst for Michael Addition Reaction 38
    2.1.3 Application in Natural Product Synthesis 41
    2.1.4 Heterogeneous Michael Addition Reaction 41
2.2 General Considerations and Concept 42
    2.2.1 Synthesis of Tertiaryamine Functionalized SBA-15 44
    2.2.2 Catalytic Activity of the Catalysts in Michael Addition Reaction 50
2.3 Summary 59
Experimental Section 61

Reference 64

3. Chapter-III Ring Opening of Epoxides with Mesoporous Silica Supported Fe(III) Catalysts 66

3.1 Introduction 66

3.1.1 Ring Opening of Epoxides with Metal Complexes 67

3.1.2 Heterogenous Ring Opening of Epoxides 68

3.2 General Consideration and Concept 70

3.2.1 Synthesis of Immobilized Fe(III) Catalyst on SBA-15 71

3.2.2 Catalytic Activity of Ext-SBA-15-en-Fe(III) in Ring Opening of Epoxides 75

3.2.3 Control Experiments 77

3.2.4 Effect of Temperature 80

3.2.5 Scope of the Reaction 80

3.2.6 Recyclability of the Catalyst 81

3.3 Summary 84

Experimental Section 86

Reference 91

4. Chapter -IV Ultrasmall Au Nanoclusters Supported in Mesoporous Channels of SBA-15 as Heterogeneous Catalysts for Selective Styrene Oxidation 93

4.1 Introduction 93

4.2 Styrene Oxidation with Ultrasmall Au Nanoparticles as Catalysts 95
4.3 General Consideration and Concept 96
    4.3.1 Synthesis and Characterization of Mesoporous Silica Supported Au Nanoparticle Catalysts 97
    4.3.2 Control Experiments 102
    4.3.3 Catalytic Activity of Mesoporous Au Nanoclusters (Ext-SBA-15-SH-Au_n) in Styrene Oxidation 104
    4.3.4 Recyclability 107
4.4 Summary 110
Experimental Section 112
Reference 117

5. Chapter-V Core-Shell-Shell Microsphere Containing Au Nanoparticles: Efficient Heterogeneous Nanocatalysts 119
5.1 Introduction 119
5.2 General Consideration and Concept 120
    5.2.1 Synthesis of Porous SiO_2-Au-SiO_2 Core-Shell-Shell Microsphere Catalyst 121
    5.2.2 Control Experiments 128
    5.2.3 Catalytic Activity of Porous SiO_2-AuNP-SiO_2 Core-Shell-Shell Microspheres in

Epoxidation of Styrene 130
5.2.4 Scope of the Reaction 132
5.2.5 Recyclability of the Catalyst 133
5.3 Summary 137
Experimental Section 138
Reference 142

6. Chapter-VI Core-Shell-Shell Microsphere Containing PAMAM Encapsulated Ultrasmall Pd Nanoparticles as Heterogeneous Nanocatalysts 144
6.1 Introduction 144
6.2 Dendrimer Encapsulated Nanoparticles (DENs) 145
6.2.1 Homogeneous Catalysis with DENs 146
6.2.2 Heterogeneous Catalysis with DENs 149
6.3 General Considerations and Concept 152
6.3.1 Synthesis of Porous SiO_2-Pd/PAMAM-pSiO_2 Core-Shell-Shell Microsphere Catalyst 155
6.3.2 Catalytic Activity of Porous SiO_2-Pd/PAMAM-SiO_2 Core-Shell-Shell Microspheres in Hydrogenation of Olefin 162
6.3.3 Scope of the Reaction 163
6.3.4 Recyclability of the Catalyst 166
6.4 Summary 167
Experimental Section 169

Reference 173

7. Chapter-VII Conclusion 176

LIST OF TABLES

Table 2.1: Control experiments to study the bifunctional nature of bis-squareamide bearing amine groups 40

Table 2.2: Elemental analysis of the catalyst and the control sample 50

Table 2.3: Catalytic activity of the supported catalyst used in Michael addition reaction 53

Table 3.1: Ring opening of epoxides using Ext-SBA-15-en-Fe(III) catalyst 77

Table 3.2: Control experiments of attempted ring-opening reactions of styrene oxide using Ext-SBA-15 containing no Fe(III) or Ext-SBA-15-Fe(III) containing no ethylenediamine, but stirred with Fe(III) solution 78

Table 3.3: Comparative catalytic results of two SBA-15-en-Fe(III) catalysts prepared from a calcined SBA-15 (Cal-SBA-15) and a solvent extracted SBA-15 (Ext-SBA-15) under the same conditions 79

Table 3.4: Temperature dependence study of ring-opening of styrene oxide with propyl alcohol using Ext-SBA-15-en-Fe(III) catalyst 80

Table 3.5: Test of recyclability of the catalyst using ring-opening of styrene oxide by MeOH using Ext-SBA-15-en-Fe(III) catalyst 82

Table 4.1: Control experiments of styrene oxidation in the presence of different reference materials or no catalyst 104

Table 4.2: Elemental analysis obtained with ICP-AES of Au in the catalysts as well as in the reaction mixture after 3rd reaction cycle 110

Table 5.1: Control reaction of styrene oxidation in TBHP and toluene at different temperatures without catalyst 130

Table 5.2: Catalytic activity of porous SiO_2-AuNPs-SiO_2 in styrene epoxidation reaction under nitrogen atmosphere 131

Table 5.3: Test of recyclability of the catalyst in epoxidation of styrene 133

Table 5.4: Elemental analysis obtained with ICP-AES of Au in the recycled catalysts as well as in the reaction mixtures 137

Table 6.2: Scope of the hydrogenation reaction 164

Table 6.3: Elemental analysis obtained of Pd with ICP-AES in the recycled catalysts and in the reaction mixtures 167

LIST OF FIGURES

Figure 1.1: Synthetic scheme of mesoporous materials by supramolecular self assembly of structure directing agents (or surfactant) in the presence of silica precursors (*e.g.* $Si(OEt)_4$) 1

Figure 1.2: Functionalization of the surfaces of mesoporous silicas with organic functional groups by post-grafting method. This method allows the grafting of catalytic active functional groups into this otherwise 'unfunctionalized' high surface area material 7

Figure 1.3: Co-condensation synthetic method to organic-functionalized mesoporous silica materials 8

Figure 1.4: (Top Panel)**.** Reaction scheme of postgrafting in ethanol at reflux, 78 °C (AP-E1) and toluene at 78 °C (AP-T1) and toluene at reflux at 112 °C. (Bottom Panel) Reaction mechanism for enhanced efficiency in Henry reaction by organoamine functionalized sample synthesized in ethanol (AP-E1) (A) compared to that synthesized in toluene (AP-T1 and AP-T2) (B). The significantly higher number of residual and spatially isolated silanol groups present in the former materials (AP-E1) led to the formation acid/base cooperative catalytic groups, which activated benzaldehyde more efficiently during the reaction 14

Figure 1.5: Reaction mechanism of the base-catalyzed
Henry reaction between nitromethane and
aromatic aldehyde with aminofunctionalized
mesoporous silica catalyst 15

Figure 1.6: Proposed mechanism of cooperative acid-base bifunctional
catalysis in aldol condensation reaction between acetone
and *p*-substituted benzaldehyde catalyzed by secondary
amine-functionalized mesoporous solid base catalyst 16

Figure 1.7: The Knoevenagel condensation reactions between
aromatic aldehydes and malononitrile catalyzed by
amine-functionalized mesoporous solid base catalyst 18

Figure 1.8: Schematic representation of entrapment of Pd
nanoparticles in sol-gel derived porous metal oxide matrix
for the synthesis of stable metal oxide-supported Pd
nanoparticle heterogeneous catalyst. 27

Figure 1.9: Schematic representation of the encapsulation of Au nanoparticles capped with 1-dodecanethiol (DT) by self-assembling 3-mercaptopropyltrimethoxysilane (MPMS) and TEOS. The synthesis resulted in porous silica encapsulated Au nanoparticles (AuNP–organic–SiO_2 nanostructured materials), which exhibited heterogeneous catalytic activity in low temperature CO oxidation reaction. 28

Figure 1.10: (A) Schematic representation of the synthesis of Pt@mSiO_2 core-shell nanoparticles. (B) TEM image of Pt@mSiO_2 nanoparticles after calcination at 350 °C 29

Figure 1.11: Synthesis procedure of silica/Au nanoparticles/silica core-shell-shell nanospheres containing embedded Au nanoparticles. These nanomaterials were shown to serve as effective heterogeneous catalysts for a number of reactions 31

Figure 1.12: Synthetic procedure and a typical TEM image of porous silica protected Fe_3O_4/SiO_2/Au composite structures 32

Figure 2.1: Activation of electrophile and nucleophile by bifunctional catalyst 39

Figure 2.2: Squaramide base bifunctional catalyst for Michael reaction 40

Figure 2.3: Application in natural products synthesis 41

Figure 2.4: Adsorption isotherm and pore size distribution of Ext-SBA-15, Ext-SBA-15-NMe_2 and Cap-SBA-15-NMe_2 45

Figure 2.5: XRD Pattern of Ext-SBA-15-NMe_2 and Cap-SBA-15-NMe_2 46

Figure 2.6: TEM Images of Ext-SBA-15-NMe_2 46

Figure 2.7: Thermogravimetric Traces of Ext-SBA-15, Ext-SBA-15-NMe_2 and Cap-SBA-15-NMe_2 47

Figure 2.8: Solid-state NMR spectra of Ext-SBA-15-NMe_2-Tol (SBA-15 grafted in toluene) and Cap- SBA-15-NMe_2 (Ext-SBA-15-NMe_2-Tol grafted in toluene and then capped with O-$SiMe_3$ groups), and Ext-SBA-15-NMe_2-IPA (SBA-15 grafted in isopropanol) 48

Figure 2.9: ^{13}C CP-MAS spectra and their peak assignments of Ext-SBA-15- NMe_2-IPA and Cap-SBA-15-NMe_2-IPA 49

Figure 2.10: Proposed mechanism of dual activation involving H-bonding by acid/base bifunctional mesoporous catalysts in Michael addition reaction 51

Figure 2.11: Percentage conversion of nitrostyrene versus reaction time in the Michael addition reaction between malononitrile and nitrostyrene catalyzed by Ext-SBA-15-NMe_2-Tol and Cap-SBA-15-NMe_2-Tol 53

Figure 2.12: Kinetic plot of a controlled experiment (without a catalyst) involving the Michael addition reaction between nitrostyrene and malononitrile at room temperature 54

Figure 2.13: Percentage conversion of nitrostyrene versus reaction time of Michael addition reaction between active methylene compounds and nitrostyrene catalyzed by Ext-SBA-15-NMe_2-Tol 55

Figure 2.14: (A) Kinetic plot of the Michael addition reaction between nitrostyrene and malononitrile at 0 °C catalyzed by Ext-SBA-15-NMe_2-IPA and Ext-SBA-15- NMe_2-Tol. (B) Kinetic plot of the Michael addition reaction between nitrostyrene and malononitrile at 0 °C Catalyzed by Ext-SBA-15-NMe_2-IPA and Cap-SBA-15- NMe_2-IPA 56

Figure 2.15: Kinetic plot of the Michael addition reaction between nitrostyrene and acetylacetone at 50 °C catalyzed by Ext-SBA-15-NMe$_2$-IPA and Ext-SBA-15-NMe$_2$-Tol 57

Figure 2.16: Kinetic plot of the Michael addition reaction between nitrostyrene and different active methylene compounds catalyzed by Ext-SBA-15-NMe$_2$-IPA 58

Figure 2.17: Recyclability studies for the Michael addition reaction between nitrostyrene and acetylacetone catalyzed by Ext-SBA-15-NMe$_2$ 59

Figure 3.1: Nitrogen gas adsorption isotherms and pore size distribution of the parent mesoporous material and the catalyst ExtSBA-15-en-Fe(III) 72

Figure 3.2: XRD patterns of Ext-SBA-15, Ext-SBA-15-en and Ext-SBA-15-en-Fe 73

Figure 3.3: (A) TEM image of Ext-SBA-15 and (B-D) TEM image of Ext-SBA-15-en-Fe(III) catalysts 74

Figure 3.4: Thermogravimetric traces of Ext-SBA-15-en and

Ext-SBA-15-en-Fe 75

Figure 3.5: UV-Vis spectra of Fe(III) solution in the filtrate obtained after mixing Ext-SBA-15 and Cal-SBA-15 with aqueous Fe(III) solution 79

Figure 3.6: Scope of catalytic activity of the Ext-SBA-15-en-Fe(III) catalyst in the ring-opening of different substituted epoxide with MeOH 81

Figure 3.7: Kinetic plot of leaching experiment, representing the % conversion of styrene oxide to time. The brown arrow indicates the time where the catalyst was filtered off and the supernatant was run by itself 82

Figure 3.8: Powder X-ray diffraction (XRD) patterns of a fresh Ext-SBA-15-en-Fe catalyst and after being used for catalysis in three cycles 83

Figure 3.9: Transmission electron microscopy (TEM) images of Ext-SBA-15-en-Fe catalyst after being used for epoxide ring-opening catalysis in (A) three cycles and (B) five cycles 84

Figure 4.1: TEM images of (A, B) Ext SBA-15 and (C, D) Ext-SBA-15-SH 100

Figure 4.2: Thermogravimetric traces of Ext-SBA-15SH, Ext-SBA-15-SH-Au_{25}, Ext-SBA-15-SH-Au_{25}-1 and Ext-SBA-15-SH-Au_{25}-5 101

Figure 4.3: UV-Vis spectra of (A) 2 µM Au_{25} and (B) 2 µM Au_{140} solutions in dichloromethane, (C) the supernatant collected after treatment of Ext-SBA-15-SH-Au_{25} with 1 mM and 5 mM $NaBH_4$ and centrifugation of the solutions, and (D) the supernatant collected after treatment of Ext-SBA-15-SH-Au_{140} with 1mM and 5 mM $NaBH_4$ and centrifugation of the solutions 102

Figure 4.4: Kinetic plot of styrene oxidation catalyzed by (A) Ext-SBA-15-SH-Au_{25}, Ext-SBA-15-SH-Au_{25}-1 and Ext-SBA-15-SH-Au_{25}-5 and (B) Ext-SBA-15-SH-Au_{140}, Ext-SBA-15-SH-Au_{140}-1 and Ext-SBA-15-SH-Au_{140}-5 nanocatalysts 106

Figure 4.5: Product distribution of styrene oxidation catalyzed by Ext-SBA-15-SH-Au_{25}-5 under oxygen at 80 ºC (solvent free conditions) 107

Figure 4.6: % Conversion versus time graphs for styrene oxidation reaction catalyzed by Ext-SBA-15-SH- Au_{140}-5 nanocatalyst 108

Figure 4.7: Percent conversion versus reaction time in a leaching experiment. The black arrow indicates the time at which the solid Au nanocatalyst was filtered and separated from the reaction mixture and the supernatant was begun to run by itself afterward 109

Figure 5.1: Thermogravimetric traces of SiO_2 and amine-functionalized SiO_2 (SiO_2-NH_2) microspheres 121

Figure 5.2: FT-IR spectra of SiO_2 and amine-functionalized SiO_2 (SiO_2-NH_2) microspheres 122

Figure 5.3: TEM images of a, b SiO_2-AuNP core-shell microspheres, c SiO_2-AuNPs-SiO_2 core-shell-Shell microspheres, and d–f etched or porous SiO_2-AuNPs-SiO_2 core-shell-shell microspheres (D = etched for 30 min, E = etched for 60 min, and F = etched for 90 min) 125

Figure 5.4: TEM image showing thick and non-uniform silica shells (indicated by red arrows) when a large amount of TEOS was used for making the silica shells around the SiO_2-AuNP core-shell Microspheres 126

Figure 5.5: Powder XRD patterns of SiO_2-Au core-shell microspheres, and SiO_2-AuNP-SiO_2 and porous SiO_2-AuNP-SiO_2 core-shell-shell microspheres 127

Figure 5.6: UV–Vis spectra of citrate-capped Au nanoparticles (AuNPs) in aqueous solution and porous SiO_2-AuNP-SiO_2 core-shell-shell microspheres 127

Figure 5.7: Plot of % conversion of styrene versus reaction time of styrene epoxidation reaction using porous SiO_2-AuNPs-SiO_2 core-shell-shell microspheres as catalyst in toluene at 80 °C under nitrogen atmosphere 129

Figure 5.8: % Conversion vs time graphs for styrene epoxidation reaction catalyzed by porous SiO_2-AuNPs-SiO_2 microsphere catalysts 133

Figure 5.9: % Conversion vs time graphs for styrene epoxidation reaction catalyzed by SiO_2/AuNPs Core-Shell microsphere catalysts 134

Figure 5.10: UV–Vis spectrum of recycled porous SiO_2-AuNP-SiO_2 core-shell-shell microspheres after three reaction cycles 135

Figure 5.11: % Conversion of styrene *vs* time to test possible leaching of Au catalyst 136

Figure 6.1: FTIR Spectra of SiO_2, SiO_2-COOH and

SiO_2-PAMAM core-shell microspheres 157

Figure 6.2: Thermogravimetric traces of SiO_2, SiO_2-COOH and SiO_2-PAMAM core-shell microspheres 158

Figure 6.3: TEM images of (A) SiO_2 microspheres, (B) SiO_2-Pd/PAMAM core-shell microspheres, (C) SiO_2-Pd/PAMAM-SiO_2 core-shell-shell microspheres, and (D–F) etched SiO_2-Pd/PAMAM-SiO_2 core-shell-shell microspheres with porous silica shell (D = etched for 30 min, E = etched for 60 min, and F = etched for 80 min) 160

Figure 6.4: UV-Vis spectrum of SiO_2-Pd/PAMAM core-shell microspheres 161

Figure 6.5: % Conversion of styrene in 15 min versus catalytic cycles for styrene hydrogenation catalyzed by SiO_2-Pd/PAMAM-pSiO_2 core-shell-shell microspheres 166

LIST OF SCHEMES

Scheme1.1: Oxidation of mesoporous silica-supported 3-mercaptopropyl groups to mesoporous silica-propylsulfonic acid catalytic groups. The resulting propylsulfonic acid-functionalized mesoporous silica catalyst was successfully used as a solid acid heterogeneous catalyst as shown in Scheme 1.2 10

Scheme 1.2: Mesoporous silica-supported solid acid-catalyzed addition reaction between 2-methylfuran and acetone 10

Scheme 1.3: Mesoporous solid acid-catalyzed reaction between alcohol and 3,4-dihydro-2H-pyran 11

Scheme 1.4: The Beckmann rearrangement reaction of cyclohexanone oxime to *ε*-caprolactam catalyzed by arenesulfonic acid-functionalized SBA-15 (SBA-Ar-SO_3H) mesoporous catalyst 12

Scheme 1.5: Asymmetric dihydroxylation reaction catalyzed by immobilized cinchona alkaloid-functionalized mesoporous silica chiral catalyst 19

Scheme 1.6: Synthesis of cinchona alkaloid immobilized SBA-17 mesoporous silica chiral catalyst for asymmetric dihydroxylation reaction 20

Scheme 1.7: Synthesis of cinchona alkaloid immobilized MCM-41 chiral catalyst for asymmetric dihydroxylation reaction of olefins 22

Scheme 1.8: Schematic representation of the synthesis of APMA-modified SBA-15 and its further immobilization with cytochrome c through Hg-cysteine binding and strong chemisorption of the enzyme on the mesoporous material 25

Scheme 2.1: *L*-Proline catalyzed enantioselective Michael addition reaction 37

Scheme 2.2: Asymmetric Michael addition reaction catalyzed by prolinamide 37

Scheme 2.3: Organocatalyst in combination with ILS-benzoic acid as a catalytic system for Michael addition reaction 38

Scheme 2.4: Michael reaction of 1,3-dicarbonyl catalyzed by P-BEMP 42

Scheme 2.5: Synthesis of Ext-SBA-15-NMe_2 and Cap-SBA-15-NMe_2 44

Scheme 2.6: Michael addition reaction between *trans*-*β*-nitrostyrene and active methylene compounds 51

Scheme 3.1: Hydrolytic kinetic resolution catalyzed by Co-salen complex 68

Scheme 3.2: Synthesis of Ext-SBA-15-en-Fe(III) 71

Scheme 3.3: Ring opening of epoxides using Ext-SBA-15-en-Fe(III) catalyst 76

Scheme 4.1: Synthesis of immobilized Au cluster on SBA-15 (Ext-SBA-15-SH-Au_n) 99

Scheme 4.2: Attempted styrene oxidation without a catalyst or in the presence of various catalysts 103

Scheme 5.1: Schematic representation of the synthesis of porous SiO_2-Au-SiO_2 Core-Shell-Shell microsphere nanocatalysts 121

Scheme 5.2: Styrene epoxidation with various catalysts 128

Scheme 5.3: Epoxidation of *trans*-stilbene catalyzed by the porous SiO_2-AuNP-SiO_2 nanocatalyst 132

Scheme 6.1: Schematic representation of the synthesis of dendrimer-encapsulated metal nanoparticles (DENs) 146

Scheme 6.2: Hydrogenation of allyl alcohol to 1-Propanol using G4OH/Pd(0)40 DECs 147

Scheme 6.3: Hydrogenation of conjugated dienes and alkynes using dendron encapsulated Pd nanoparticles 148

Scheme 6.4: C-C coupling reaction between aryl halides and n-butylacrylate catalyzed by Pd nanoparticles containing DEC 148

Scheme 6.5: Hydroformylation of styrene with rhodium-complexed dendrimers that are anchored onto polystyrene beads 150

Scheme 6.6: Heterogeneous Pd nanoparticle containing DEC for the hydroalkoxylation of 2-Phenylethynylphenol 151

Scheme 6.7: Schematic representation of the synthesis of

core-shell-shell microsphere containing SiO_2 microsphere-supported PAMAM-encapsulated Pd nanoparticles that are further coated with nanoporous silica shell.
(a) Functionalization of SiO_2 microspheres with carboxylic acid group by grafting the SiO_2 microspheres with carboxyethylsilanetriol, (b) 1-ethyl-3-(3-dimethylaminopropyl)carbodiimide (EDC) coupling of SiO_2-COOH with NH_2 terminated PAMAM dendrimers, (c) synthesis of PAMAM encapsulated Pd nanoparticles within the SiO_2-COOH supported PAMAM dendrimers forming SiO_2-Pd/PAMAM microspheres, (d) synthesis of SiO_2 shell around the SiO_2-Pd/PAMAM using TEOS, and (e) controlled etching of SiO_2 shell using aqueous NaOH solution 154

Scheme 6.8: Evaluation of the catalytic activity of the control samples and the catalyst towards hydrogenation reaction 162

Chapter I

Introduction

"Chemistry without catalysis would be a sword without a handle, a light without brilliance, a bell without sound." - Alwin Mittasch, 1948.[1]

In today's perspective, this quotation by the German chemist Prof. Alwin Mittasch about the importance of catalysis in chemistry is still not an exaggeration. Since the term "catalyst" was coined by Berzelius[2] in 1836, the area of "catalysis" has grown enormously. Moreover, catalysis plays significant roles in the production of many things we use in our daily lives today as about 90% of all the chemical processes currently used for industrial production of various commodity chemicals and synthetic materials involve at least one catalyst for their production. Though, the importance of catalysis is well-understood and highly recognized (most recently with the Nobel Prize awarded in Chemistry to Prof. Richard F. Heck, Prof. Ei-ichi Negishi and Prof. Akira Suzuki in 2010 for their works in catalysis), the potential implications of catalysis for environmental remediation, renewable energy and sustainability have started to emerge and are opening up new opportunities as well as challenges for the scientific community. Fortunately, thanks to the recent developments in powerful instrumentations and the willingness of the scientific community that these issues are increasingly being addressed through the use of effective catalysts that lead to higher yields of the desired products, energy intensive processes, atom economy and greener reactions. However, much work still remains as many conventional catalytic processes are not highly efficient.

Owing to the vast variety of catalysts that have been developed and are being utilized both in industry and academia, different kinds of classifications for catalysts are possible. Based on the phase of the catalyst with respect to substrate, they are broadly or most commonly divided into two groups: homogeneous catalysts and heterogeneous catalysts, which result in homogeneous catalysis and heterogeneous catalysis, respectively. In homogeneous catalysis, the catalyst is in the same phase as the reactants, whereas in heterogeneous catalysis, the catalyst is in different phase (often in solid phase) while the reactants are in liquid or gaseous phase.

1.1 Heterogeneous Catalysts and Catalysis

Heterogeneous catalysts are particularly attractive in industry because of their advantages in minimizing possible environmental pollution, reducing some labor-intensive and time-consuming synthetic work up procedures, and enabling separation of catalysts from reaction mixtures more easily at the end of catalytic reactions. Thus, the field of heterogeneous catalysis has been growing rapidly over the last few decades, especially for the purpose of addressing environmental and sustainability issues. Many of the research efforts in heterogeneous catalysis have also already led to many important and commercially used heterogeneous catalysts.

The most attractive synthetic approach to many types of heterogeneous catalysts involves immobilization of well-prepared homogeneous catalysts onto insoluble solid support materials such as polymers,[3-6] zeolite,[7-10] or silica.[11] Heterogeneous catalytic reactions typically occur through the adsorption of reactants on the surface of the catalyst, followed by cleavage or recombination of the chemical bonds of the reactants on the catalyst surfaces. Therefore, the catalytic activity, selectivity, and shelf-lives of heterogeneous catalysis strongly depend on the surface structures of the support materials. Hence, to successfully develop efficient heterogeneous catalysts, the rational choice of the support material and the use of the right synthetic strategy for placing the active catalytic groups on the support material are vital. Among many materials that are used as support material for heterogeneous catalysts, mesoporous silica materials are appealing because of their inherent physical robustness, high surface areas, tunable monodisperse nanometer pores and suitable structural features to serve as hosts for a variety of catalytic groups.[12-14]

1.2 Mesoporous Silica Materials

In 1992, scientists at Mobil Oil Company in New Jersey developed a new family of periodic mesoporous silica materials, also known as M41S or MCM type materials, where MCM stands for Mobil Composition of Matter.[15] The most notable examples of M41S materials include MCM-41, which has hexagonally ordered cylindrical mesoporous structures with p6mm space group; MCM-48, which has cubic ordered cylindrical mesoporous structures with space group Ia$\bar{3}$

d; and MCM-50, which has a laminar structure with a P2 space group.[16] These mesostructured or mesoporous silica materials are synthesized by using the combination of the sol-gel process and supramolecular self-assembly in the presence of surfactant templates, as represented in Figure 1.1. In typical synthesis, surfactant or a structure directing agent, *e.g.* cetyltrimethylammonium bromide (CTAB), is mixed at certain concentrations with water to form cylindrical micelles. These cylindrical micelles then spontaneously self-assemble into hierarchically ordered liquid crystalline structures that can serve as soft-templates for inorganic systems. For example, these liquid crystalline self-assembled micelle templates can self-assemble with inorganic sol-gel precursors such as tetraethylorthosilicate (TEOS), which undergo hydrolysis and condensation and form silica networks around the micelle templates. The resulting materials are finally treated by calcination or solvent extraction to remove the soft templates and yield well-ordered mesoporous silica materials, *e.g.,* hexagonally ordered MCM-41 mesoporous silica, which is one of the most widely studied mesoporous silica materials.[12]

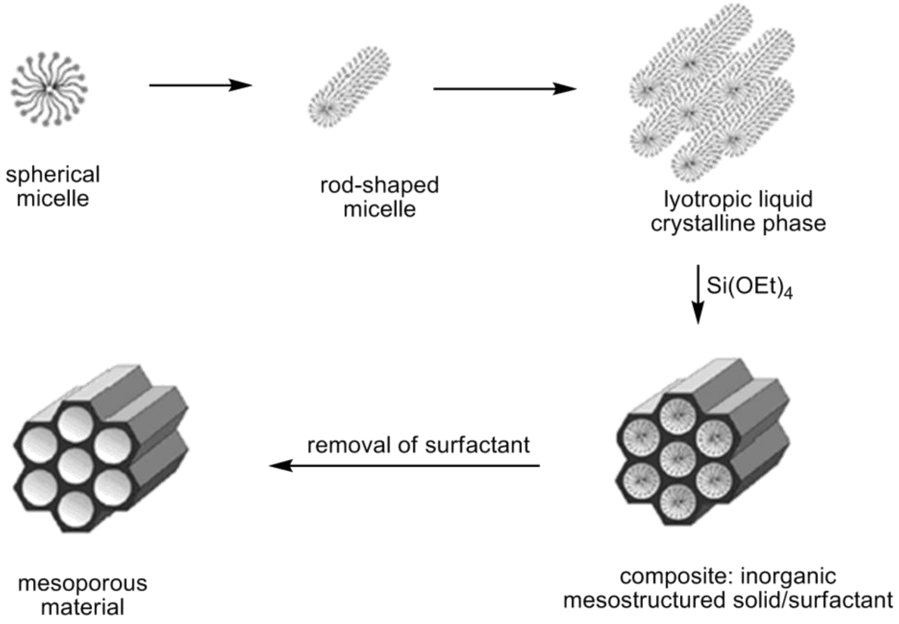
spherical micelle
rod-shaped micelle
lyotropic liquid crystalline phase
Si(OEt)4
removal of surfactant
mesoporous material
composite: inorganic mesostructured solid/surfactant

Figure 1.1: Synthetic scheme of mesoporous materials by supramoleclar self-assembly of structure directing agents (or surfactants) in the presence of silica precursors (*e.g.,* $SiOEt_4$).[10]

After the pioneering works of Kresge and co-workers on the surpramolecular self-assembly route to M41S materials, this synthetic method was extended to produce a number of other types of mesoporous silica materials. This was achieved by simply changing the types of templates, the silica source, the solvents, the ratios of reagents, or the reaction conditions used during the synthesis of the materials. For instance, SBA-15 (Santa Barbara Amorphous-15) mesoporous silica materials, which is another most commonly studied mesoporous material, was synthesized by using a Pluronic-123 tri-block copolymer, poly(ethylene glycol)-poly(propylene glycol)-poly(ethylene glycol), as template.[17] Ever since its report, this material has also attracted many researchers' attention, including those working in the field of heterogeneous catalysis. This is because this material has large pore sizes, high surface area and robust structure or structural features that make it possible for SBA-15 to serve as excellent host material for various types of catalytic groups: molecular, biocatalytic or nanoparticles.[12]

1.2.1 Functionalization of Mesoporous Silicas

In order to utilize mesoporous silicas in catalysis, their surfaces have to be functionalized by catalytic active groups. This is typically achieved by modifying the surfaces or the structures of the mesoporous silicas with reactive or catalytic active organic groups, such as thiols, sulfonic and carboxylic acids, and amines as shown in Figure 1.2.[18] The symbiosis of the robust inorganic matrix and the presence of such reactive surface organic groups can lead to various types of good heterogeneous catalysts. The organic or catalytic active functional groups are introduced into mesoporous silicas by using one of the two general surface modification synthetic methods developed: (a) grafting and (b) co-condensation synthetic method.

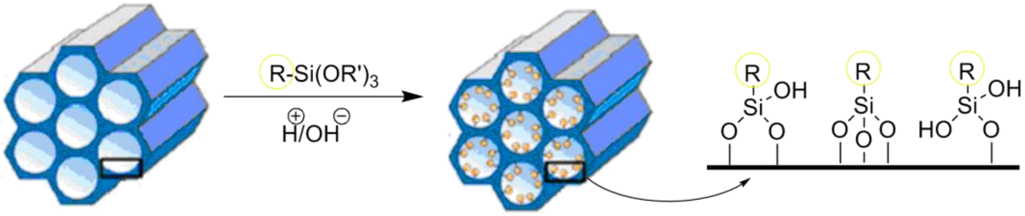

Figure 1.2: Functionalization of the surfaces of mesoporous silicas with organic functional groups by post-grafting method.[10] This method allows the grafting of catalytic active functional groups into this otherwise ‘unfunctionalized’ high surface area material.

Grafting refers to the process by which the surfaces of pre-made mesoporous silica materials are modified by organic groups using organosilane coupling agents. This process is often carried out by simply reacting mesoporous silica with organosilanes of the type trialkoxysilane $(R'O)_3SiR$, or less frequently chlorosilanes $ClSiR_3$ or silazanes $HN(SiR_3)_3$ (Figure 1.2).[10] The reaction leads to the conjugation between the free silanol groups of the parent mesoporous silica material and the incoming organosilane. This process often leaves the mesostructure of the parent material intact; however, inherently leads to nonhomogeneous distribution of the organic groups in the material, where higher density of functional groups is formed around the pore mouth and less density in the middle of the cylindrical channel pores of the material.[19] An alternative synthetic method to organic-functionalized mesoporous silica materials is achieved by one-pot co-condensation method, in which tetraalkoxysilane [$(RO)_4Si$, *e.g.*, TEOS or tetramethoxysilane (TMOS)] is co-condensed with terminal trialkoxyorganosilanes of the type $(R'O)_3SiR$ in the presence of structure-directing agents.[57-58] This leads to mesostructured materials with the organic functional groups (R) anchored covalently to the walls of the material (Figure 1.3). The removal of the organic templates results in organic-functionalized mesoporous materials with functional groups (R) inside and outside for external surface.

Although the drawback associated with grafting synthetic method, *i.e.*, non-homogeneous distribution of functional groups, can be overcome by using the direct co-condensation synthetic method, the latter has also its own disadvantages. The most notable drawback of co-condensation synthetic method is that the content of organic functional groups in the organic-modified materials cannot exceed about 40 mol% without significantly compromising the ordered mesostructure of the organic-functionalized material.[10]

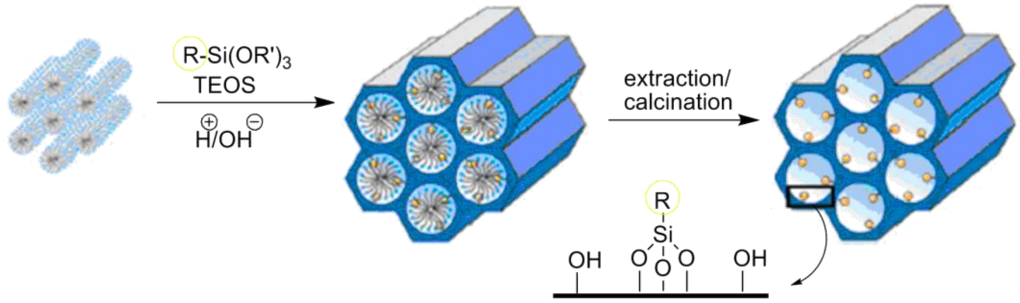

Figure 1.3: Co-condensation synthetic method to organic-functionalized mesoporous silica materials.

1.2.2 Literature Review on Functionalized Mesoporous Silica Materials for Heterogeneous Catalysis

Mesoporous silicas are versatile materials for the development of heterogeneous catalysts because, besides their high surface areas and robust structures, their surfaces can easily be functionalized by a number of different types of functional catalytic active functional groups such as acid[20,21], base,[22,23] cinchona alkaloids,[24-26] enzymes,[20,27,28] etc. Hence, there is currently many literature reports on synthesis of functionalized mesoporous silica materials for heterogeneous catalysis. In the following section, selected examples of mesoporous materials functionalized with various catalytic active groups and their use as heterogeneous catalysts for different reactions are discussed.

1.2.2.1. Mesoporous Materials Acid Catalyst

Acid catalytic sites can be incorporated into mesoporous silicas to produce high surface area, solid acid heterogeneous catalysts. For example, Jacobs *et al*.[29] reported the synthesis of mesoporous solid acid catalysts containing covalently attached alkylsulfonic acid groups on the surfaces of hexagonally ordered mesoporous silica (HMS) by using both grafting and direct co-condensation synthetic methods. In the case of the co-condensation method, tetralkoxysilane and 3-mercaptopropyltriethoxysilane were self-assembled in the presence of surfactant as structure directing agent. This gave mesoporous silica-supported 3-mercaptopropyl groups, which were then oxidized with hydrogen peroxide into propylsulfonic acid groups (Scheme 1.1). When the catalytic activity of the resulting mesoporous silica-supported propylsulfonic acid (solid acid catalyst) was tested in the reaction between 2-methylfuran and acetone, the reaction gave 2,2-bis(5-methylfuryl)propane (DMP) product in good yields (Scheme 1.2).

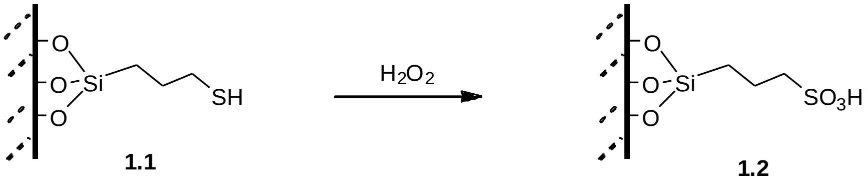

Scheme 1.1: Oxidation of mesoporous silica-supported 3-mercaptopropyl groups to mesoporous silica-propylsulfonic acid catalytic groups. The resulting propylsulfonic acid-functionalized mesoporous silica catalyst was successfully used as a solid acid (or a heterogeneous catalyst) for addition reaction between 2-methylfuran and acetone, as shown in Scheme 1.2.

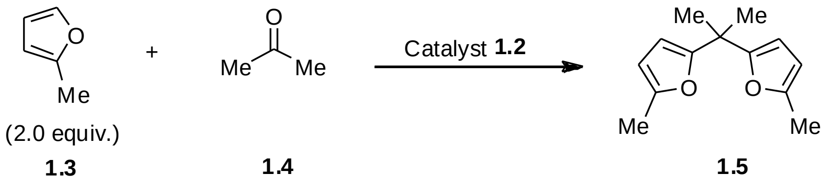

Scheme 1.2: Mesoporous silica-supported solid acid-catalyzed addition reaction between 2-methylfuran and acetone.

Similarly, Stein *et al.*[30] used direct one-pot co-condensation synthetic method to produce MCM-41 type organic-inorganic hybrid silicates that contained uniformly distributed 3-mercaptopropyl groups (thiol-MCM-41). After letting the 3-mercaptopropyl groups oxidize in the subsequent step, the authors obtained propylsulfonic acid-functionalized mesoporous solid acid catalyst, which exhibited catalytic activity for alcohol dehydration and protection reactions (Scheme 1.3).

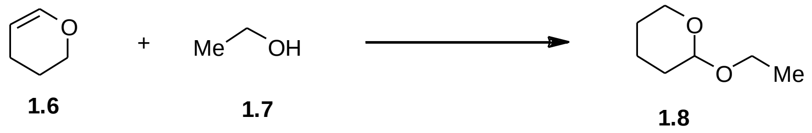

Scheme 1.3: Mesoporous solid acid-catalyzed reaction between alcohol and 3,4-dihydro-2H-pyran.

In a related example, Sastre *et al.*[31] synthesized sulfonic acid-functionalized MCM-41 by mixing 3-mercaptopropyltrimethoxysilane (MPTMS) and tetramethoxysilane (TMOS) with surfactants such as dodecyltrimethylammonium bromide and hexadecyltrimethylammonium as structure directing agents and tetramethylammonium hydroxide (TMAOH) as a co-structure directing agent and a base catalyst. The resulting material was then successfully shown to serve as a catalyst in the esterification reaction between glycerol and fatty acids (oleic and lauric acids). The results indicated that the catalysts synthesized by using a mixture of the two surfactants were more selective to monoglyceride products than those synthesized by using only hexadecyltrimethylammonium bromide. This was suggested to be the result of the higher degree of order in the mesoporous structure and the higher surface area in the former material.[31]

By using arenesulfonic acid-functionalized SBA-15 mesoporous silica (SBA-Ar-SO_3H) as a solid acid catalyst, Wang *et al.* demonstrated the Beckmann rearrangement reaction of cyclohexanone oxime to ε-caprolactam (Scheme 1.4) in liquid phase.[20] The catalyst was synthesized by co-condensation synthetic method involving 2-(4-chlorosulfonylphenyl)ethyltrimethoxysilane (CSPTMS) and tetraethyl orthosilicate (TEOS) in the presence of triblock co-polymer Pluronic 123 ($EO_{20}PO_{70}EO_{20}$) as surfactant.

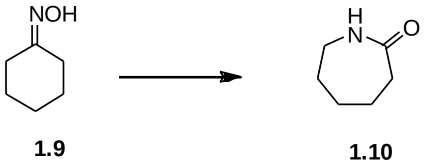

Scheme 1.4: The Beckmann rearrangement reaction of cyclohexanone oxime to ε-caprolactam catalyzed by arenesulfonic acid-functionalized SBA-15 (SBA-Ar-SO_3H) mesoporous catalyst.

1.2.2.2. Mesoporous Materials Base Catalyst

Amine-functionalized MCM- and SBA-type materials have been among the most widely studied mesoporous solid-base catalysts for various reactions, including the aldol, Knoevenagel, Michael and Henry reactions. Our group has also extensively studied the design and synthesis of various amine functionalized, efficient solid-base mesoporous catalysts for the Henry[23,32,33] and aldol reactions.[34] The work showing how the catalytic properties of amine-functionalized MCM-41 materials base-catalyzed catalytic reactions can be significantly enhanced by rational design and synthesis of the amine-functionalized materials by grafting in polar, protic solvents is the most notable example of our group's contributions.[23] The polar, protic solvents led to the formation of bifunctional mesoporous catalysts, which contained spatially distributed organoamine and silanol groups that exhibited excellent (or the highest ever reported) catalytic activity in the Henry reaction between nitromethane and *p*-substituted benzaldehyde. The catalytic activity of the organoamine groups obtained using polar, protic solvents were more effective than those obtained with non-polar solvents—the traditionally used solvents for grafting organosilanes on mesoporous silicas—because the former gave less density of surface grafted organoamines, or conversely large enough silanol (weak acid) groups. The site-isolated organoamine groups paired up with the neighboring residual surface silanol (weak acid) groups to form optimized combination of acid and base groups or cooperative acid-base catalysts that could efficiently catalyzed the Henry or aldol condensation reaction between acetone and *p*-substituted benzaldehyde, as shown in Figure 1.4.

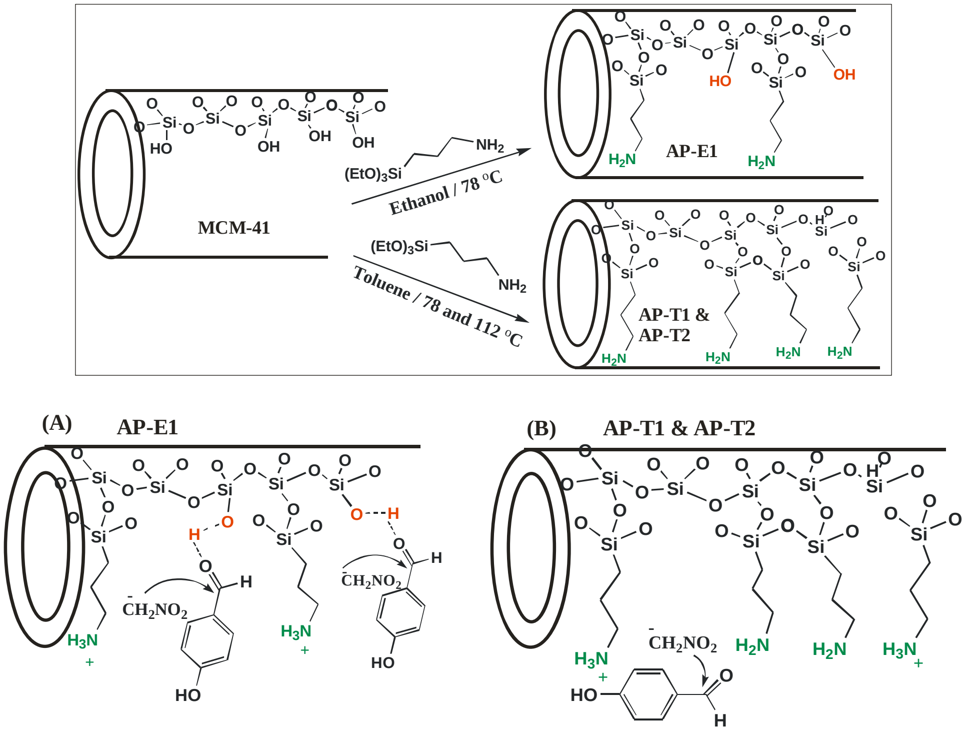

Figure 1.4. (Top Panel)**.** Reaction scheme of postgrafting in ethanol at reflux, 78 °C (AP-E1) and toluene at 78 °C (AP-T1) and toluene at reflux at 112 °C. (Bottom Panel) Reaction mechanism for enhanced efficiency in Henry reaction by organoamine functionalized sample synthesized in ethanol (AP-E1) (A) compared to that synthesized in toluene (AP-T1 and AP-T2) (B). The significantly higher number of residual and spatially isolated silanol groups present in the former materials (AP-E1) led to the formation acid/base cooperative catalytic groups, which activated benzaldehyde more efficiently during the reaction.[23]

Our group also reported that the catalytic activity and product selectivity of the amine-functionalized mesoporous catalysts could be tuned by judiciously choosing the organoamine (primary, secondary, or tertiary amine) catalytic groups supported on the mesoporous silicas.[33] For example, while primary amine-functionalized mesoporous silicas favored an alkene (the dehydrated) product in the Henry reaction, the secondary and tertiary amine-functionalized mesoporous silicas gave predominantly an alcohol (a non-dehydrated) product, as shown in Figure 1.5

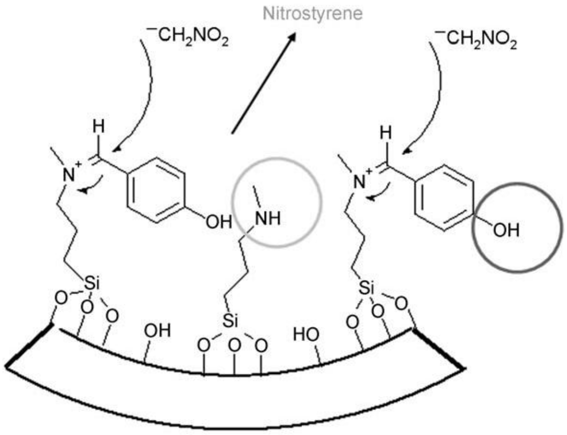
Nitrostyrene
⁻CH₂NO₂
⁻CH₂NO₂
H
N⁺
OH
NH
H
N⁺
OH
Si
O
OH
Si
O
HO
Si
O

Imine mechanism

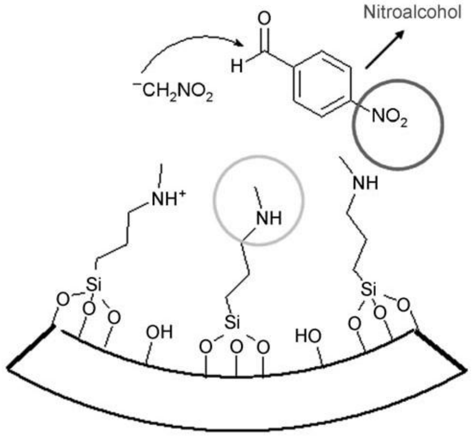
Nitroalcohol
O
H
⁻CH₂NO₂
NO₂
NH⁺
NH
NH
Si
O
OH
Si
O
HO
Si
O

Ion-pair mechanism

Figure 1.5: Reaction mechanism of the base-catalyzed Henry reaction between nitromethane and aromatic aldehyde with aminofunctionalized mesoporous silica catalyst.[56]

Besides the work on the Henry reaction, our group also described the synthesis of highly efficient solid-base catalyst for aldol condensation reaction by grafting site-isolated secondary amine groups onto the channel walls of MCM-41 mesoporous silica, again using polar-protic solvents. The organoamine-functionalized materials obtained with polar-protic solvents, such as ethanol and isopropanol, showed higher catalytic efficiency toward the aldol reaction compared to the corresponding materials obtained with non-polar solvents such as toluene and chloroform. This was explained again based on the cooperative acid-base catalytic activity toward the aldol reaction due to the presence of site-isolated secondary amine groups and many residual silanol groups on the surfaces of the mesoporous catalyst, as shown in Figure 1.6.

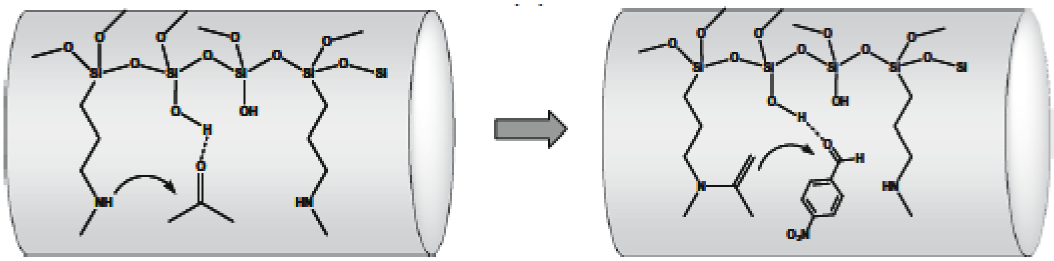

Figure 1.6: Proposed mechanism of cooperative acid-base bifunctional catalysis in aldol condensation reaction between acetone and *p*-substituted benzaldehyde catalyzed by secondary amine-functionalized mesoporous solid base catalyst.

The Knoevenagel reaction, which is sometimes considered as a modified version of the aldol condensation reaction, can also be catalyzed by similar, solid base mesoporous catalysts. Bhaumik *et. al*.[36] demonstrated successfully the use of amino-functionalized mesoporous silica material as catalyst for the

Knoevenagel condensation reaction. Furthermore, the authors described the mechanism of the catalytic reaction for the reactions involving aromatic aldehydes and malononitrile as substrates (Figure 1.7). In the catalytic reaction, the mesoporous silica-supported amine groups abstracted protons from the active methylene groups of malononitrile, and in the process, malononitrile produced its corresponding conjugate base (carbanion). The resulting carbanion species then attacked the carbonyl carbon atoms of the substituted aromatic aldehydes, yielding alkoxy intermediates, which subsequently took up the proton from the conjugate acid of the catalyst to form β-hydroxyl compounds, leading also to the regeneration of the catalyst. Finally, the β-hydroxyl molecules were transformed into α,β-unsaturated dicyano species (the final product) via elimination of water molecules as byproducts, which was catalyzed also by the same material.

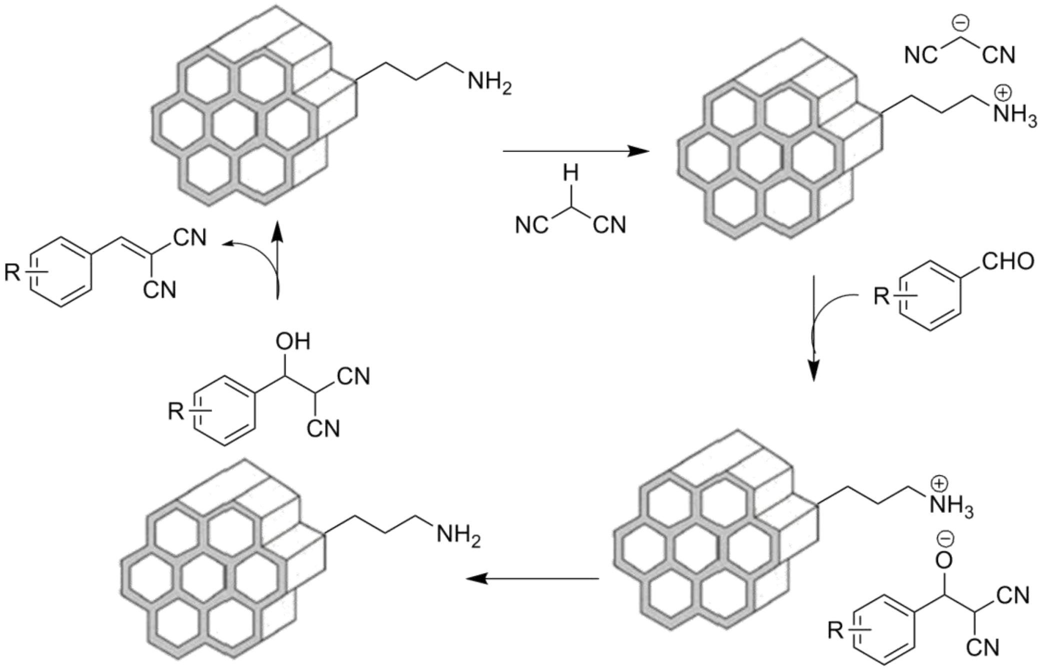

Figure 1.7: The Knoevenagel condensation reactions between aromatic aldehydes and malononitrile catalyzed by amine-functionalized mesoporous solid base catalyst.

Besides primary amine-functionalized mesoporous silicas, diamine-grafted MCM-41 mesoporous silicas were also shown to catalyze the Knoevenagel condensation reaction. In fact, the diamine-functionalized mesoporous silicas were found to exhibit higher catalytic activity in the Knoevenagel reaction than their primary-amine functionalized counterparts. Park *et al.*[37] synthesized amino-functionalized-SBA-15 catalysts and showed their efficient catalytic activity toward the Knoevenagel condensation reaction between aldehyde or ketones and ethyl cyanoacetate, yielding olefin products without any intermediate alcohol or other side products. In the catalytic reaction, aromatic aldehydes were found to be more readily reactive under milder condition (303 K) giving higher conversions, whereas aromatic ketones reacted well enough only at higher temperatures (e.g., 353 K), and yet gave only lower conversions.

1.2.2.3. Cinchona Alkaloid-Immobilized Mesoporous Silica Catalysts for Asymmetric Catalysis

Cinchona alkaloids can be immobilized on the pore surfaces of mesoporous silicas to produce chiral mesoporous catalysts for asymmetric catalysts.[24,27,38] Lee *et al*.[26] have successfully grafted cinchona alkaloids on SBA-15 mesoporous silica, producing a chiral catalyst that successfully catalyzed the asymmetric dihydroxylation reaction. The reaction gave high enantiomeric excess (ee) (up to > 99.5%), especially when a dimeric alkaloid ligand with six-carbon link between the ligand and the support material was employed as the catalyst (Scheme 1.5).

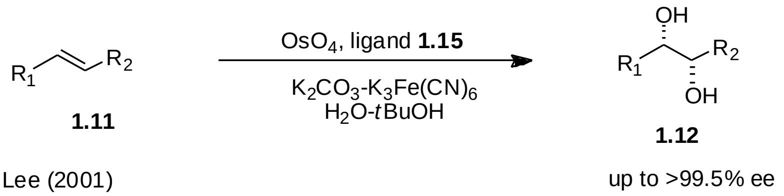

Scheme 1.5: Asymmetric dihydroxylation reaction catalyzed by immobilized cinchona alkaloid-functionalized mesoporous silica chiral catalyst.

In a related example, Motorina *et al*.[38] reported the synthesis of cinchona alkaloid-grafted SBA-17 mesoporous silica and its use as chiral catalyst for the asymmetric dihydroxylation reaction. To prepare the catalyst, the authors first synthesized an organosilane containing the cinchona alkaloid group on it by using a hydrosilation reaction, as shown in Scheme 1.6. Specifically, the authors treated cinchona alkaloid (**1.13**) with $HSi(OEt)_3$ in the presence of H_2PtCl_6 catalyst. This produced a silylated cinchona alkaloid (**1.14**), which was then grafted onto hexagonally ordered SBA-17 at room temperature. The condensation of the organosilane (**1.14**) with the surface hydroxyl groups of SBA-17 finally produced the cinchona alkaloid-immobilized SBA-17 mesoporous silica (**1.15**) catalyst (Scheme 1.6).

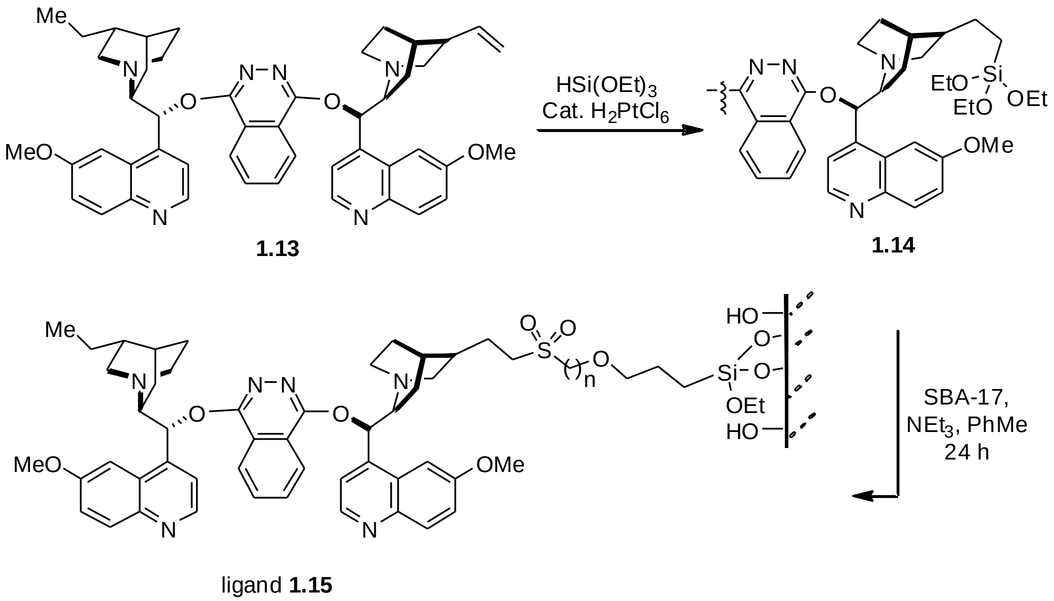

Scheme 1.6: Synthesis of cinchona alkaloid immobilized SBA-17 mesoporous silica chiral catalyst for asymmetric dihydroxylation reaction.

Chiral mesoporous heterogeneous catalysts have been successfully synthesized by using a slightly different approach as shown in Scheme 1.7. Choudary *et al.*[39] reported the synthesis of 1,4-bis(9-O-quininyl)phthalazine-functionalized MCM-41 mesoporous silica by letting vinyl terminated cinchona alkaloid (**1.13**) to conjugate across the alkylthiol groups of alkythiol-functionalized mesoporous silica through radical intermediates (Scheme 1.7). First, MCM-41 was pretreated with 3-mercaptopropyltrimethoxysilane producing 3-mercaptopropyl-functionalized MCM-41. The MCM-41-supported 3-mercaptopropyl groups were then reacted with divinyl groups of 1,4-bis(9-O-quininyl)phthalazine (**1.13**) in the presence of azobisisobutyronitrile (AIBN) (Scheme 1.7). This led to the formation of cinchona alkaloid-immobilized mesoporous MCM-41 catalyst. The authors then successfully employed the resulting material as catalyst for asymmetric dihydroxylation reaction of olefins in the presence of *N*-methylmorpholine *N*-oxide (NMO), $K_3Fe(CN)_6$ or molecular oxygen as co-oxidants, affording diol products with good *ee*. For example, styrene gave an *ee* of 95%, 96% and 88% when NMO, $K_3Fe(CN)_6$ or molecular oxygen, respectively, were used as co-oxidant.

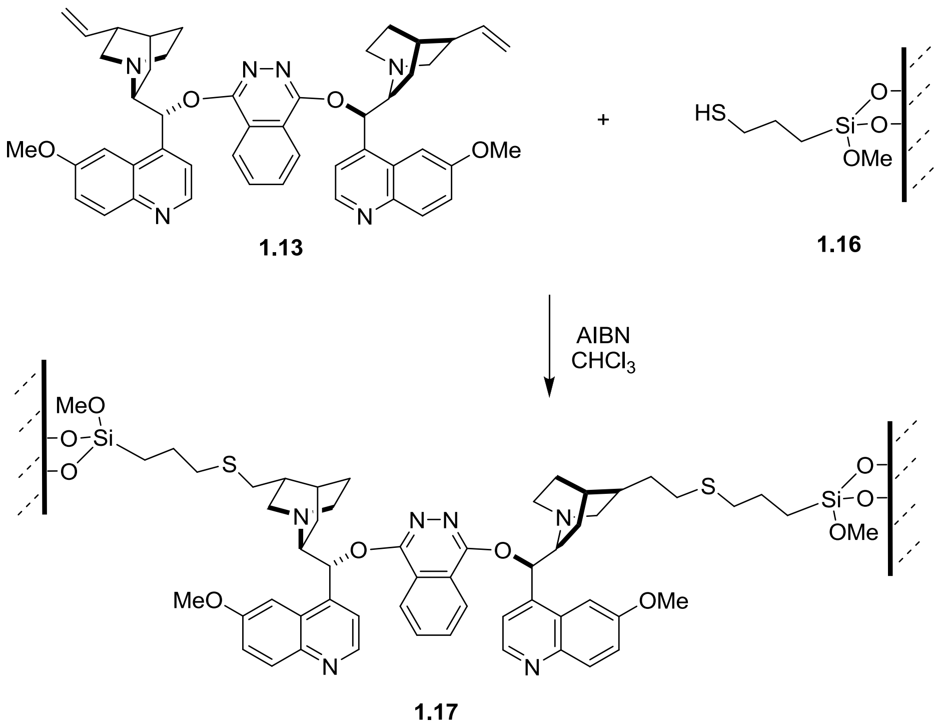

Scheme 1.7: Synthesis of cinchona alkaloid immobilized MCM-41 chiral catalyst for asymmetric dihydroxylation reaction of olefins.

Recently, Yu *et al.*[24] described the synthesis of 9-thiourea epiquinine-functionalized SBA-15 mesoporous silica catalysts by employing the widely used radical synthetic method initiated by the common radical initiator AIBN. The authors then demonstrated that the resulting material could serve as efficient chiral heterogeneous catalyst for the asymmetric Friedel–Crafts reaction between imines and indoles, giving very high enantioselectivity (99.2%).

1.2.2.4 Enzyme-Immobilized Mesoporous Catalyst (Heterogeneous Bio-Catalysts)

Like organocatalytic groups, enzymes can also be immobilized within mesoporous silica materials to produce mesoporous biocatalysts. Since the potential industrial uses of enzymes are often hampered by the lack of long-term operational stability and the difficulty of the recovery and re-use of enzymes, supporting enzymes on solid support materials and preparing their corresponding heterogeneous catalysts are very appealing for the utilization of enzymes effectively in synthetic processes. This has been successfully demonstrated by using mesoporous silicas as support materials for enzymes. For example, Frunz *et al.*[40] showed that the immobilization of the short peptide sequence His-Gly-Gly-Glu, which is found in the active center of methanemonooxygenase, on mesoporous silica produced an effective mesoporous silica/peptide-based solid biocatalyst. To synthesize the material, the authors first made the peptide using a solid-phase peptide synthesizer. Then, they coupled the peptide onto the amino-functionalized mesoporous silica support material with step-by-step synthetic procedure, in the same way as the peptides are synthesized on the peptide synthesizer. After the peptide chain was supported directly on the mesoporous silica support material, iron or copper complexes were anchored on the system by mixing the material with solutions containing iron and copper ions. The catalytic activity of the resulting material was then examined by using the oxidation reaction of cyclohexane by H_2O_2. While modest catalytic activity, with turn-over-numbers (TON) (in x 10^{-1} mol(mol metal)$^{-1}$) in the range of 0.2 to 5.9 was observed, the selectivity towards cyclohexanol over cyclohexanone were very good (with rations ranging from 0.2 to 0.8). Interestingly, the catalytic activity of the material was higher than that obtained with metal complexes immobilized with single amino acids.

In another example, a hydrothermally stable and highly reactive cytochrome c (cyt c) enzyme was immobilized within the nanochannel pores of mesoporous silica (SBA-15).[55] This was achieved by first modifying the surfaces of SBA-15 mesoporous silica with 4-aminophenylmercuric acetate (APMA) groups. The 4-aminophenylmercuric containing mesoporous silica was subsequently stirred with cyt c enzyme. This allowed the supported Hg ions to bind to cysteine groups of cyt c enzyme through strong Hg-S interactions and produce adsorption and high loading of cyt c within the mesoporous silica material, as shown in Scheme 1.8. The resulting mesoporous silica-immobilized enzyme was then successfully applied as a heterogeneous biocatalyst for oxidation of polyaromatic hydrocarbon pyrene, giving an activity of 0.841 min^{-1}.

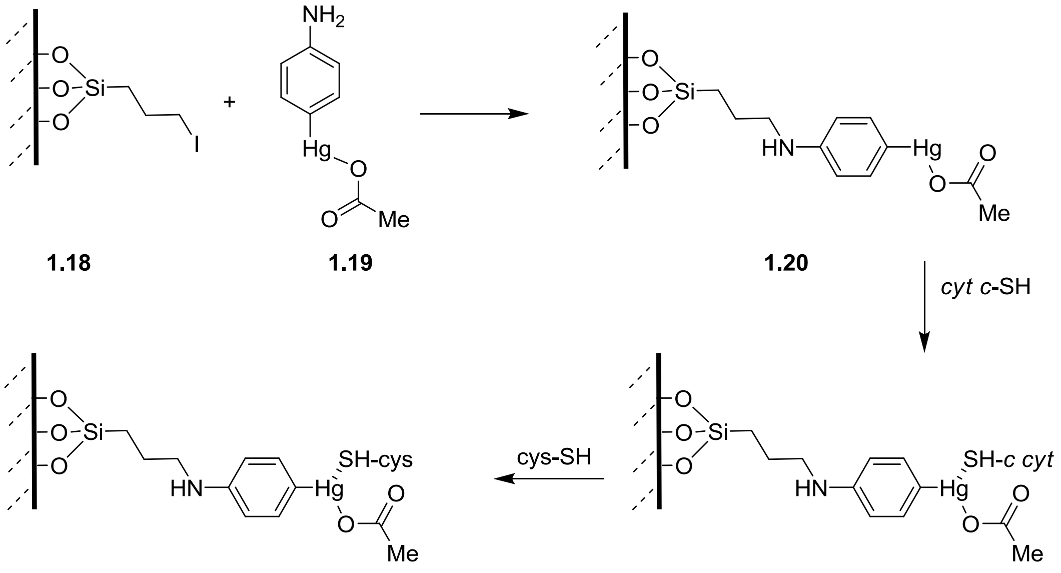

1.18 **1.19** **1.20** **1.21** **1.22**

Scheme 1.8: Schematic representation of the synthesis of APMA-modified SBA-15 and its further immobilization with cytochrome c through Hg-cysteine binding and strong chemisorption of the enzyme on the mesoporous material.

1.3. Core-Shell Nanostructured Materials for Synthesis of Heterogeneous Catalysts

Recently nanomaterials have been the subject of extensive interest because of their extremely small size, which renders them a wide range of unique and size- and shape-dependent physical, electronic and optical properties. Owing to larger surface-to-volume ratio compared to their bulk counterparts, nanoparticles also possess advantageous features for use as support materials in heterogeneous catalysis[41-43] and they give higher catalytic activity per unit mass than their corresponding bulk counterparts.[44] However, their high surface area-to-volume ratios is a “double-edged sword” as it can lead to high surface energies, making many of them to have a great tendency to aggregate, and thereby lose their unique nanoscale properties and inherent catalytic activities. This is more serious especially for metallic nanoparticles under high temperature conditions, which many catalytic reactions require. Aggregation or sintering of metallic nanoparticles results in increased particle size and decreased metal surface area, and quick loss of their catalytic activity.[45] Fortunately, metal sintering can be effectively avoided by placing stabilizing agents around the metal nanoparticles. In particular, porous inorganic shells such as porous silica are appealing for use as shells around nanoparticle catalysts and overcome these problems because they are highly stable, withstand harsh reaction conditions, chemically inert, and can be permeable.[46,47]

1.3.1. Metal Nanoparticles Embedded in Sol-Gel Synthesized Metal Oxide Matrices for Catalysis

In 1999, Reetz[48] developed a synthetic method for heterogenization of of $R_4N^+Br^-$-stabilized Pd colloidal nanoparticles in a metal oxide for catalysis. The entrapment of the nanoparticles was accomplished by fluoride-catalyzed hydrolysis of a mixture of $CH_3Si(OCH_3)_3$ and $Mg(OC_2H_5)_2$ (Figure 1.8). The catalytic activity of the resulting material was tested in hydrogenation reaction of 1,5-cyclooctadiene to cyclooctene product. The selectivity of the reaction for cyclooctene product was found to be 93%. Furthermore, sol–gel-entrapped Pd catalysts exhibited a considerably higher activity than a commercially available Pd/Al_2O_3 sample. Most importantly, the material allowed ease of recycling of the nanoparticle catalysts.

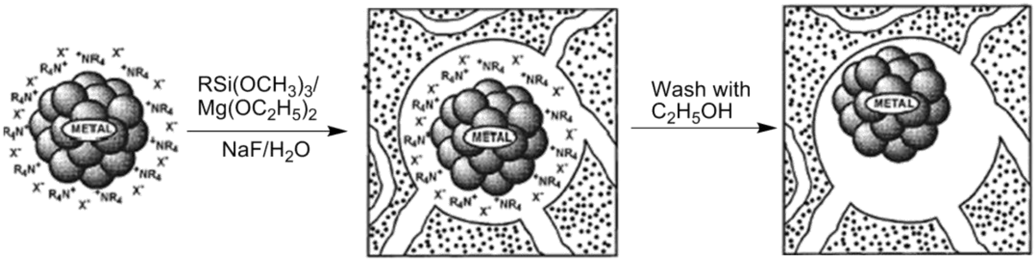

Figure 1.8: Schematic representation of entrapment of Pd nanoparticles in sol-gel derived porous metal oxide matrix for the synthesis of stable metal oxide-supported Pd nanoparticle heterogeneous catalyst.

In a related example, Corma *et al*.[49] presented a modified sol–gel synthetic approach for the synthesis of silica encapsulated Au nanoparticles that served as heterogeneous catalysts. The synthesis first produced a three-component metal–organic–inorganic nanostructure composed of 3-mercaptopropyltrimethoxysilane-capped Au nanoparticles (AuNPs). The alkoxysilyl groups around of the nanoparticles were then hydrolyzed and polymerized with tetraethyl orthosilicate (TEOS), which was added into the solution, producing the silica-encapsulated Au nanoparticles (Figure 1.9). The resulting material, when properly activated, was found to be highly active heterogeneous catalyst for the oxidation of CO at low temperature.

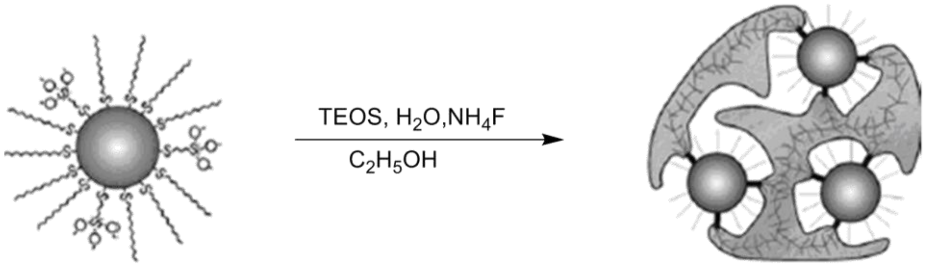

Figure 1.9: Schematic representation of the encapsulation of Au nanoparticles capped with 1-dodecanethiol (DT) by self-assembling 3-mercaptopropyltrimethoxysilane (MPMS) and TEOS. The synthesis resulted in porous silica encapsulated Au nanoparticles (AuNP–organic–SiO_2 nanostructured materials), which exhibited heterogeneous catalytic activity in low temperature CO oxidation reaction.

1.3.2. Metal@Core-Shell Catalyst

Recently, Somorjai *et al.*[50] reported the synthesis of Pt/mesoporous silica core shell (Pt@mSiO_2) nanoparticles that are thermally stable at high temperatures. The core-shell structured Pt@mSiO_2 nanoparticles were synthesized via the following three steps (Figure 1.10): (1) synthesis of Pt nanoparticles using tetradecyltrimethylammonium bromide (TTAB) as the capping agent; (2) polymerization of silica around the Pt cores, generating the as-synthesized Pt@SiO_2 mesostructures; and (3) the removal of the TTAB molecules by calcination of the material to produce the Pt@mSiO_2 core-shell nanoparticles. The resulting Pt@mSiO_2 core-shell nanoparticles exhibited efficient catalytic activity for ethylene hydrogenation and CO oxidation.

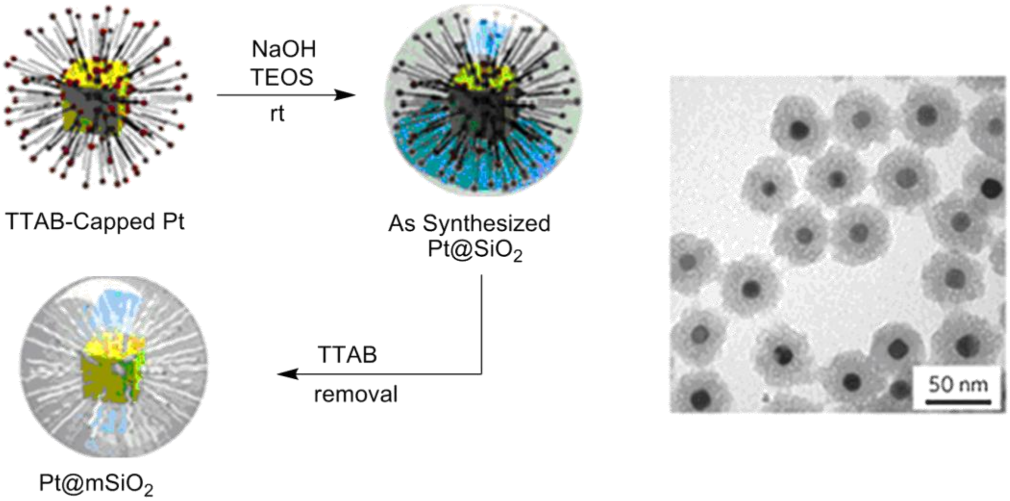

Figure 1.10: (A) Schematic representation of the synthesis of Pt@mSiO_2 core-shell nanoparticles. (B) TEM image of Pt@mSiO_2 nanoparticles after calcination at 350 °C.

Park *et al.*[51] developed a similar synthetic route to sinter-resistant Pd@SiO_2 nanocatalysts. Colloidal Pd particles were first prepared in the aqueous droplets of microemulsions by reducing $Pd(NO_3)_2$ with hydrazine inside the microemulsions. The resulting Pd nanoparticles were then mixed with silicon alkoxides (tetraethylorthosilicate and *n*-octadecyl trimethoxysilane) inside the microemulsions. This led to hydrolysis and condensation the silicon alkoxides around the preformed Pd nanoparticles, producing the Pd@SiO_2 core-shell nanoparticles. The catalytic activity of the resulting Pd@SiO_2 core-shell nanoparticle was tested by using CO oxidation and acetylene hydrogenation as model reaction. Although the control sample, Pd/$SiO_{2,}$ which was prepared by impregnation method showed a better activity (apparent activation energy = 103.0±3.7 $kJmol^{-1}$) than the Pd@SiO_2 catalyst (apparent activation energy =

129.0±5.3 kJ mol^{-1}) at lower temperature, this trend was reversed after heat treatments of the samples at higher temperatures, *i.e.*, temperatures that are typically necessary for many catalytic reactions these nanomaterials are used for. The catalyst (Pd@SiO_2) calcined in air at 700 ºC for 6 h retained its catalytic activity much more than the reference material (*i.e.*, Pd/SiO_2 nanoparticles), indicating the higher stability of the former against sintering and deactivation at higher reaction temperature.

1.3.3. Metal@Core-Shell-Shell Catalyst

For most of the previously reported core-shell type nanostructured catalysts, only one metal per particle was encapsulated with silica shell for a given nanoparticle. Although this synthetic approach reduces the chances of agglomeration or aggregation of the encapsulated metal nanoparticles, such nanomaterials suffer from having low metal loading. To achieve a higher metal loading and more efficient catalysis per unit mass of catalyst, the given nanosphere must possess multiple metal catalytic active nanoparticles. Our group recently developed a new method to overcome this problem. Specifically, our group described a new synthetic method to novel nanomaterials called core-shell-shell nanoparticles, which contained a silica core with many gold nanoparticles shell that was further coated by a nanoporous silica shell with a tunable size and tailored structure (Figure 1.11).[52] The thickness of the silica shells was controlled by changing the concentrations of TEOS used during silica coating step of the synthesis (Figure 1.11). Furthermore, its porosity and pore sizes were tuned by changing the etching synthetic method we developed.

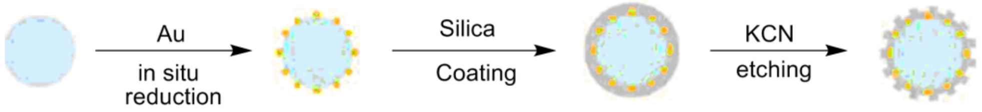

Figure 1.11: Synthesis procedure of silica/Au nanoparticles/silica core-shell-shell nanospheres containing embedded Au nanoparticles. These nanomaterials were shown to serve as effective heterogeneous catalysts for a number of reactions.

Later, Yin *et al.*[53] followed a similar synthetic procedure to encapsulate electrostatically linked Au nanoparticles on the silica core with a silica shell. By controlled etching of the silica shell, the authors produced mesoporous silica structure around the Au nanoparticles (AuNPs). The porous silica shell around the Au nanoparticles allowed the Au nanoparticles to be accessed by the reactants (Figure 1.12). The introduction of magnetic active species into the cores of the materials further provided the material the benefit of facile recovery and regeneration of the catalysts using an external magnetic field. Liquid-phase reduction of 4-nitrophenol by $NaBH_4$ was used as a model reaction to ascertain the catalytic performance of this Au nanoparticles in this core-shell-shell nanocatalytic system.

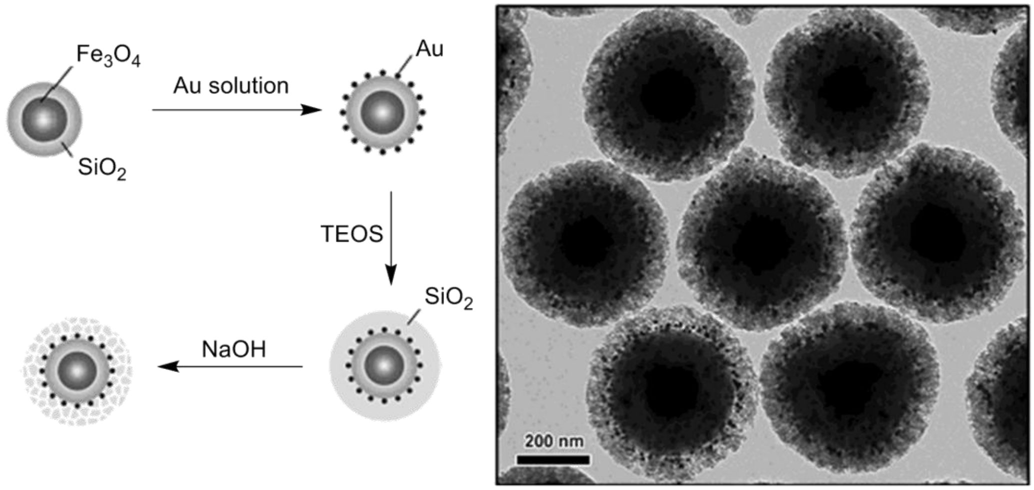

Figure 1.12: Synthetic procedure and a typical TEM image of porous silica protected $Fe_3O_4/SiO_2/Au$ composite structures.

We also recently reported the successful synthesis of core-shell-shell nanospheres, with each nanosphere containing several octahedral-shaped 5 nm or 20 nm Pd nanoparticles sandwiched between a silica nanosphere core and a nanoporous silica shell.[54] By using these core-shell-shell nanospheres as heterogeneous catalyst, we demonstrated highly efficient and recyclable catalytic properties for the nanomaterials in hydrogenation and C–C coupling reactions.

1.4. Objective

The primary objective of this dissertation was to develop novel multifunctional mesoporous and nanostructured catalysts containing different judiciously chosen functional / catalytic groups and explore their unique or unprecedented catalytic activities in various useful organic reactions. The functional or catalytic groups can comprise organocatalytic groups, weak acid groups such as silanols, organometallic complexes or metallic nanoparticles. The dissertation is divided into two parts: (a) multifunctional mesoporous material and (b) core-shell-shell nanostructured material. In Chapter II, the development of synthetic strategies to make tertiary amine/silanol-based bifunctional mesoporous catalysts that can efficiently catalyze the base-catalyzed the Michael addition reaction is discussed. In Chapter III the application of the iron-containing SBA-15 type mesoporous silica catalysts, in which Fe(III) is coordinated to organoamine groups grafted onto the surface of the mesoporous silica (SBA-15) and its catalytic activity in the alcoholysis or hydrolysis of various epoxides is discussed. Chapter IV is focused on the immobilization of Au_n nanocluster in thiol functionalized SBA-15 and the effect of removal of thiol groups from the surface of gold cluster on selective oxidation of styrene. Chapter V describes synthesis of stable and robust core-shell-shell microspheres containing AuNPs that are sandwiched between metal oxide cores and nanoporous metal oxide shells and their efficient catalytic activity for epoxidation reaction. Chapter VI describes the synthesis of dendrimer encapsulated ultrasmall palladium nanoparticles core-shell-shell microspheres and the application in hydrogenation reactions. Finally, Chapter VII provides a brief conclusion of the dissertation, along with an overview of potential future applications or prospects for the reported catalysts.

Reference

(1) Desper, R B. 'Alwin Mittasch'. *J. Chem. Edu*. **1948**, *25*, 531.

(2) Laidler, K J.; Meiser, J H. *Phys. Chem*. **1982**, 423.

(3) Kumar, S.; Rayalu, S.; Russo, N.; Kanade, G. S.; Kusaba, H.; Teraoka, Y.; Labhsetwar, N. *Catal. Lett.* **2009**, *132*, 248.

(4) Shimada, H.; Sato, K.; Honna, K.; Enomoto, T.; Ohshio, N. *Catal. Today*. **2009**, *141*, 43.

(5) Chen, H. Y.; Sun, Q.; Wen, B.; Yeom, Y. H.; Weitz, E.; Sachtler, W. M. H. *Catal. Today* **2004**, *96*, 1.

(6) Durap, F.; Rakap, M.; Aydemir, M.; OÌˆzkar, S. *Appl. Catal. A: Chem*, *382*, 339.

(7) Jones, C. W.; McKittrick, M. W.; Nguyen, J. V.; Yu, K. *Top. Catal.* **2005**, *34*, 67.

(8) Gill, C. S.; Venkatasubbaiah, K.; Jones, C. W. *Adv. Synth. Catal.* **2009**, *351*, 1344.

(9) Kouachi, K.; Lafaye, G.; Especel, C.; Cherifi, O.; Marecot, P. *J. Mol. Catal. A: Chem.* **2009**, *308*, 142.

(10) Hoffmann, F.; Cornelius, M.; Morell, J.; Fröba, M. *Angew. Chem. Int. Ed* **2006**, *45*, 3216.

(11) Salechi, P.; Khodaei, M. M.; Ghareghani, S. B.; Motlagh, A. R. *Russian J. Org. Chem.* **2003**, *39*, 794.

(12) Wan, Y.; Zhao, D. *Chem. Rev* **2007**, *107*, 2821.

(13) Heravi, M. M.; Baghernejad, B.; Oskooie, H. A. *Catal. Lett.* **2009**, *130*, 547.

(14) Barreca, D.; Copley, M. P.; Graham, A. E.; Holmes, J. D.; Morris, M. A.; Seraglia, R.; Spalding, T. R.; Tondello, E. *Appl. Catal., A: Gen.* **2006**, *304*, 14.

(15) Beck, J. S.; Vartuli, J. C.; Roth, W. J.; Leonowicz, M. E.; Kresge, C. T.; Schmitt, K. D.; Chu, C. T. W.; Olson, D. H.; Sheppard, E. W. *J. Am. Chem. Soc* **1992**, *114*, 10834.

(16) Kresge, C T.; Leonowicz, M E.; Roth, W J.; Vartuli, J C.; Beck, J S. *Nature*. **1992**, *359*, 710..

(17) Zhao, D.; Feng, J.; Huo, Q.; Melosh, N.; Fredrickson, G H.; Chmelka, B F.; Stucky, G D. *Science*. **1998**, *279*, 548.

(18) Wight, A. P.; Davis, M. E. *Chem. Rev.* **2002**, *102*, 3589.

(19) Lim, M. H.; Stein, A. *Chem. Mater.* **1999**, *11*, 3285.

(20) Wang, X.; Chen, C.-C.; Chen, S.-Y.; Mou, Y.; Cheng, S. *Appl. Catal., A:Gen.* **2005**, *281*, 47.

(21) Shen, J. G. C.; Herman, R. G.; Klier, K. *J. Phys. Chem. B.* **2002**, *106*, 9975.

(22) Bass, J. D.; Solovyov, A.; Pascall, A. J.; Katz, A. *J. Am. Chem. Soc.* **2006**, *128*, 3737.

(23) Sharma, K. K.; Asefa, T. *Angew Chem.* **2007**, *119*, 2937.

(24) Yu, P.; He, J.; Guo, C. *Chem. Commun.* **2008**, 2355.

(25) Motorina, I.; Crudden, C. M. *Org Lett* **2001**, *3*, 2325.

(26) Lee, H. M.; Kim, S.-W.; Hyeon, T.; Kim, B. M. *Tetrahedron: Asymmetry* **2001**, *12*, 1537.
(27) Wang, Y.; Caruso, F. *Chem. Mater* **2005**, *17*, 953.
(28) Sheldon, R. A. *Adv. Synth. Catal.* **2007**, *349*, 1289.
(29) M. Van Rhijn, W.; E. De Vos, D.; F. Sels, B.; D. Bossaert. W, Jacobs, P A. *Chem. Commun.* **1998**, 317.
(30) Lim, M. H.; Blanford, C. F.; Stein, A. *Chem. Mater.* **1998**, *10*, 467.
(31) Díaz, I.; Mohino, F.; Pérez-Pariente, J. Ì. N.; Sastre, E. *Appl. Catal., A: Gen.* **2001**, *205*, 19.
(32) Anan, A.; Sharma, K. K.; Asefa, T. *J. Mol. Catal., A: Chem* **2008**, *288*, 1.
(33) Sharma, K. K.; Anan, A.; Buckley, R. P.; Ouellette, W.; Asefa, T. *J. Am. Chem. Soc.* **2007**, *130*, 218.
(34) Xie, Y.; Sharma, K. K.; Anan, A.; Wang, G.; Biradar, A. V.; Asefa, T. *J. Catal* **2009**, *265*, 131.
(35) Xie, Y.; Sharma, K. K.; Anan, A.; Wang, G.; Biradar, A. V.; Asefa, T. *J. Catal.* **2009**, *265*, 131.
(36) Mondal, J.; Modak, A.; Bhaumik, A. *J. Mol. Catal. A: Chem.*, **2011**, *335*, 236.
(37) Sujandi; Prasetyanto, E. A.; Park, S.-E. *Appl. Catal. A: Gen.* **2008**, *350*, 244.
(38) Motorina, I.; Crudden, C. M. *Org. Lett.* **2001**, *3*, 2325.
(39) Choudary, B. M.; Chowdari, N. S.; Jyothi, K.; Kantam, M. L. *Catal Lett* **2002**, *82*, 99.
(40) Frunz, L.; Prins, R.; Pirngruber, G. D. *Chem. Mater.* **2007**, *19*, 4357.
(41) Lewis, L. N. *Chem. Rev.* **1993**, *93*, 2693.
(42) Moreno-Maňas, M.; Pleixats, R. *Acc. Chem. Res.* **2003**, *36*, 638.
(43) Narayanan, R.; El-Sayed, M. A. *J. Phy. Chem. B.* **2005**, *109*, 12663.
(44) Cheong, S.; Watt, J. D.; Tilley, R. D. *Nanoscale.***2010**, *2*, 2045.
(45) Jia, C.-J.; Schuth, F. *Phys. Chem. Chem. Phys.* **2011**, *13*, 2457.
(46) Mulvaney, S. P.; Musick, M. D.; Keating, C. D.; Natan, M. J. *Langmuir* **2003**, *19*, 4784.
(47) Lee, J.; Park, J. C.; Bang, J. U.; Song, H. *Chem. Mater.* **2008**, *20*, 5839.
(48) Reetz, M.; Dugal, M. *Catal. Lett.* **1999**, *58*, 207.
(49) Budroni, G.; Corma, A. *Angew. Chem. In. Ed.* **2006**, *45*, 3328.
(50) Joo, S. H.; Park, J. Y.; Tsung, C.-K.; Yamada, Y.; Yang, P.; Somorjai, G. A. *Nat Mater.* **2009**, *8*, 126.
(51) Park, J.-N.; Forman, A. J.; Tang, W.; Cheng, J.; Hu, Y.-S.; Lin, H.; McFarland, E. W. *Small.* **2008**, *4*, 1694.
(52) Shi, Y.-L.; Asefa, T. *Langmuir.* **2007**, *23*, 9455.
(53) Ge, J.; Zhang, Q.; Zhang, T.; Yin, Y. *Angew. Chem. Int. Ed.* **2008**, *47*, 8924.
(54) Wang, Y.; Biradar, A. V.; Duncan, C. T.; Asefa, T. *J. Mater. Chem.* **2010**, *20*, 7834.
(55) Cheng, S-H.; Kao, K-C.; Liao, W-N.;Chen. L-M.; Mou, C-Y.; Lee, C-H. *New J. Chem.* **2011**,*35*, 1809.
(56) Sharma, K. K.; Biradar, A. V.; Asefa, T. *ChemCatChem.* **2010**, *2,* 61.

(57) Burkett, S. L.; Sims, S.D.; Mann, S. *Chem. Commun*. **1996**, *11*, 1367.
(58) Macquarrie, D.J. *Chem. Commun*. **1996**, 1961.

Chapter II

Amine/Silanol Bifunctionalized Mesoporous Silica Catalysts for Michael Addition Reactions between Active Methylene Compounds and Nitroolefin

2.1 Michael Addition Reaction

The Michael addition reaction is the nucleophilic addition of a carbanion (Michael donor) or another nucleophile to an α,β-unsaturated compound (Michael acceptor). As originally defined by Arthur Michael[1,2] the reaction is the addition of an enolate of a ketone or aldehyde to an α,β-unsaturated carbonyl compound at the β carbon. During the course of the reaction, electronic charge migrates from the carbon in the donor molecule to a better acceptor atom, usually oxygen, in the electrophile. A base is used to form the carbanion by abstracting a proton from an activated methylene precursor. The ease of the reaction and the involvement of a base and the corresponding conjugate acid to catalyze the reaction have made the development of catalysts which can catalyze the reactions reversibly and efficiently the subject of intense research in catalysis. Below are discussed some of the examples of Michael addition reaction.

2.1.1 Homogeneous Michael Addition Reaction

The products of 1,4-additions of nitroalkanes to α,β-unsaturated enones are useful precursors for a variety of structures such as aminocarbonyl compounds, aminoalkanes, and pyrrolidines.[3] Efforts toward achieving asymmetric conjugate additions of enones to α,β-unsaturated compounds are listed below. Hanessian *et al.*[4] reported the catalytic asymmetric conjugate addition of various nitroalkanes to cyclic enones such as cyclopentenone, cyclohexenone, and cycloheptenone in the presence of *L*-proline (3–7 mol%) as a catalyst and *trans*-2,5-dimethylpiperazine as an additive (Scheme 2.1). The reaction proceeds with good to high enantioselectivities of 62–93% *ee* and in yields of up to 88%. The highest enantioselectivity was found with 2-nitropropane and cyclohexenone (93% *ee*).

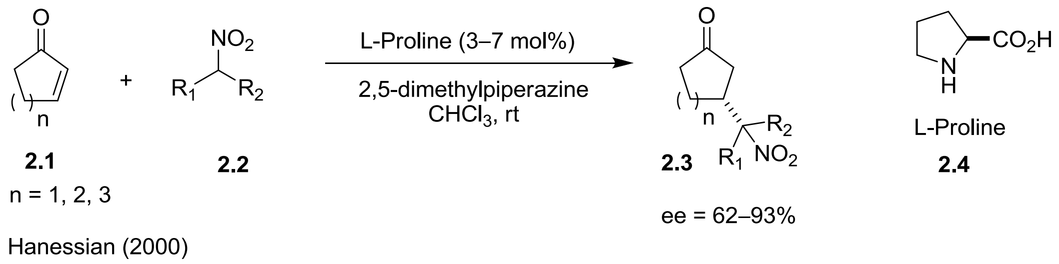

O
n
2.1
n = 1, 2, 3
+
NO2
R1
R2
2.2
L-Proline (3–7 mol%)
2,5-dimethylpiperazine
CHCl3, rt
O
n
R2
R1
NO2
2.3
ee = 62–93%
N
H
CO2H
L-Proline
2.4
Hanessian (2000)

Scheme 2.1: *L*-Proline catalyzed enantioselective Michael addition reaction.

Palomo *et al.*[5] demonstrated asymmetric Michael addition of aldehydes to nitroalkenes (Scheme 2.2) catalyzed by a simple *trans*-4-hydroxyprolylamide with 92 % ee and high conversion (> 99%).

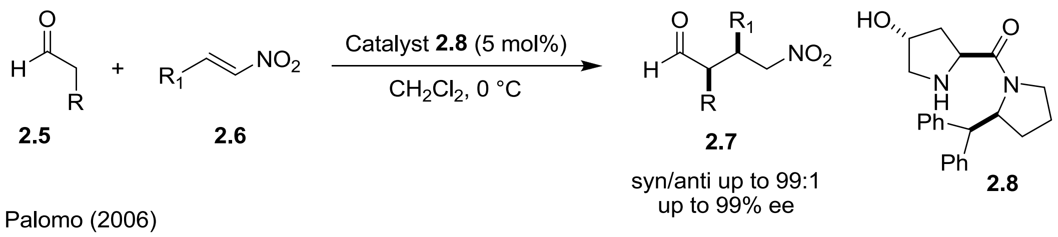

O
H
R
2.5
+
R1
NO2
2.6
Catalyst 2.8 (5 mol%)
CH2Cl2, 0 °C
O
R1
H
NO2
R
2.7
syn/anti up to 99:1
up to 99% ee
HO
O
N
H
N
Ph
Ph
2.8
Palomo (2006)

Scheme 2.2: Asymmetric Michael addition reaction catalyzed by prolinamide.

Ni and co-workers[6] have developed a highly efficient organocatalyst containing ILS-benzoic acid as the catalytic system for Michael additions of aldehydes to nitroolefins in water (Scheme 2.3). The catalytic system gave excellent enantioselectivities and high diastereoselectivities for a wide range of nitroolefins, including aromatic and aliphatic nitroolefins and it can be easily recovered and reused for at least 12 times without significant loss of stereoselectivities.

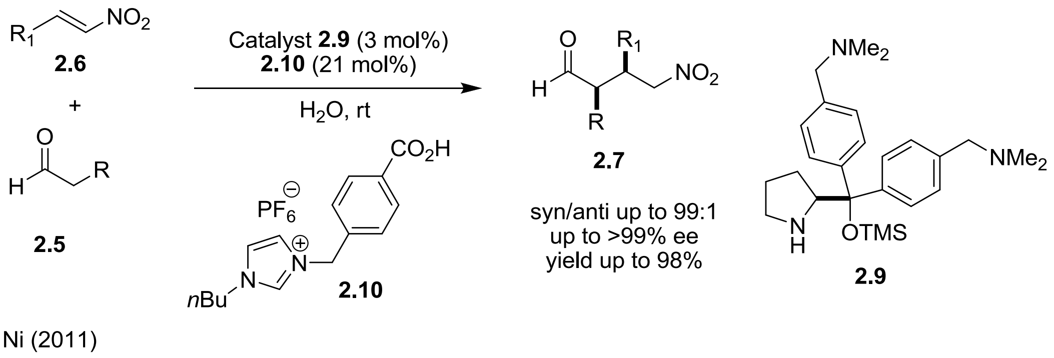

R1
NO2
2.6
+
O
H
R
2.5
Catalyst 2.9 (3 mol%)
2.10 (21 mol%)
H2O, rt
CO2H
PF6
N
N
nBu
2.10
O
R1
H
NO2
R
2.7
syn/anti up to 99:1
up to >99% ee
yield up to 98%
NMe2
NMe2
N
H
OTMS
2.9
Ni (2011)

***Scheme 2.3*:** Organocatalyst in combination with ILS-benzoic acid as a catalytic system for Michael addition reaction.

2.1.2 Bifunctional Catalyst for Michael Addition Reaction

A different vista has been opened up by some recent contributions from some research groups, who have shown that chiral thiourea based bifunctional compounds can act as efficient organocatalysts for asymmetric Michael reactions between ketones and nitroolefins.[7-10] Takemoto *et al.*[11] have designed a new class of bifunctional catalysts bearing both a thiourea moiety and an amino group on a chiral scaffold. These bifunctional catalysts would be able to activate both nitroolefins and nucleophiles simultaneously and could control the approach of nucleophiles to nitroolefins (Figure 2.1). On the basis of this concept, they have recently reported that novel bifunctional catalysts realized Michael reaction of 1,3-dicarbonyl compounds to nitroolefins with high enantioselectivity up to 93% *ee*.

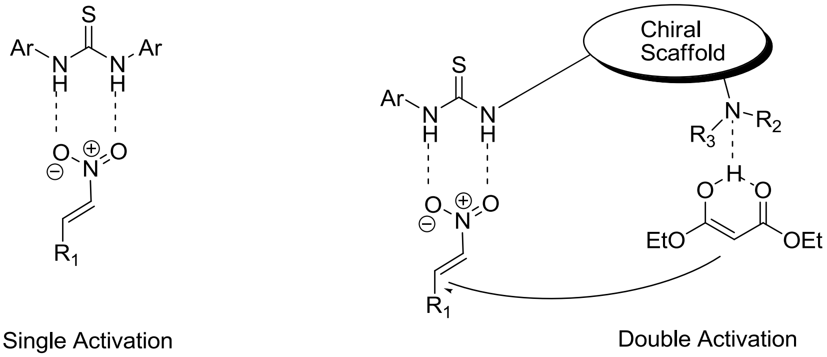

Figure 2.1**:** Activation of electrophile and nucleophile by bifunctional catalyst.

Rawal *et al.*[12] developed a new family of H-bonding catalysts based on the squaramide backbone analogous to Takemoto’s catalyst.[11] The chiral squareamide catalyst proved to be an effective H-bond donor catalyst for the conjugate addition of 2,4-pentanedione to *β*-nitrostyrene. A series of experiments has been performed to demonstrate the bifunctional nature of squareamides bearing amine groups (Figure 2.2 and Table 2.1). Simple squaramide **2.14** was not an effective catalyst for the reaction of **2.11** and **2.12** (Entry 1).

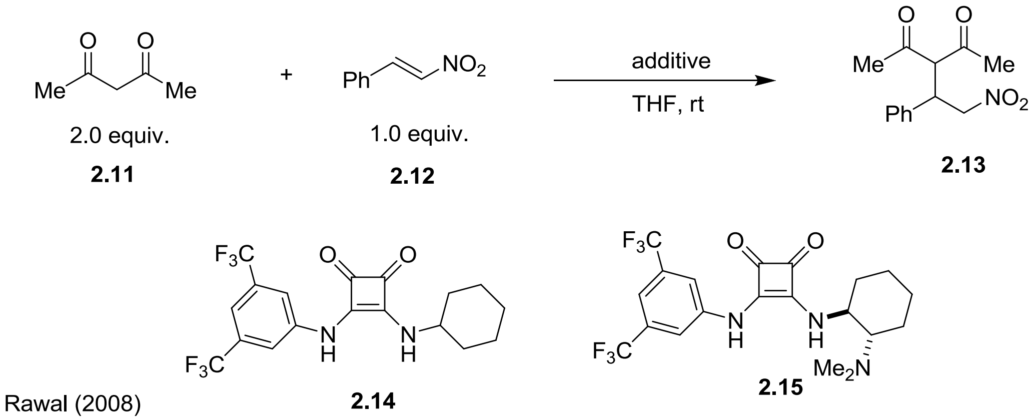

***Figure 2.2*:** Squaramide base bifunctional catalyst for Michael reaction.

In the presence of Et_3N, partial conversion was observed after 6 h (Entry 2). The addition of both **2.14** and Et_3N (Entry 3) significantly increased the rate of production of **2.13** compared to either of the isolated components. Utilizing catalyst **2.15**, which incorporates a basic tertiary amine into the squaramide, gives further rate acceleration. These results suggest that while basic activation of the nucleophile is required for the reaction to take place, further rate increase can be attributed to activation of the electrophile by hydrogen bonding.

Table 2.1: Control experiments to study the bifunctional nature of bis-squareamide bearing amine groups.

Entry	Additive	Time (h)	Conversion (%)
1	**2.14** (10 mol%)	17	NR
2	Et_3N (10 mol%)	6	30
3	Et_3N (10 mol%) + **2.14** (10 mol%)	6	95
4	**2.15** (10 mol%)	2	100

2.1.3 Application in Natural Product Synthesis

Michael addition reaction has been applied in the organocatalytic total synthesis of natural products. Most recently, Fan and coworkers[13] reported Michael addition of α-cyanoketones and acrylates as the key step for the diversity oriented asymmetric synthesis of bioactive hydrodibenzofuran alkaloids. Three natural hydrodibenzofuran alkaloids, (-)-lycoramine **2.16**, (-)-galanthamine and (+)-lunarine **2.17**, were constructed on the basis of this method (Figure 2.3).

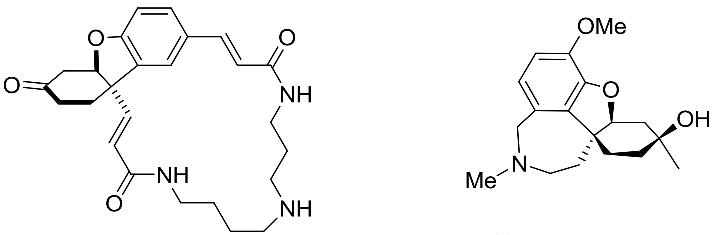

(-)-galanthamine
2.16

(-)-galanthamine
(+)-lunarine
2.17

Figure 2.3**:** Application in natural products synthesis.

2.1.4 Heterogeneous Michael Addition Reaction

Michael addition reaction is also well known in heterogeneous system. In 1998 Macquarrie and coworker[14] demonstrated the Michael addition of nitroalkane to *α,β*-unsaturated ketone catalyzed by N,N-dimethyl-3-aminopropyl derivatised hexagonal mesoporous silica which gave a yield of 70 % in 3 h under reflux conditions. In 2003, the same group[15] reported four aminopropylsilica materials, prepared from different siliceous precursors or by different methods, namely by the grafting method producing MCM-41-NH_2 and KG-60-NH_2, and by the sol-gel method producing HMS-NH_2 and APS-NH_2. The resulting materials were then utilized as solid base catalysts to promote Michael addition reaction.

Cheng *et al*.[16] functionalized SBA-15 mesoporous silica with aminopropyl groups through a simple co-condensation approach of tetraethyl orthosilicate (TEOS) and (3-aminopropyl)triethoxysilane (APTES) using amphiphilic block copolymers under acidic conditions. The catalyst was tested for intramolecular Michael addition of benzaldehyde and 2'-hydroxyacetonphenone to flavanone at 140 °C and a conversion of 92 % was achieved in 8 h.

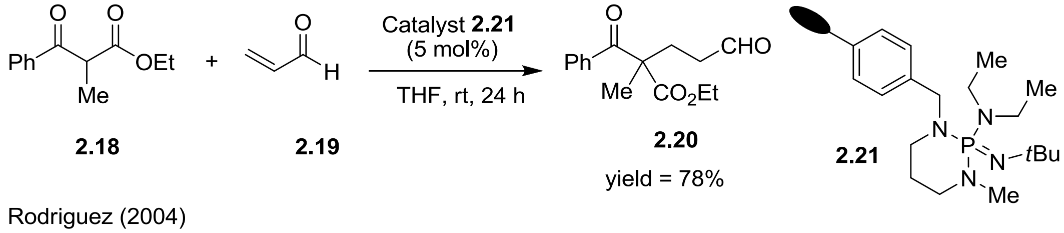

Scheme 2.4: Michael reaction of 1,3-dicarbonyl catalyzed by P-BEMP.

Rodriguez and coworkers[17] demonstrated the Michael addition of 1,3-dicarbonyls with various Michael acceptors catalyzed by commercially available, user-friendly and recyclable *N*-phenyl-tris(dimethylamino)iminophosphorane immobilized on polystyrene resin (P-BEMP) (Scheme 2.4).

2.2 General Considerations and Concept

Our goal was to develop a bifunctional mesoporous catalyst that contains tertiary amine and silanol groups for the Michael addition reaction. Traditionally, the Michael reaction is catalysed by mild to moderately strong bases such as diisopropylamine, potassium *t*-butoxide[18] and tetramethylguanidine[19] in homogeneous phase. However, production of significant amounts of multiple Michael adducts, other side reactions, difficult product separation and catalyst recovery, have always been problematic. These problems, plus the recent increase in the interest of developing environmentally friendly solid catalysts, have led to the development of heterogeneous catalytic systems for this reaction. Examples of such systems are those based on KF- and CsF-alumina,[20] potassium *t*-butoxide on xonotlite,[21] and Amberlyst A-27,[22] which have been used with different degrees of success.

We envisioned that mesoporous silica can be used as an insoluble solid surface to develop bifunctional catalysts. Recently in our group we have shown that the presence of surface silanol groups can be beneficial for the catalytic performance when appropriate catalytic functions like amines are introduced into the pore channels.[23, 24] These bifunctional catalysts are like enzymes which are able to accelerate organic reactions through cooperative acid-base interaction,[25] which inspired chemists to build a library of homogenous bifunctional catalysts.[26] But the use of both acidic and basic species in a homogeneous single reactor is impossible due to neutralization of acid and base to form inactive salts. Because of this limitation in homogeneous systems, several acid-base bifunctional heterogeneous systems are developed[27-31] where the co-existence of acid and base is possible.

2.2.1 Synthesis of Tertiaryamine Functionalized SBA-15

The synthesis of the bifunctional catalyst Ext-SBA-15-NMe_2-Tol containing tertiary-organoamine and silanol groups was achieved by stirring an excess amount of DATS in toluene at 80 °C for 6 h using SBA-15 as support. The corresponding control sample (labelled as Cap-SBA-15-NMe_2-Tol) was prepared by capping the external residual silanol (weak acid) groups of the Ext-SBA-15-NMe_2-Tol with methyl groups as depicted in Scheme 2.5. The latter sample was synthesized in such a way that its accessible silanol groups would be capped by trimethylsilyl (O-$SiMe_3$) groups so that it would not have accessible external silanol (active weak acid) groups, which could aid in hydrogen bonding during the Michael reaction.

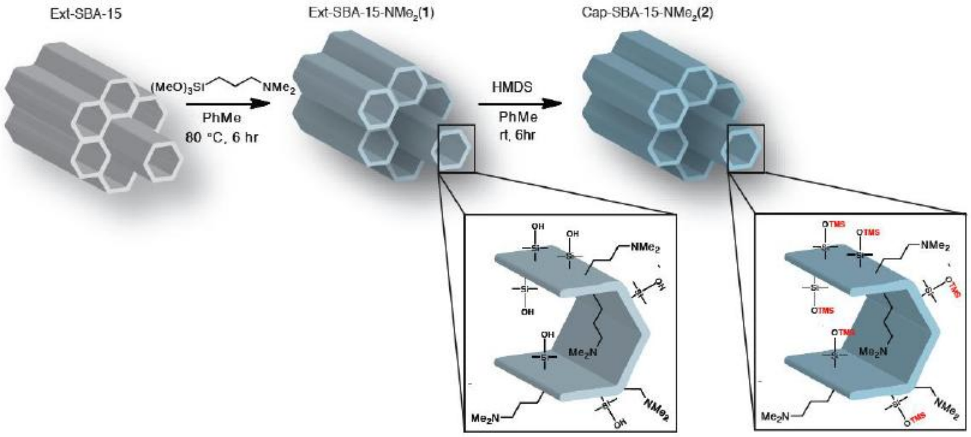

***Scheme 2.5*: ** Synthesis of Ext-SBA-15-NMe_2 and Cap-SBA-15-NMe_2.

The N_2 gas adsorption measurement was used to characterize the mesoporous structure, surface area and pore diameter of the catalyst and the parent material. The N_2 gas adsorption measurements showed type IV isotherm, which were characteristic of mesoporous materials (Figure 2.4) and their BJH pore size distribution was monodisperse. Furthermore the BET surface area and pore diameter of the parent material (Ext-SBA-15) was 427 m^2/g and 118.28 Å which decreased successively with grafting of organoaminosilane in the mesopore. For instance the surface area and pore diameter of Ext-SBA-15-NMe$_2$ was 235 m^2/g and 84.0 Å and to that of Cap-SBA-15-NMe$_2$ was 225 m^2/g and 84.28 Å respectively. These results indicated the decrease in surface area and pore diameter of the latter material than the parent material was due to the presence of grafted amine.

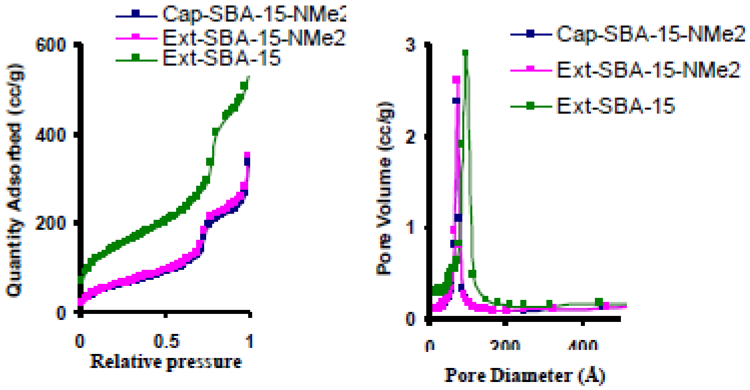

Figure 2.4: Adsorption isotherm and pore size distribution of Ext-SBA-15, Ext-SBA-15-NMe$_2$ and Cap-SBA-15-NMe$_2$.

These materials, both before and after postgrafting were also characterized by powder X-ray diffraction (Figure 2.5) and transmission electron microscope (TEM) (Figure 2.6). The XRD pattern of all the samples showed a sharp peak corresponding to the (100) peak which indicates that the materials possess hexagonally ordered mesostructures, which remain intact even after postgrafting. The peaks were indexed to give unit cell sizes of 11.7 nm. The TEM images of the sample also revealed the presence of ordered mesostructures in the materials.

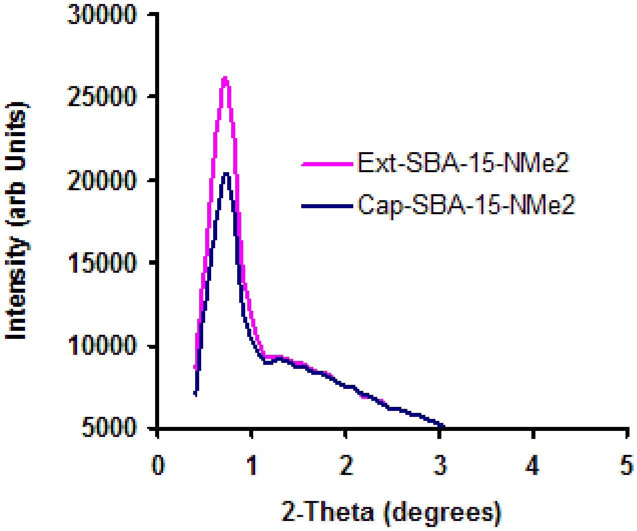

Figure 2.5: XRD Pattern of Ext-SBA-15-NMe$_2$ and Cap-SBA-15-NMe$_2$.

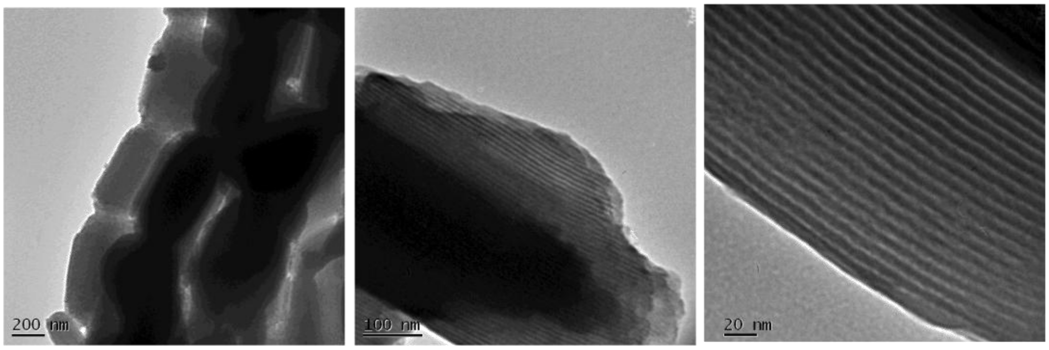

Figure 2.6: TEM Images of Ext-SBA-15-NMe$_2$.

The thermogravimetric traces (Figure 2.7) indicated a weight loss below 100 °C for all the samples due to loss of water adsorbed on the material. The weight loss in Ext-SBA-15 in between 100 to 600 °C may be due to the residual surfactant. The weight loss in the catalyst samples in between 100 to 600 °C is due to the organoamine group. The Ext-SBA-15-NMe_2 and Cap-SBA-15-NMe_2 samples showed almost same weight loss (20.58 %), which indicates the same amount of organoamine group grafted on both the samples.

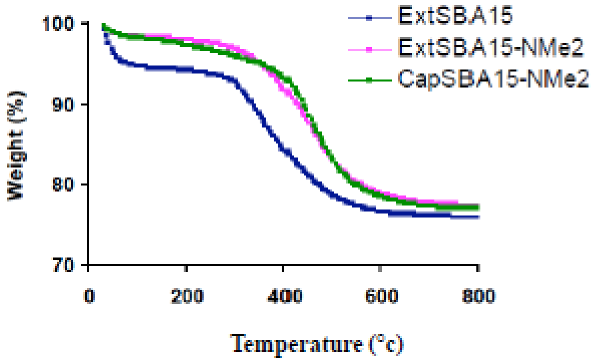

Figure 2.7: Thermogravimetric Traces of Ext-SBA-15, Ext-SBA-15-NMe_2 and Cap-SBA-15-NMe_2.

The catalysts Ext-SBA-15-NMe_2-Tol, Cap-SBA-15-NMe_2-Tol and Cap-SBA-15-NMe_2-IPA were also characterized by ^{13}C cross polarization magic angle spinning (CP-MAS), ^{29}Si CP-MAS and ^{29}Si MAS (^{29}Si-1H-Decoupled) solid-state NMR spectroscopy (Figure 2.8). In case of ^{13}C CP-MAS NMR spectra for Ext-SBA-15-NMe_2-Tol, the peaks at 10.2, 20.1, 43.2 and 61.6 ppm were designated as C4, C3, C1 (NMe_2) and C2 of alkyl-chain (Figure 2.9). The peaks marked with asterisks (*) correspond to the peaks from residual surfactant.[32] Similar pattern (as well as similar chemical shift) was observed in case of Cap-SBA-15-NMe_2-Tol.

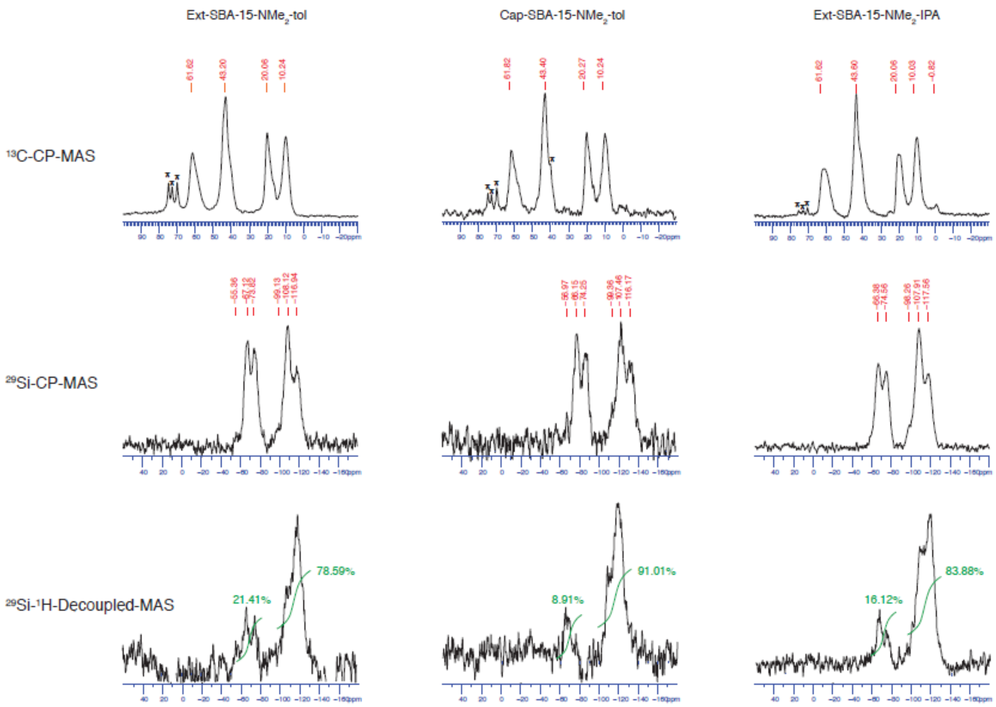

Figure 2.8**:** Solid-state NMR spectra of Ext-SBA-15-NMe2-Tol (SBA-15 grafted in toluene) and Cap- SBA-15-NMe2 (Ext-SBA-15-NMe2-Tol grafted in toluene and then capped with O-SiMe3 groups), and Ext-SBA-15-NMe2-IPA (SBA-15 grafted in isopropanol).

However, the peaks corresponding to methyl groups due to the capping of –Si-OH groups by HMDS and formation of -Si-OSiMe$_3$ did not show up in the spectra (at least under the same experimental condition). On the other hand, in case of Cap-SBA-15-NMe$_2$-IPA, the peak at 0.82 ppm indicates the presence of –OSiMe$_3$ into the material.[33]

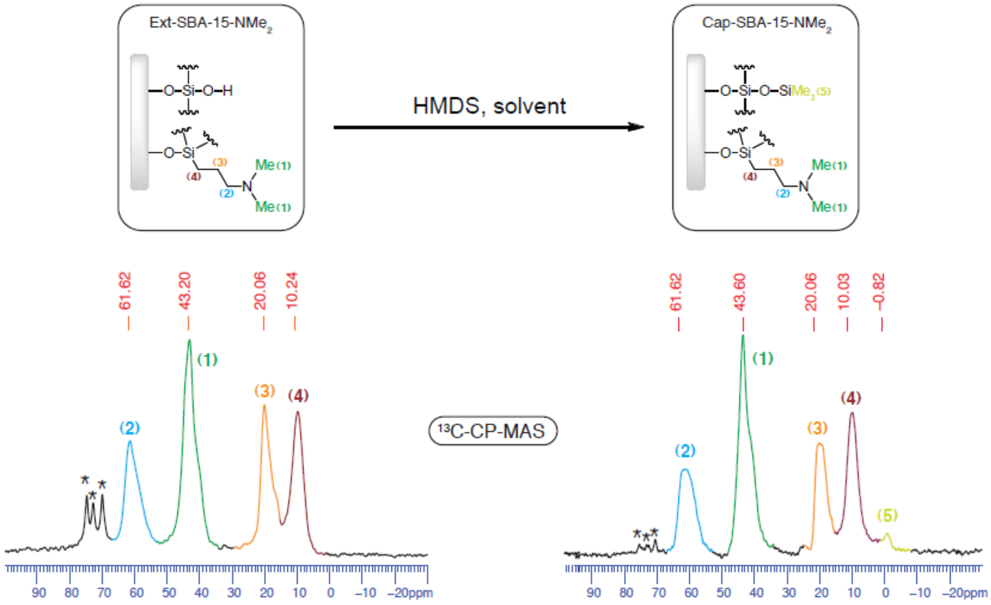

Figure 2.9: ^{13}C CP-MAS spectra and their peak assignments of Ext-SBA-15-NMe$_2$-IPA and Cap-SBA-15-NMe$_2$-IPA.

Based on these observations, it seems likely that because of the higher degree of grafting in toluene the number of free -Si-OH groups gets reduced resulting into lower number of free –Si-OH for capping whereas in case of grafting in IPA, the relative number of -Si-OH sites have increased due to less-grafting.[24] As a result, the latter material gets more capped by the treatment of HMDS and shows –O-SiMe$_3$ peak in its ^{13}C-CP-MAS spectrum. Our effort to characterize this further using ^{29}Si-CP-MAS and ^{29}Si-1H-Decoupled offer satisfactory information regarding the Q(s) and T(s) states of the material but failed to identify the peaks for M state corresponding to the Si in -OSiMe$_3$ for Cap-SBA-15-NMe$_2$ under the same experimental condition because of low S/N ratio as well as lower number of capping sites.[34] Comparative studies of Ext-

SBA-15-NMe$_2$ and Cap-SBA-15-NMe$_2$ (obtained from the same batch of SBA-15) revealed that Ext-SBA-15-NMe$_2$ sample had higher % of T(s) states (see Figure 2.8). The amount of amine groups present in both catalysts was obtained using CHN elemental analysis (Table 2.2).

***Table 2.2*:** Elemental analysis of the catalyst and the control sample.

Entry	**Sample**	**C (%)**	**H (%)**	**N (%)**
1.	Ext-SBA-15-NMe$_2$	17.71	3.95	3.06
2.	Cap-SBA-15-NMe$_2$	17.53	3.78	3.07

2.2.2 Catalytic Activity of the Catalysts in Michael Addition Reaction

The catalytic activity of Ext-SBA-15-NMe$_2$-Tol and Cap-SBA-15-NMe$_2$-Tol was tested in the Michael addition reaction between *trans*-β-nitrostyrene and active methylene compounds at various temperatures (Scheme 2.6). In order to establish the dual effect of the amine catalyst and surface silanol groups towards this reaction, Cap-SBA-15-NMe$_2$-Tol, which does not have active residual (weak acid) groups in it, was used as a reference material. Though the effect was less prominent at higher temperatures, it was observed that the reaction was faster with Ext-SBA-15-NMe$_2$-Tol than with Cap-SBA-15-NMe$_2$-Tol. This was presumably because the surface silanol groups in the former aided in the H-bonding, which was absent in the later catalyst. In other words, the Si-OH groups in the former activated the nitro group of nitro-styrene, making it more electrophilic, so a facile addition of the nucleophile took place (Figure 2.10). This observation suggests that while activation of the nucleophile with basic groups is required for the reaction, a further rate acceleration can be achieved by activation of the electrophile via H-bonding. This effect is limited in Cap-SBA-15-NMe$_2$-Tol because this material does not have many free or accessible Si-OH groups as a result of its treatment with HMDS. The results of these experiments clearly showed that Ext-SBA-15-NMe$_2$-Tol, which was not treated with HMDS, could serve as an effective H-bond donor catalyst towards the conjugate addition of various active methylene compounds to *trans*-*β*-nitrostyrene.

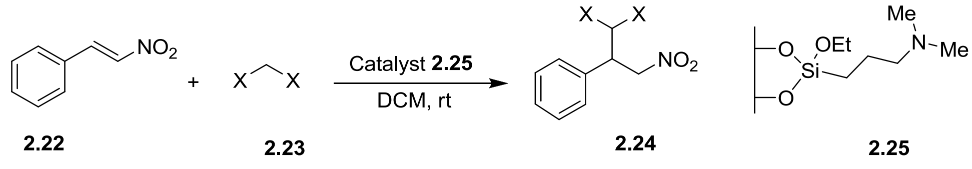
NO2
+
X X
Catalyst 2.25
DCM, rt
X X
NO2
O OEt
Si
O
Me
N
Me
2.22
2.23
2.24
2.25

X = CN, COCH$_3$, CO$_2$Et

Scheme 2.6: Michael addition reaction between *trans*-*β*-nitrostyrene and active methylene compounds.

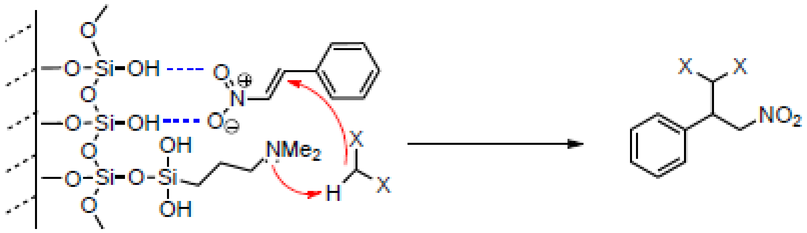
O-Si-OH
O
N
O
O-Si-OH
O
OH
NMe2
X
O-Si-O-Si
H
X
OH
X X
NO2

Figure 2.10: Proposed mechanism of dual activation involving H-bonding by acid/base bifunctional mesoporous catalysts in Michael addition reaction.

A kinetic study using variable temperature ^{1}H NMR-array technique was performed which closely matched with the results of the bench-top experiments. Because of smaller amount of catalyst employed in the former, this technique actually eliminated the risk of potential rate difference between NMR and bench-top experimental condition due to external influences (e.g. stirring) and allowed us to study the reactions at different temperatures in real time. In addition, based on our current results, this technique seems to be more reliable than (our) GC experimental results. Despite its apparent usefulness, such experiment for monitoring heterogeneous catalysis is, however, rarely performed, and this is one of the first examples that demonstrate the use of such method successfully for probing the catalytic activities of organoamine-functionalized mesoporous heterogeneous catalysts. The reaction was studied with three different active methylene compounds, which clearly showed the activity of Michael donor species (Table 2.3).

The solid catalyst with 3.42 mmol catalytic groups (calculated based on ~3 wt % or 2.14 mol/g of amine obtained from elemental analysis) was used for the reaction between 0.2 M nitrostyrene and 0.25 M active methylene compounds. The reaction with malononitrile and nitrostyrene was almost completed within 0.3 h at 0 °C in presence of the catalyst Ext-SBA-15-NMe$_2$-Tol (Figure 2.11) whereas the control experiment without the catalyst showed 80 % conversion in 1.5 h at room temperature (Figure 2.12).

Table 2.3: Catalytic activity of the supported catalyst used in Michael addition reaction.

Entry	Catalyst	X	Temp(°C)	Time(h)	Conv%	TOF(h^{-1})
1	**1**	CN	0	0.3	90	17142
2	**2**	CN	0	0.3	80	15238
3	**1**	COMe	50	3	85	1619
4	**2**	COMe	50	3	88	1676
5	**1**	CO_2Et	50	12	62	295
6	**2**	CO_2Et	50	-	-	-

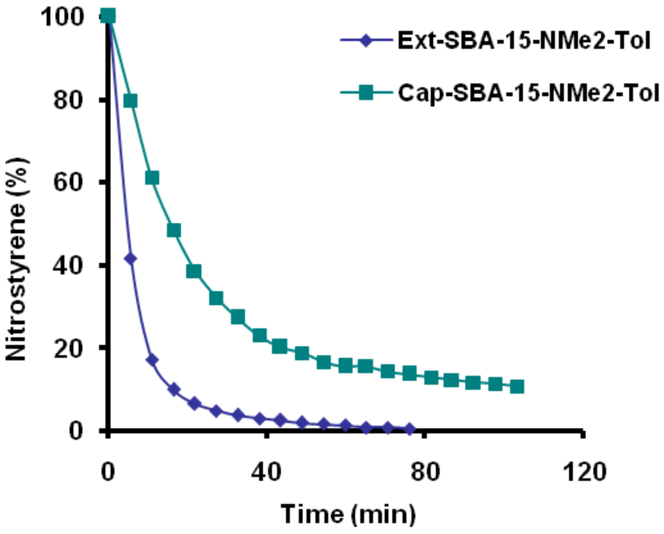

Figure 2.11: Percentage conversion of nitrostyrene versus reaction time in the Michael addition reaction between malononitrile and nitrostyrene catalyzed by Ext-SBA-15-NMe_2-Tol and Cap-SBA-15-NMe_2-Tol.

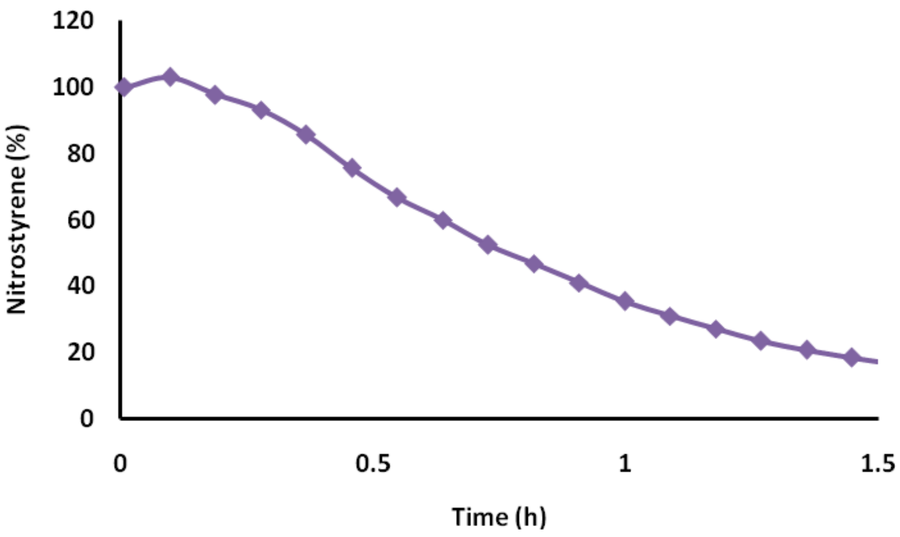

Figure 2.12**:** Kinetic plot of a controlled experiment (without a catalyst) involving the Michael addition reaction between nitrostyrene and malononitrile at room temperature.

Other reactions with acetylacetone and diethylmalonate reacted at much higher temperature (50 °C) yielding the desired products respectively (Figure 2.13). The trend in reactivity closely corresponds to the pK_a values of the respective substrates and can be explained by the ease of formation of the carbanion from the substrates. The relative acidity of active methylene compounds in DMSO follows the trend malononitrile (pKa = 11.1) > acetylacetone (pK_a 13.3) > diethylmalonate (pK_a 16.4).[35] Hence, in the presence of amine catalyst (base), the compound with lower pK_a showed greater propensity to form the carbanion (also the nucleophile). Consequently, the reaction between malononitrile and nitrostyrene showed faster reactivity, followed by acetylacetone, and finally diethylmalonate (Table 2.2).

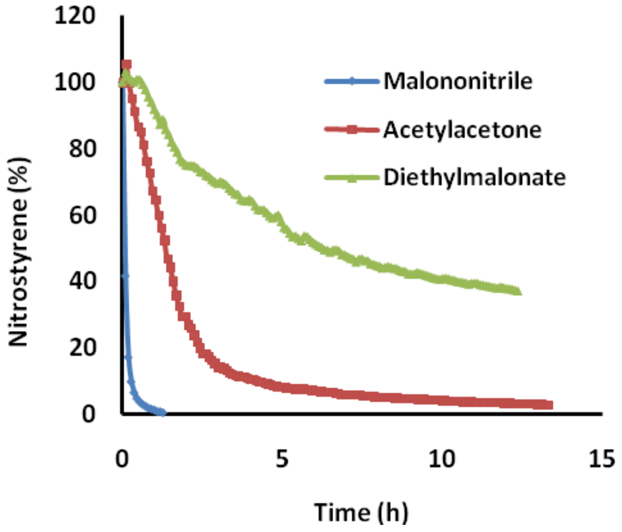

***Figure 2.13*:** Percentage conversion of nitrostyrene versus reaction time of Michael addition reaction between active methylene compounds and nitrostyrene catalyzed by Ext-SBA-15-NMe$_2$-Tol.

We further investigated the reaction in more detail with the catalysts Ext-SBA-15-NMe$_2$-IPA and Cap-SBA-15-NMe$_2$-IPA, whose *t*-amine groups were grafted in a more polar solvent, isopropanol. However, it is worth mentioning here that the choice of solvent is not arbitrary. Previously it was shown by our group that grafting aminosilanes on mesoporous silicas in polar solvents results in lesser amount of amine groups leaving more accessible silanol groups than the one in the more commonly used or the conventional non-polar solvent used for grafting, *i.e.*, toluene.[23, 24] In presence of Ext-SBA-15-NMe$_2$-IPA, the Michael addition between *trans*-β-nitrostyrene and malononitrile at 0 °C showed faster reactivity than its counterpart, which involved Ext-SBA-15-NMe$_2$-Tol as catalyst (Figure 2.14A). This diminishing catalytic efficiency in case of Ext-SBA-15-NMe$_2$-Tol can be attributed to the fewer silanol (weak acid) sites the material has for dual activation, but the possibility of catalyst aggregation resulting into densely populated organic groups in mesopores cannot be ruled out.[36] When comparing Ext-SBA-15-NMe$_2$-IPA with Cap-SBA-15-NMe$_2$-IPA, the latter showed lower catalytic activity, as expected, because of the lesser number of silanol groups present in it to activate the nitrostyrene (Figure 2.14B).

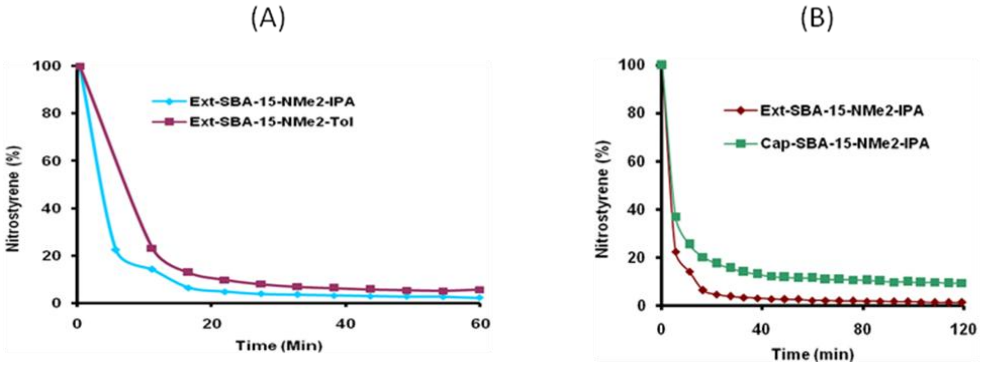

Figure 2.14**:** (A) Kinetic plot of the Michael addition reaction between nitrostyrene and malononitrile at 0 °C catalyzed by Ext-SBA-15-NMe$_2$-IPA and Ext-SBA-15-NMe$_2$-Tol. (B) Kinetic plot of the Michael addition reaction between nitrostyrene and malononitrile at 0 °C catalyzed by Ext-SBA-15-NMe$_2$-IPA and Cap-SBA-15- NMe$_2$-IPA.

These experiments signify the importance of silanol groups, or conversely spatially isolated amine groups, for dual catalysis. This study was further extended to other substrate and catalyst combination. For instance, comparative study of the catalytic activity of Ext-SBA-15-NMe_2-IPA and Ext-SBA-15-NMe_2-Tol was also performed for the substrate acetylacetone at 50 °C, and a similar trend was observed. The reaction was again faster with Ext-SBA-15-NMe_2-IPA compared with Ext-SBA-15-NMe_2-Tol (Figure 2.15). Finally, the substrate scope was studied with the catalyst Ext-SBA-15-NMe_2-IPA, which also showed similar trend as that obtained with Ext-SBA-15-NMe_2-Tol (Figure 2.16).

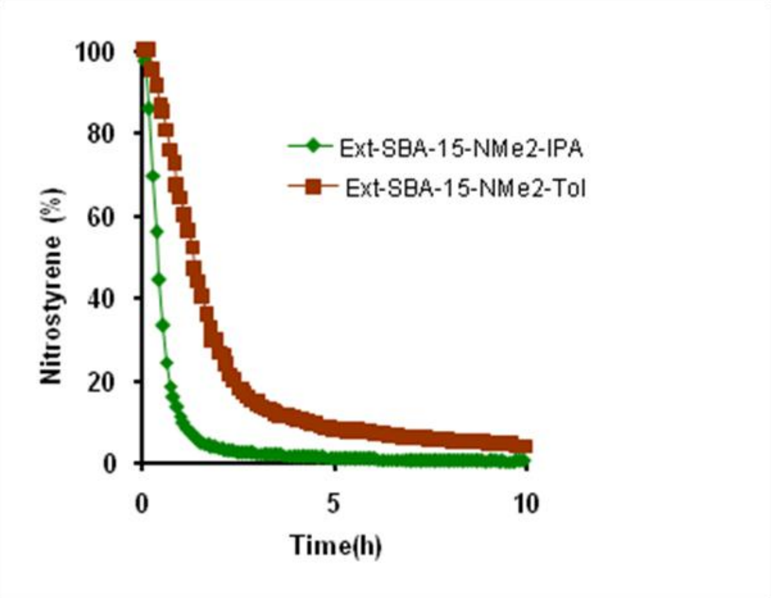

Figure 2.15**:** Kinetic plot of the Michael addition reaction between nitrostyrene and acetylacetone at 50 °C catalyzed by Ext-SBA-15-NMe_2-IPA and Ext-SBA-15-NMe_2-Tol.

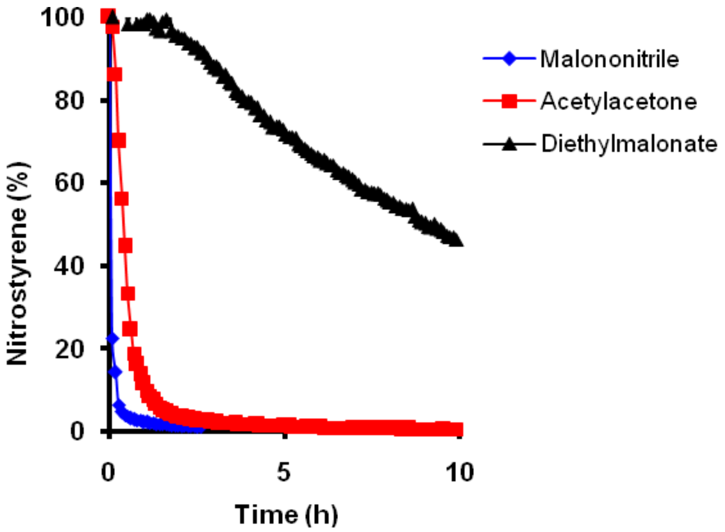

Figure 2.16**:** Kinetic plot of the Michael addition reaction between nitrostyrene and different active methylene compounds catalyzed by Ext-SBA-15-NMe$_2$-IPA.

Recyclability studies using such a small amount of catalyst (16 mg) was challenging under NMR kinetic condition mainly because of poor recovery of the catalyst at the end of the reaction after each cycle. In order to overcome these difficulties, a different approach was adopted. For the first recyclability studies, the reaction between nitrostyrene and acetylacetone was carried on a larger scale (4 times than used in the usual catalytic studies) on benchtop using Ext-SBA-15-NMe$_2$-Tol as catalysts at 50 °C. Once the reaction was complete, the catalyst was isolated by centrifugation, washed with dichloromethane and air-dried to use it for the next cycle. From the recovered catalyst, 16 mg was used for NMR kinetic studies, and the reaction was performed under the original catalytic condition. Rest of the catalyst was utilized for the same reaction but under benchtop condition, and the same procedure is repeated for the subsequent cycles.

As shown in Figure 2.17, the reaction between nitrostyrene and acetylacetone at 50 °C showed 85% conversion to the desired Michael product within 3 h. After second and third cycles of reactions, the reaction with the recycled catalyst gave 41% and 36% conversion after 4 and 5 h, respectively. The lower catalytic activity with the recycled catalysts can be attributed to the possibility of partial binding of product to catalytic surface (indirectly confirmed by the pale yellow color of the recovered catalyst), thereby decreasing the active catalytic sites as well as the amount of catalyst.

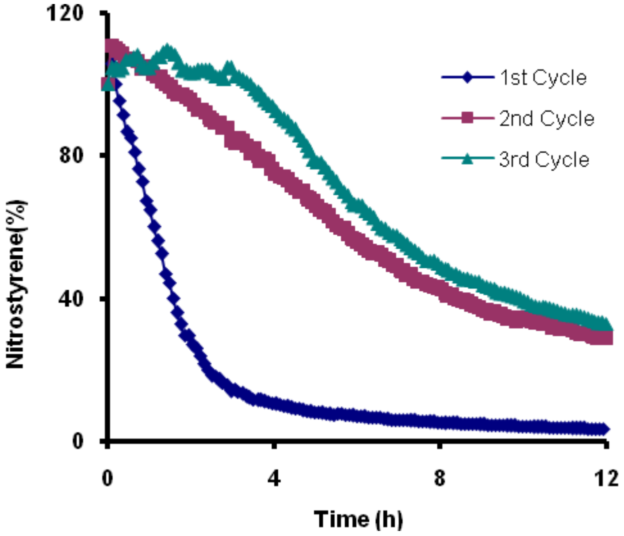

***Figure 2.17*:** Recyclability studies for the Michael addition reaction between nitrostyrene and acetylacetone catalyzed by Ext-SBA-15-NMe_2-Tol.

2.3 Summary

We have described the synthesis of efficient mesoporous nanocatalysts for Michael addition by postgrafting of organoamine groups on mesoporous silica.

The synthesis of these nanocatalysts was achieved by reacting organoaminesilanes with mesoporous silica in toluene and isopropanol. It was observed that the catalysts with tertiary amine and enough silanol (weak acid) groups in them exhibited cooperative catalytic properties, and thereby more efficient catalytic activities than the ones without silanol groups in them. Furthermore, the catalysts were investigated with different active methylene compounds as nucleophiles to study the scope of the catalytic reaction and the versatility of the catalysts. It was observed that the reaction was the fastest with malononitrile. Besides their high catalytic activity, the catalysts reported here have many advantages, including its ease of separation from reaction mixtures and greater shelf life.

Experimental Section

General Procedure for Preparation of Catalyst

Synthesis of Mesoporous (SBA-15) Material. SBA-15 was synthesized as reported previously by Zhao et al.[32b] and by using Pluronic P123 (average molecular mass ~5800 g/mol) as a templating agent in acidic solution. Typically, a solution of Pluronic P123 : 2 M HCl : TEOS : H_2O = 2 : 12 : 4.25 : 26 (mass ratio in g) was prepared and stirred at 40 °C for 24 h. The solution was then aged at 65 °C for another 24 h. The resulting solution was filtered, and the solid material was washed with copious amount of water, producing a material labelled as “as-synthesized mesostructured SBA-15”. Then, 4 g of the as-synthesized mesostructured SBA-15 was dissolved in ethanol (400 mL) and diethyl ether (400 mL) and stirred at 50 °C for 5 h to remove the templating agent. After filtration and washing with ethanol, the final solid material was dried in oven, giving mesoporous silica, SBA-15.

Synthesis of Tertiary Amine-Functionalized Mesoporous Silica, SBA-15. 500 mg of the dried mesoporous SBA-15 sample was stirred with excess 3-(N,N-Dimethylaminopropyl trimethoxysilane (DATS) (3.68 mmol, 1.5 mL) in 250 mL of anhydrous toluene or anhydrous isopropanol at 80 °C for 6 h. The solution was filtered, and the residue was washed with toluene (3 x 20 mL) or isopropanol, and then ethanol, and finally air-dried. The resulting dried samples, which contained tertiary amine catalytic groups and many residual silanol groups in them, were denoted as “Ext-SBA-15-NMe_2-Tol” and “Ext-SBA-15-NMe_2-IPA”, respectively. It is worth mentioning here that the relative ratios of the two groups in the two materials were, however, different.

To prepare a control sample containing the tertiary amine catalytic groups but no active residual silanol groups in it, 200 mg of the Ext-SBA-15-NMe_2-Tol or Ext-SBA-15-NMe_2-IPA was suspended in 11.5 mL of toluene and 1.5 mL of HMDS, and the solution was stirred for 6 h at room temperature to functionalize the external Si-OH groups of Ext-SBA15-NMe_2 with $–Si(CH_3)_3$. The solid sample was recovered by filtration, washed with toluene and ethanol, and then air dried. The resulting sample—SBA-15-NMe_2 with almost all of its accessible silanol groups capped with methyl groups—was denoted as “Cap-SBA-15-NMe_2-Tol” and “Cap-SBA-15-NMe_2-IPA”.

General Procedure for the Catalytic Reaction

The Michael addition reaction was performed both in reaction flasks as well as in NMR tubes. The latter allowed us to monitor the reaction progress and to reliably quantify the % conversion or yield of the reaction in real time at different temperatures. In a typical Michael addition experiment, a NMR tube was charged with either Ext-SBA-15-NMe_2 or Cap-SBA15-NMe_2 (16 mg), and dried at 80 °C for 30 min. The NMR spectrometer was set up at the desired temperature. Freshly prepared stock solution (in $CDCl_3$) of *trans-β*-nitrostyrene (1 eq., 0.2 M in NMR tube) and the corresponding active methylene compound (1.25 eq., 0.25 M in NMR tube) in $CDCl_3$ (total volume of 0.6 mL) were added to the NMR tube, capped (sealed with parafilm) and shaken well. For an experiment at 0 °C, this addition was performed in an ice-bath and transferred quickly to the spectrometer. The tube was inserted into the spectrometer and the reaction was monitored by following the rate of disappearance of olefinic proton peaks of the starting materials in ^{1}H NMR.

Reference:

(1) Michael, A. *J. Praktische Chemie*. **1894**, 49, 20.
(2) Michael, A. *J. Praktische Chemie*. **1887**, 35, 349.
(3) Tsogoeva, S. B. *Eur. J. Org. Chem.* **2007**, 2007, 1701.
(4) Hanessian, S.; Pham, V. *Org. Lett.* **2000**, 2, 2975.
(5) Palomo, C.; Vera, S.; Mielgo, A.; Gómez-Bengoa, E.; *Angew. Chem. Int. Ed.* **2006**, 45, 5984.
(6) Sarkar, D.; Bhattarai, R.; Headley, A. D.; Ni, B. *Synthesis.* **2011**, 1993.
(7) Tsogoeva, S. B.; Yalalov, D. A;. Hateley, M. J.; Weckbecker, C.; Huthmacher, K. *Eur. J. Org. Chem.* **2005**, 2005, 4995.
(8) Huang, H.; Jacobsen, E. N. *J. Am. Chem. Soc.* **2006**, 128, 7170.
(9) Lalonde, M. P.; Chen, Y.; Jacobsen, E. N. *Angew. Chem.* **2006**, 118, 6514.
(10) Cao, C.-L.; Ye, M.-C.; Sun, X.-L.; Tang, Y. *Org. Lett.* **2006**, 8, 2901.
(11) Okino, T.; Hoashi, Y.; Furukawa, T.; Xu, X.; Takemoto, Y. *J. Am. Chem. Soc.* **2004**, 127, 119.
(12) Malerich, J. P.; Hagihara, K.; Rawal, V. H. *J. Am. Chem. Soc.* **2008**, 130, 14416.
(13) Peng, F. Z.; Shao, Z. H.; Fan, B. M.; Song, H.; Li, G. P.; Zhang, H. B., *J. Org. Chem.* **2008,** 73, 5202.
(14) Mdoe, J. E. G.; Clark, J. H.; Macquarrie, D. J. *Synlett.* **1998**, 625,627.
15. Macquarrie, D. J.; Maggi, R.; Mazzacani, A.; Sartori, G.; Sartorio, R. *Appl. Catal. A.* **2003**, 246, 183.
(16) Wang, X.; Lin, K. S. K.; Chan, J. C. C.; Cheng, S. *J. Phys. Chem. B.* **2005**, 109, 1763.
(17) Bensa, D.; Constantieux, T.; Rodriguez, J. *Synthesis.* **2004**, 2004, 923, 927.
(18) Eisch, J. J.; Gadek, F. J.; Gupta, G. *J. Org. Chem.* **1973**, 38, 431.
(19) Miller, D. D.; Moorthy, K. B.; Hamada, A. *Tetrahedron Lett.* **1983**, 24, 555.
(20) Clark, J. H.; Cork, D. G.; Robertson, M. S. *Chem. Lett.* **1983**, 12, 1145.
(21) Laszlo, P.; Pennetreau, P. *Tetrahedron Letters.* **1985**, 26, 2645.
(22) Ballini, R.; Marziali, P.; Mozzicafreddo, A. *J. Org. Chem.* **1996**, 61, 3209.
(23) Sharma, K. K.; Asefa, T. *Angew. Chem. Int. Ed.* **2007**, 46, 2879.
(24) Sharma, K. K.; Anan, A.; Buckley, R. P.; Ouellette, W.; Asefa, T. *J. Am. Chem. Soc.* **2007**, 130, 218.
(25) Notestein, J. M.; Katz, A. *Chem. Eur. J.* **2006**, 12, 3954.
(26) Breslow, R.; Graff, A. *J. Am. Chem. Soc.* **1993**, 115, 10988.
(27) Huh, S.; Chen, H.-T.; Wiench, J. W.; Pruski, M.; Lin, V. S. Y. *Angew. Chem. Int. Ed.* **2005**, 44, 1826.
(28) Motokura, K.; Tada, M.; Iwasawa, Y. *Angew. Chem. Int. Ed.* **2008**, 47, 9230.
(29) Bass, J. D.; Solovyov, A.; Pascall, A. J.; Katz, A. *J. Am. Chem. Soc.* **2006,** 128, (11), 3737-3747.

(30) Motokura, K.; Tada, M.; Iwasawa, Y., Heterogeneous Organic Base-Catalyzed Reactions Enhanced by Acid Supports. *J. Am. Chem. Soc.* **2007**, 129, 9540.

(31) Margelefsky, E. L.; Zeidan, R. K.; Davis, M. E. *Chem. Soc. Rev.* **2008**, 37, 1118.

(32) (a)Margolese, D.; Melero, J. A.; Christiansen, S. C.; Chmelka, B. F.; Stucky, G. D. *Chem. Mater.* **2000**, 12, 2448.(b) D.Y. Zhao, J. L. Feng, Q, S. Huo, N. Melosh, G. H. Fredrickson, B. F. Chmelka, G. D. Stucky, *Science*. **1998**, *279*, 548-552.

(33) Xie, Y.; Quinlivan, S.; Asefa, T. *J. Phys. Chem. C.* **2008**, 112, 9996.

(34) Suratwala, T. I.; Hanna, M. L.; Miller, E. L.; Whitman, P. K.; Thomas, I. M.; Ehrmann, P. R.; Maxwell, R. S.; Burnham, A. K. *J. Non-Cryst. Solids.* **2003**, 316, 349.

(35) Matthews, W. S.; Bares, J. E.; Bartmess, J. E.; Bordwell, F. G.; Cornforth, F. J.; Drucker, G. E.; Margolin, Z.; McCallum, R. J.; McCollum, G. J.; Vanier, N. R. *J. Am. Chem. Soc.* **1975**, 97, 7006.

(36) McKittrick, M. W.; Jones, C. W. *J. Am. Chem. Soc.* **2004**, 126, 3052.

Chapter III

Ring Opening of Epoxides with Mesoporous Silica Supported Fe(III) Catalysts

3.1 Introduction

Epoxide is cyclic ether with a three membered ring. In organic synthesis, epoxides are invaluable building blocks for introduction of diverse functionalities into a hydrocarbon backbone in a 1,2-fashion.[1-3] The strain of the epoxide makes it much more reactive than the cyclic ether, as a result epoxides can be ring opened easily. Ring opening of epoxides with nucleophiles is an important route to achieve compounds with versatile 1,2-type functional groups, including β-alkoxyalcohols.[3-5] β-Alkoxyalcohols, in turn, are an important class of organic compounds and precursors for a broad range of pharmaceuticals.[6-13] The general procedure for β-alkoxyalcohols synthesis is via alcoholysis[4] involving ring-opening of epoxides with alcohols, which usually requires acid or base catalysts. For instance, the ring-opening of styrene oxide with water or alkyl alcohols in the presence of acidic catalyst produces 1-phenyl-1,2-ethanediol and 2-alkoxy-2-phenylethanol, respectively.[14-16] These compounds, in turn, are useful precursors for pharmaceuticals such as mandelic acids, which are antibacterial agents and oral antibiotics and also useful intermediates for the synthesis of β-lactam antibiotics.[9-12]

3.1.1 Ring Opening of Epoxides with Metal Complexes

Due to their ring strain (having a high thermodynamic driving force, usually greater than 20 kcal/mol),[17] the reactivity of the epoxides by ring-opening can be enhanced by using a Lewis acid coordinating the oxygen atom. Ring-opening of epoxides can be achieved with various nucleophiles in the presence of many metal complexes composed of transition and rare earth metals. Oliverio *et al.*[18] has studied the ring opening of epoxides with trimethylsilyl azide and cyanide under neutral conditions in presence of erbium(III) triflate which acts as a Lewis acid catalyst, affording the corresponding ring opened products in high yields. Singh and coworkers[19] studied the ring opening with different amines catalyzed by $Cu(OTf)_2$ and $Sn(OTf)_2$. The worthy feature of the reaction is that highly deactivated amines such as *p*-nitroaniline also opened the epoxides in a reasonable yield. Although the isolated yield in the epoxide opening reaction with aromatic amines catalyzed by $Cu(OTf)_2$ and $Sn(OTf)_2$ is comparable, the reaction was faster with the latter catalyst. Kühn and coworkers[20] studied the ring opening reactions of epoxides with aromatic/aliphatic amines efficiently catalyzed by nitrile ligated aluminum-based Lewis acids under solvent-free conditions at room temperature, affording 2-amino alcohols in high yields (up to 99%) within 4 h.

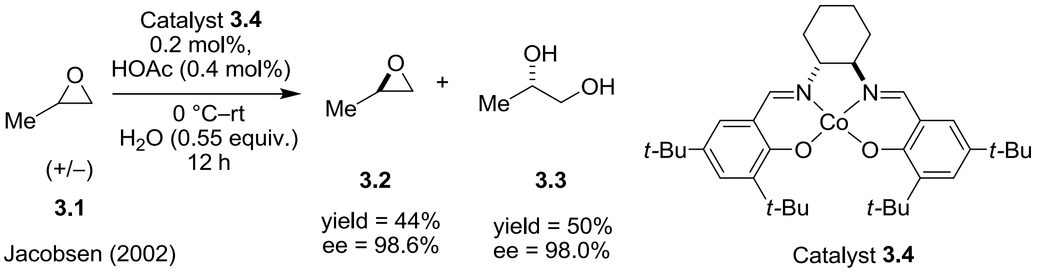

Scheme 3.1**:** Hydrolytic kinetic resolution catalyzed by Co-salen complex.

Jacobsen and coworkes[21] discovered that (salen)Co complex catalyzed the efficient hydrolytic kinetic resolution (HKR) of a variety of terminal epoxides affording both recovered unreacted epoxide and 1,2-diol product in highly enantioenriched form. Xia and coworkers[22] also demonstrated that the nucleophilic opening of epoxide rings by amines leading to the efficient synthesis of β-amino alcohols can be catalyzed by transition metal-based Lewis acids, such as $SnCl_4{\cdot}5H_2O$, $Co(OAc)_2{\cdot}4H_2O$, $Ni(OAc)_2{\cdot}2H_2O$, $NiCl_2$, $Mn(OAc)_2{\cdot}4H_2O$ etc under solvent free condition.

3.1.2 Heterogenous Ring Opening of Epoxides

The high cost and the toxicity associated with many of the previously reported metal complex catalysts for epoxide ring opening reactions have necessitated an increased interest in immobilizing the metal complexes onto solid support materials to generate their heterogeneous forms. There are many examples of heterogenous catalysis of ring opening of epoxides are reported. Recently, Otani *et al.*[23] have reported the synthesis of a novel chiral porous metal–organic framework (R)-3 and its application to the asymmetric catalyst for asymmetric ring opening reaction of epoxide with amine under heterogeneous conditions. Nano-TiO_2 also is an effective heterogeneous catalyst for the ring opening of epoxides with aromatic amines to afford β-amino alcohols in good to excellent yields at room temperature under solvent-free conditions.[24] It is well known that there are many Lewis acidic sites (Ti^+) on the surface of TiO_2, which may activate the epoxide through the weak interaction with the oxygen atom of the epoxide. Tondello *et al*.[25] demonstrated the catalytic activity of zirconium incorporated mesoporous silica for the methanolysis of styrene oxide in a single-mode microwave reactor. Motlagh *et al*.[26] demonstrated that aliphatic alcohols and water in the presence of catalytic amounts of Fe^{3+} ion introduced as iron(III) perchlorate on silica gel carrier perform efficient regiospecific opening of an epoxy ring with aliphatic alcohols and water. Lee *et al*.[27] demonstrated polymer-supported metal (Fe or Ru) complexes for epoxide ring opening reactions which can be successfully prepared by anchoring the bis(2-picolyl)amine ligand onto the polymer poly(chloromethylstyrene-co-divinylbenzene) (PCD); the catalysts showed heterogeneous catalytic activity and easy recyclability in the ring opening reactions of various epoxide substrates with methanol or H_2O at room temperature under mild and neutral conditions. Lee et al.[28] synthesized a novel Fe mono(terpyridine) complex by choosing the polymer surface anchored terpyridine as a chelating ligand and it showed an excellent catalytic activity with an easy reusability on the ring-opening reaction of various epoxides by alcohol and water under mild and neutral conditions to give stereospecific and regioselective products. Garcia and coworkers[29] studied an iron-based metal–organic framework, [Fe(BTC)] (BTC: 1,3,5-benzenetricarboxylate) as an efficient catalyst in the ring opening of styrene oxide with alcohols and aniline under mild reaction conditions. [Fe(BTC)] was a truly heterogeneous catalyst and could be reused without loss of activity. The analogous compound [$Cu_3(BTC)_2$] was also found to be effective, although with somewhat lower activity than [Fe(BTC)].

3.2 General Consideration and Concept

As discussed above the ring opening of epoxide can be achieved in the presence of many metal complexes acting as Lewis acid**.** However, many of these metals have high toxicity, are less abundant, or both. In contrast, iron is one of the most inexpensive, most abundant, and more environmentally friendly transition metals.[30] Moreover, many iron salts and complexes are commercially available[31] or reported in the literature.[32] Our goal was to develop an iron-containing SBA-15 type mesoporous silica catalyst, in which Fe(III) is coordinated to organoamine groups grafted onto the surface of the mesoporous silica (SBA-15) and its catalytic activity in the alcoholysis or hydrolysis of various epoxides. The organoamine group in this case is ethylenediamine which served as a bidentate ligand for coordinating to Fe(III). Traditionally Epoxides can be ring-opened by various nucleophiles under acidic, basic, or neutral conditions.[21, 33-35] However, in some cases, the ring-opening of epoxides such as styrene oxide with methanol to achieve the alcoholysis products under basic or acidic conditions results in polymerization and low regioselectivity at high temperatures.[36] In our case, mild reaction conditions would be used to give high regioselectivity.

3.2.1 Synthesis of Immobilized Fe(III) Catalyst on SBA-15

The synthesis of the catalyst consists of three steps. First our parent material, mesoporous silica was synthesized (in this case it is SBA-15) and it was grafted with ethylenediamine to act as the bidentate ligand and finally Fe(III) was coordinated to the bidentate ligand. The synthesis of SBA-15 functionalized with organoamine groups was achieved by stirring surfactant-extracted Ext-SBA-15 with an excess amount of N-(2-aminoethyl)-3-aminopropyltrimethoxysilane in toluene at 80 °C for 6 h. This produced an ethylenediamine-functionalized mesoporous silica sample or Ext-SBA-15-en. Then the Ext-SBA-15-en was stirred with iron(III) nitrate nonahydrate to obtain the desired iron catalyst, which was denoted as Ext-SBA-15-en-Fe(III) (Scheme 3.2).

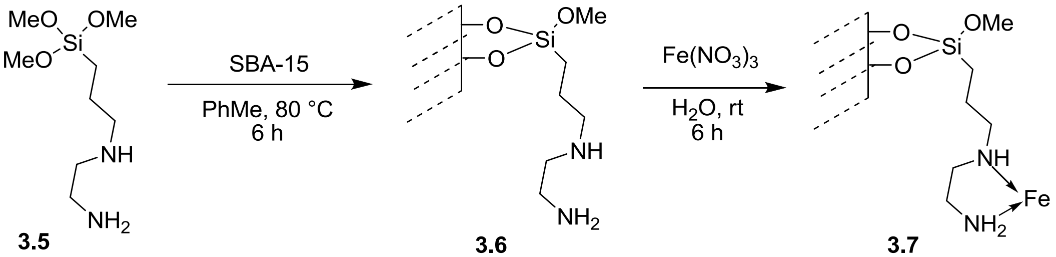

Scheme 3.2**:** Synthesis of Ext-SBA-15-en-Fe(III).

The catalyst (Ext-SBA-15-en-Fe(III)) and the parent materials (Ext-SBA-15 and Ext-SBA-15-en) were characterized by N_2 gas adsorption measurement

(Figure 3.1). The N_2 gas adsorption measurements showed a type IV isotherm that is characteristic of mesoporous materials for all the three samples (Figure 1A). Their BJH pore size distributions showed that the materials had monodisperse pore sizes (Figure 1B). Furthermore, the BET surface areas of Ext-SBA-15, Ext-SBA-15-en, and Ext-SBA-15-en-Fe(III) were 470, 204, and 194 m^2/g, respectively. These results indicated that the surface area of the SBA-15 material decreased in the presence of organic groups in the mesopores of the material. N-(2-Aminoethyl)-3-aminopropyl groups are rather bulkier and thus take up a significant portion of the void space of the mesopores.

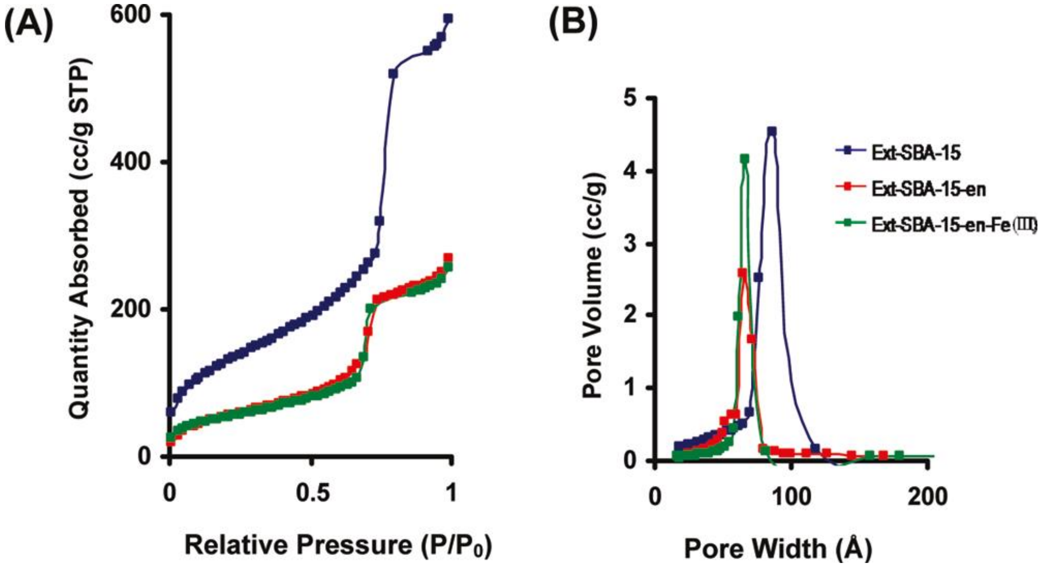

***Figure 3.1*:** Nitrogen gas adsorption isotherms and pore size distribution of the parent mesoporous material and the catalyst, ExtSBA-15-en-Fe(III).

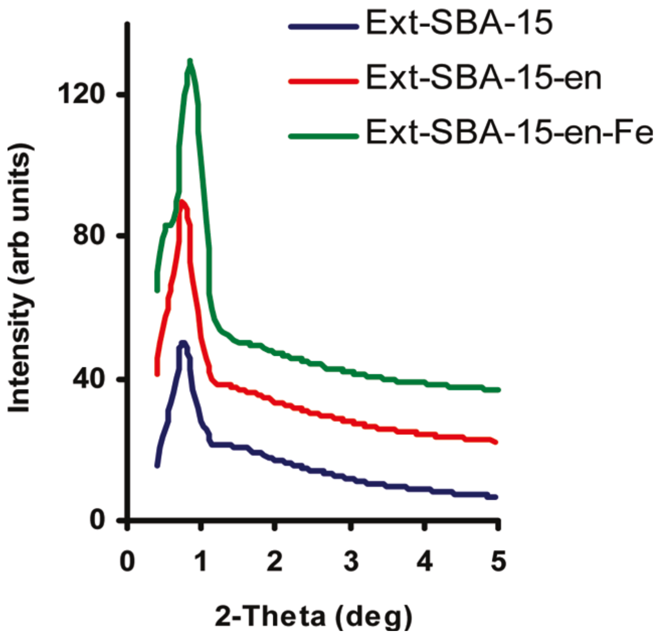

Figure 3.2**:** XRD patterns of Ext-SBA-15, Ext-SBA-15-en and Ext-SBA-15-en-Fe.

The mesoporous materials, both before and after postgrafting, were also characterized by powder X-ray diffraction (XRD) (Figure 3.2) and TEM (Figure 3.3). The XRD patterns of all the samples showed sharp peaks corresponding to the (100) Bragg reflection, indicating that the materials possessed hexagonally ordered mesostructures. Furthermore, the result suggested that the ordered SBA-15 mesostructure remained intact, even after postgrafting it with the organoamines or organoamine Fe(III) complexes. The (100) peaks were indexed and gave unit cell sizes of ~12-13 nm.

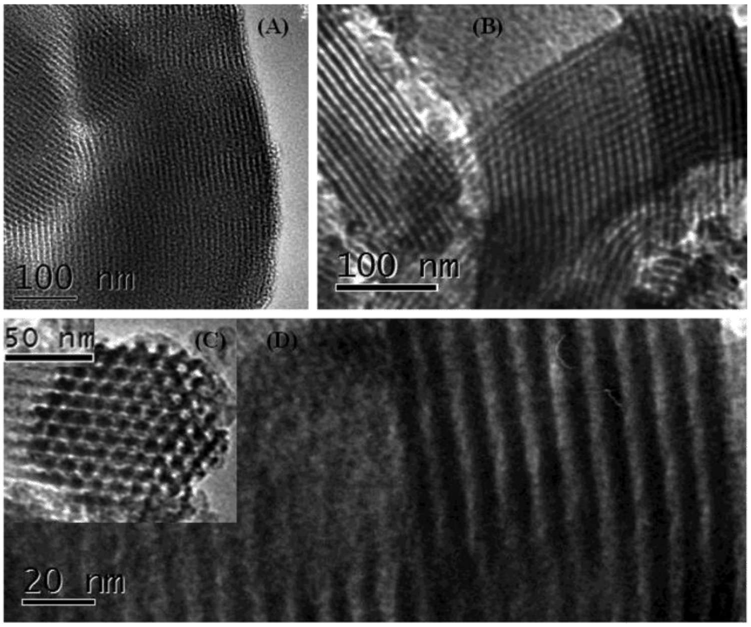

Figure 3.3**:** (A) TEM image of Ext-SBA-15 and (B-D) TEM image of Ext-SBA-15-en-Fe(III) catalysts.

The TEM images of the samples before and after postgrafting also revealed the presence of ordered mesostructures in the materials (Figure 3.3). Thus, except for the pore size reduction, the monodispersity and mesoporosity of the pores remained unchanged after immobilization of organoamine and organoamine Fe(III) complexes within the pores of the materials.

The materials were also characterized by thermogravimetric analysis. The thermogravimetric traces (Figure 3.4) indicated a weight loss below 100 °C for all the samples due to loss of water adsorbed on the materials. The weight loss in Ext-SBA-15-en in the range 100-450 °C could be due mainly to the loss of organoamine groups. The amount of amine or organodiamine groups in the fresh catalyst was obtained by CHN elemental analysis, which gave C (10.72%), H (1.75%), and N (6.17%).

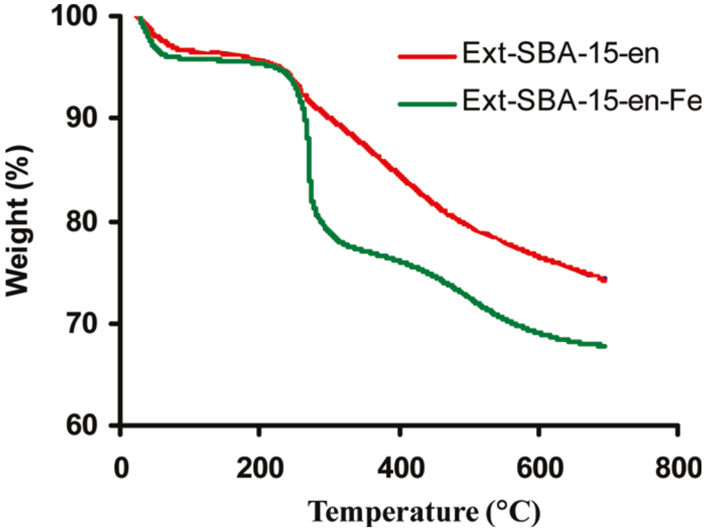

Figure 3.4**:** Thermogravimetric traces of Ext-SBA-15-en and Ext-SBA-15-en-Fe.

3.2.2 Catalytic Activity of Ext-SBA-15-en-Fe(III) in Ring Opening of Epoxides

The catalytic properties of Ext-SBA-15-en-Fe(III) in epoxide ring-opening reactions were evaluated using the reaction between styrene oxide and water or different alcohols including primary, secondary, and tertiary alcohols (Scheme 3.3) at room temperature or at an elevated temperature of 80 °C.

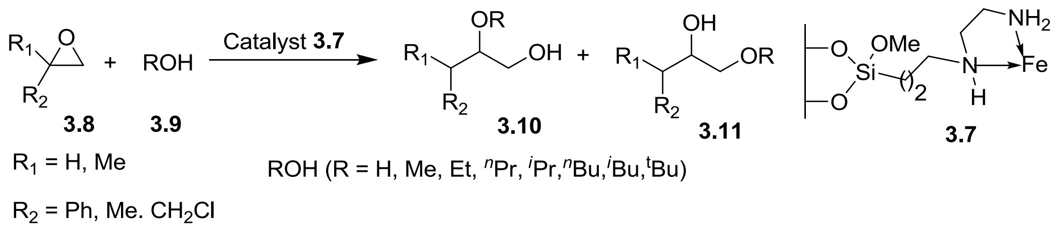

Scheme 3.3**:** Ring opening of epoxides using Ext-SBA-15-en-Fe(III) catalyst.

The rate of the reaction varied depending on the type of reactant used. Water was found to ring open styrene oxide the fastest, giving ~100% 1-phenyl-1,2-ethanediol in 2 h. The rates of the reactions with alcohols varied significantly depending on their structures. Methanol gave a yield of 100% 2-methoxy-2-phenylethanol in 6 h at room temperature. Styrene oxide also reacted with ethanol at room temperature, but took a slightly longer time of 9 h compared with methanol to give ~100% yield of 2-ethoxy-2-phenylethanol. Similarly propyl alcohol reacted with styrene oxide to give a 93% yield of the corresponding product, but only after a longer reaction time of 45 h. Isopropyl alcohol gave even a much lower yield after longer reaction times in comparison with methanol, ethanol, and propyl alcohol (Table 3.1). The decrease in the rates of the reactions became even more pronounced when butyl alcohol, isobutyl alcohol, and tert-butyl alcohol were used as nucleophiles. Butyl alcohol gave a yield of 96% in 56 h at 80 °C, whereas isobutyl alcohol and *tert*-butyl alcohol gave a yield of 62% and 9%, respectively, when the reaction was run for 6 days (144 h) at 80 °C. The difference in reactivity may due to the steric hindrance imparted by the alcohols when going from primary to secondary to tertiary.

Table 3.1: Ring opening of epoxides using Ext-SBA-15-en-Fe(III) catalyst.

Entry	**Alcohol**	**Temp (°C)**	**Time (h)**	**Yield (%)**	**TOF (h^{-1})**
1	H_2O	RT	2	~ 100	157343
2	MeOH	RT	6	~ 100	52448
3	EtOH	RT	9	~ 100	34965
4	*n*PrOH	80	45	93	6503
5	*i*PrOH	80	72	50	2185
6	*n*BuOH	80	56	96	5395
7	*i*BuOH	80	144 (6days)	62	1355
8	*t*BuOH	80	144 (6days)	9	197

3.2.3 Control Experiments

Some control experiments were performed to evaluate the catalytic property of the catalysts. A control reaction between styrene oxide and MeOH at room temperature with no catalyst or mesoporous material in the reaction solution gave no reaction product in 48 h. Similarly, the control experiment of attempted ring-opening reactions of styrene oxide using Ext-SBA-15 containing no Fe(III) also gave no product (Table 3.2). Even the material, Ext-SBA-15-Fe, which contained no ethylenediamine but was stirred with Fe(III) solution, gave no reaction product in the reaction mixture of styrene oxide and MeOH at room temperature in 48 h-reaction time. Furthermore, it gave 11% yield of 2-methoxy-2-phenylethanol product only after 96 h-reaction time. This clearly showed that the reaction was catalyzed by Fe(III). Furthermore, it indicated the importance of a ligand such as organoamine in the material to anchor Fe(III) better and to produce an efficient catalyst.

Table 3.2**:** Control experiments of attempted ring-opening reactions of styrene oxide using Ext-SBA-15 containing no Fe(III) or Ext-SBA-15-Fe(III) containing no ethylenediamine, but stirred with Fe(III) solution.

Entry	Catalyst	Reactant	Time (h)	Yield (%)
1	Ext-SBA-15	MeOH	48	NR
2	Ext-SBA-15-Fe	MeOH	48	NR
3	Ext-SBA-15-Fe	MeOH	86	11.31

In addition to the solvent extracted SBA-15 mesoporous silica, a calcined SBA-15, whose P123 polymer templates were removed by calcination, was used for the preparation of the Fe(III) catalyst, Cal-SBA-15-en-Fe(III). The latter showed less catalytic efficiency than the corresponding catalyst made from the solvent extracted Ext-SBA-15 (Table 3.3). The two catalysts Cal-SBA-15-en-Fe and Ext-SBA-15-en-Fe were prepared from the same batch of mesostructured SBA-15 but by using calcinations or solvent-extraction, respectively, to remove their P123 polymer templates. The calcination to remove the polymer template was performed by heating the sample in air in tube furnace at 600 °C for 5h. This was then grafted with diamineorganosilane and then stirred in Fe(III) under the same procedure as in the Experimental Section. The catalyst Ext-SBA-15-en-Fe showed better efficiency than Cal-SBA-15-en-Fe. This is possibly because the former sample had higher density of Fe(III) anchored per given gm of sample, which was proved by the UV-Vis of the filtrate obtained after the complexation reaction of the grafted diamines with Fe(III) (Figure 3.5). The absorbance intensity in case of Cal-SBA-15 is more than Ext-SBA-15 which signifies the presence of more uncomplexed Fe(III) in the solution. This in turn is due to the presence of more silanols and ethylene diamine in the solvent-extracted SBA-15 than Calcined SBA-15 sample.

Table 3.3: Comparative catalytic results of two SBA-15-en-Fe(III) catalysts prepared from a calcined SBA-15 (Cal-SBA-15) and a solvent extracted SBA-15 (Ext-SBA-15) under the same conditions.

Entry	**Catalyst**	**Surface Area (m^2/g)**	**Pore Volume (cc/g STP)**	**Time (h)**	**Yield (%)**
1	Calc-SBA-15-en-Fe	225	0.99	2	~0
2	Ext-SBA-15-en-Fe	164	0.81	2	8.1
3	Calc-SBA-15-en-Fe	225	0.99	5	39.8
4	Ext-SBA-15-en-Fe	164	0.81	5	~100

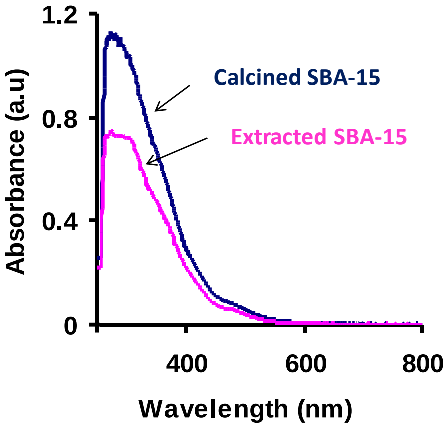

Figure 3.5: UV-Vis spectra of Fe(III) solution in the filtrate obtained after mixing Ext-SBA-15 and Cal-SBA-15 with aqueous Fe(III) solution.

3.2.4 Effect of Temperature

The effect of temperature on the epoxide ring-opening catalytic reaction was studied by using the reaction between styrene oxide and propyl alcohol. The reaction was done at RT and 40, 60, and 80 °C, and the reaction yield after 24 h was monitored by GC. The results are summarized in Table 4. It was observed that the rate of the reaction increased with increasing temperature. For example, at room temperature there was no formation of product after 24 h. When the temperature was slightly increased to 40 °C, the yield was 3.2% after 24 h. But, when the reaction temperatures were increased to 60 and 80 °C, a moderate yield of 43.9%and a good yield of 97.6%, respectively, were obtained after 24 h.

***Table 3.4*:** Temperature dependence study of ring-opening of styrene oxide with propyl alcohol using Ext-SBA-15-en-Fe(III) catalyst.

Entry	**Temp (°C)**	**Time (h)**	**Yield (%)**
1	RT	24	0
2	40	24	3.2
3	60	24	43.9
4	80	24	97.6

3.2.5 Scope of the Reaction

The scope of the reaction was explored under the optimized conditions. The catalyst can ring open other epoxides, such as chloropropylene oxide and 2-methyl-1,2-epoxypropane (Figure 3.6). The chloropropylene oxide was found to react much more slowly than the 2-methyl-1,2-epoxypropane, whereas the 2-methyl-1,2-epoxypropane underwent catalytic reaction more slowly than styrene oxide under the same reaction conditions. Furthermore, the regioselectivity of the products was found to vary depending on the type of the reactant. While the ring-opening reaction between styrene oxide or 2-methyl-1,2-epoxypropane and MeOH with Ext-SBA-15-en-Fe(III) catalyst gave the corresponding less-substituted alcohol regioisomers, the reaction between chloropropylene oxide and MeOH resulted in the more-substituted alcohol regioisomer product. These differences in reactivity as well as regioselectivity can be attributed to the relative steric and electronic differences among the reactants, which affect the reaction mechanism.

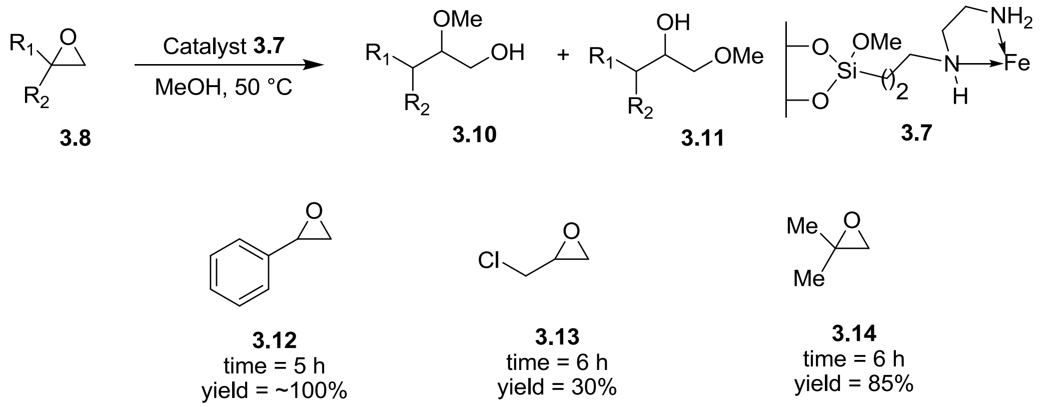

3.8 **3.10** **3.11** **3.7**

3.12
time = 5 h
yield = ~100%

3.13
time = 6 h
yield = 30%

3.14
time = 6 h
yield = 85%

***Figure 3.6*:** Scope of catalytic activity of the Ext-SBA-15-en-Fe(III) catalyst in the ring-opening of different substituted epoxide with MeOH.

3.2.6 Recyclability of the Catalyst

The Ext-SBA-15-en-Fe(III) mesoporous silica catalyst was shown to be easily recyclable at least five times. Upon completion of the reaction, the catalyst was recovered from the reaction mixture by simple filtration, washed with the corresponding alcohol and was then used in the next reaction run. The fresh catalyst as well as the recycled catalysts (after recycling one, two, three, four, and five times) gave ~100% conversion for the reaction between styrene oxide and MeOH in 5 h at 50 °C (Table 3.5).

Table 3.5**:** Test of recyclability of the catalyst using ring-opening of styrene oxide by MeOH using Ext-SBA-15-en-Fe(III) catalyst.

Entry	**Time (h)**	**Temp (°C)**	**Yield (%)**
1st run	5	50	~ 100
2nd run	5	50	~ 100
3rd run	5	50	~ 100
4th run	5	50	~ 100
5th run	5	50	~ 100

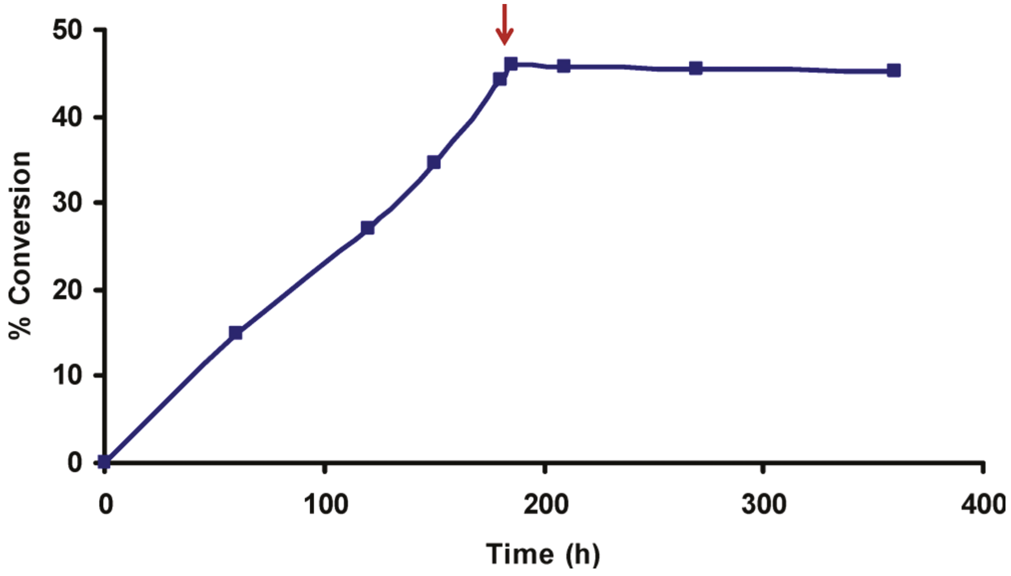

Figure 3.7**:** Kinetic plot of leaching experiment, representing the % conversion of styrene oxide to time. The brown arrow indicates the time where the catalyst was filtered off and the supernatant was run by itself.

A hot-filtration based leaching test was also performed to determine if iron(III) leached from the catalyst into the reaction mixture and possibly participated in the catalytic reaction. The catalyst was centrifuged and separated from the reaction mixture, and the supernatant was further run by itself. There was almost no further conversion of styrene oxide, even after 3 h reaction time (Figure 3.7) when the supernatant was stirred by itself after removing the catalyst from it. The structure of the material also remained intact even after the material was used as catalyst in catalytic reactions multiple times, as confirmed by powder X-ray diffraction patterns (Figure 3.8) and TEM images (Figure 3.9). The XRD patterns show that the degree of order of the mesostructure remained reasonably unchanged after catalytic reactions. On the basis of our recyclability and leaching tests, our Ext-SBA-15-en-Fe(III) catalyst was shown to be “truly heterogenous”.

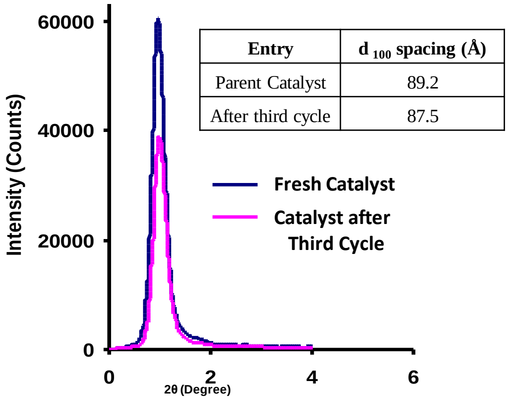

Entry	d_{100} spacing (Å)
Parent Catalyst	89.2
After third cycle	87.5

Figure 3.8: Powder X-ray diffraction (XRD) patterns of a fresh Ext-SBA-15-en-Fe catalyst and after being used for catalysis in three cycles.

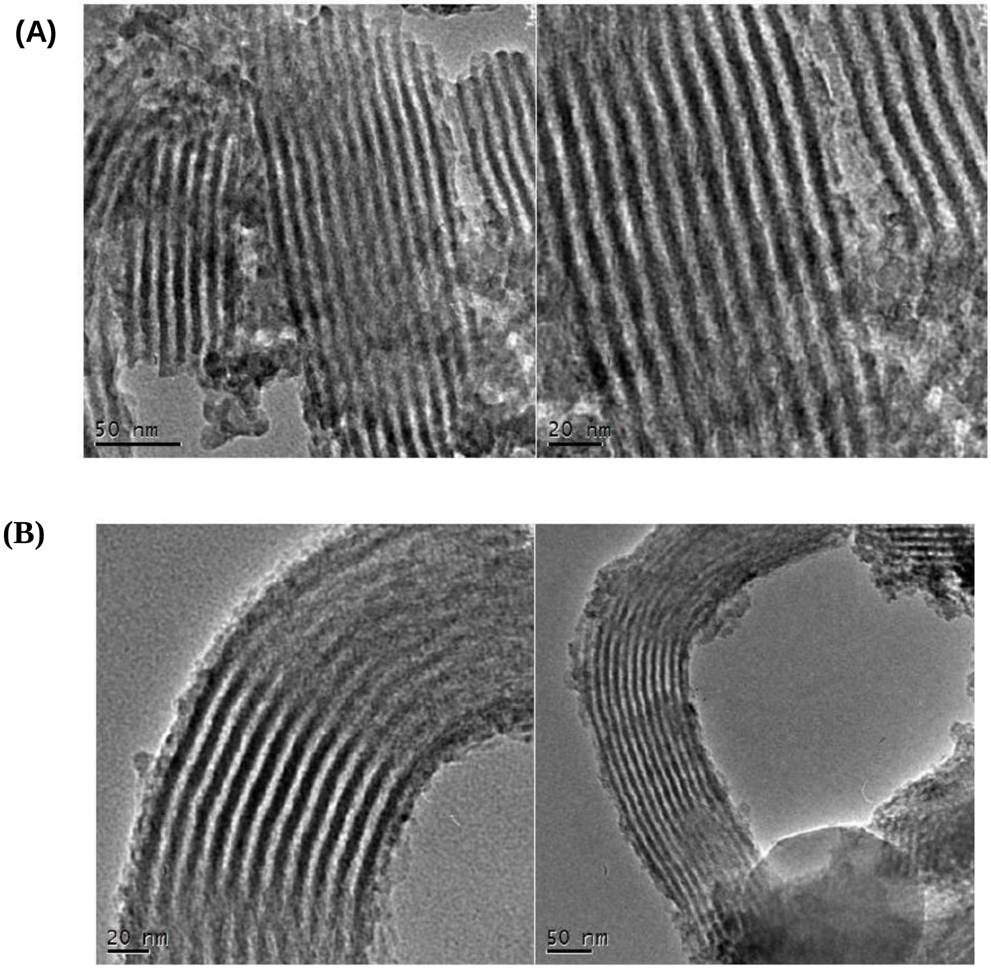

Figure 3.9 Transmission electron microscopy (TEM) images of Ext-SBA-15-en-Fe catalyst after being used for epoxide ring-opening catalysis in (A) three cycles and (B) five cycles.

3.3 Summary

In summary, we have described the synthesis of an active iron-containing mesoporous silica catalyst for ring-opening of various epoxides with water and a variety of alcohols. The material was synthesized by postgrafting of ethylenediamine groups on mesoporous silica and subsequently letting Fe(III) attach onto the ethylenediamine groups. This synthetic method has advantages because it involves easily available, less costly and nontoxic reagents and produces an easily recyclable catalyst that shows no leaching and generates high yields of the products.

Experimental Section

General Procedure for Preparation of Catalyst

Synthesis of Mesoporous Silica, SBA-15: SBA-15 was synthesized as reported previously[37] by using Pluronic P 123 as a templating agent in acidic solution.[38] Typically, a solution of Pluronic P 123/HCl/TEOS/H_2O = 2:12:4.3:26 (mass ratio in g) was stirred at 40 °C for 24 h and then aged at 65 °C for another 24 h. The resulting solution was filtered, and the solid was washed with copious amounts of water, resulting in “as synthesized” SBA-15. Then 4 g of “as synthesized” SBA-15 was dispersed in a solution of ethanol (400 mL) and diethyl ether (400 mL) and stirred at 50 °C for 5 h to remove the template. The solid material was separated by filtration and was dried in an oven at 40 °C for 2 h. This produced surfactant-extracted mesoporous silica, labeled as Ext-SBA-15.

Synthesis of Ethylenediamine-Functionalized Mesoporous Silica and It’s Immobilization with Fe(III): A 500 mg portion of the dried Ext-SBA-15 sample was stirred with excess N-(2-aminoethyl)-3-aminopropyltrimethoxysilane (3.68 mmol) in 250 mL toluene at 80 °C for 6 h. The solution was filtered, and the residue was quickly washed with toluene (3 × 20 mL), and then with ethanol (3×20 mL) and air-dried. The resulting dried sample was denoted as Ext-SBA-15-en. Then the dried Ext-SBA-15-en (200 mg) was dispersed in an aqueous solution containing iron(III) nitrate nonahydrate (400 mg, 1 mmol) and distilled water (100 mL) and stirred at room temperature for 6 h. The resulting solution from a mixture of Ext-SBA-15-en and Fe(III) was deep orange in color. The solid was filtered after 6 h, and the residue was washed with 500 mL of distilled water. After washing, the filtrate was checked for free Fe(III) by potassium thiocyanate test. The resulting pale beige solid was air dried and labeled as Ext-SBA-15-en-Fe(III).

A calcined SBA-15 material was also used to make a catalyst labeled as Cal-SBA-15-en-Fe(III) for comparison purposes. The mesostructured SBA-15 was kept in a furnace and heated at 600 °C for 5 h to remove the polymer templates and prepare calcined SBA-15 (Cal-SBA-15). Then N-(2-aminoethyl)-3-aminopropyltrimethoxysilane was grafted onto Cal-SBA-15, and the material was filtered, washed, and dried in the same way as above. The resulting sample was treated with aqueous Fe(III) solution in the same way as above, producing Cal-SBA-15-en-Fe(III) catalyst.

Ring-Opening of Epoxides with Alcohols: In a typical epoxide ring-opening reaction, the catalyst, Ext-SBA-15en-Fe-(III) (20 mg), was added into a solution of styrene oxide (0.9mmol) and 5 mL of anhydrous alcohol (MeOH, ethanol, propylalcohol, isopropyl alcohol, butyl alcohol, isobutyl alcohol, or tert-butyl alcohol). The solution was stirred at room temperature or at elevated temperature to get the corresponding β-alkoxyalcohols. The progress of the reaction was monitored with TLC in a 20:80 ratio of ethyl acetate/hexane solution and by gas chromatography(GC). The product was also characterized by ^{1}H NMR in $CDCl_3$

and mass spectrometry. The ring-opening reactions for the other epoxide substrates, that is, chloropropylene oxide and 2-methyl-1,2-epoxypropane, and characterization of their products were also conducted in the same way.

Ring-Opening of Epoxides with Water as a Nucleophile: The catalyst (20 mg) was added into a solution containing styrene oxide (0.9 mmol) and a 1:1 mixture of distilled water and acetone (5 mL). The solution was stirred at room temperature to get the corresponding 1-phenyl-1,2-ethanediol. The progress of the reaction was monitored with TLC in a 20:80 ratio of ethyl acetate/hexane solution and by gas chromatography (GC). The product was also characterized by 1H NMR in $CDCl_3$.

^{1}H NMR and ^{13}C NMR of the Products

2-methoxy-2-phenylethanol: ^{1}H NMR (400 MHz, $CDCl_3$) δ 7.40-7.23 (m, 5H), 4.31 (dd, J = 3.8, 8.5 Hz, 1H), 3.75-3.57 (m, 2H), 3.30 (s, 3H), 2.73 (br s, 1H).

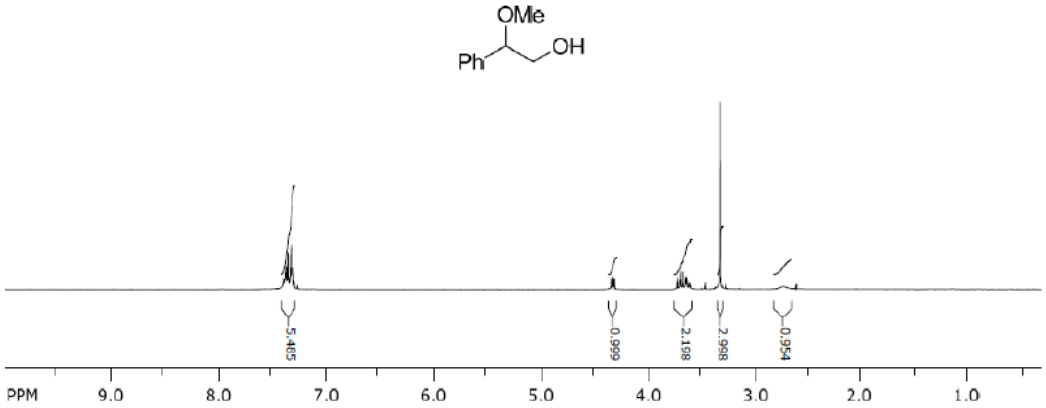

1-chloro-3-methoxypropan-2-ol : ^{1}H NMR (500 MHz, CDCl$_3$) δ 3.98 (quintet, *J* = 3.4 Hz, 1H), 3.64 (dd, *J* = 5.4, 11.1 Hz, 1H), 3.59 (dd, *J* = 5.8, 11.1 Hz, 1H), 3.51 (d, *J* = 5.1 Hz, 2H), 3.41 (s, 3H); ^{13}C NMR (125 MHz, CDCl$_3$) δ 73.4, 70.4, 59.5, 46.2.

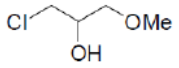

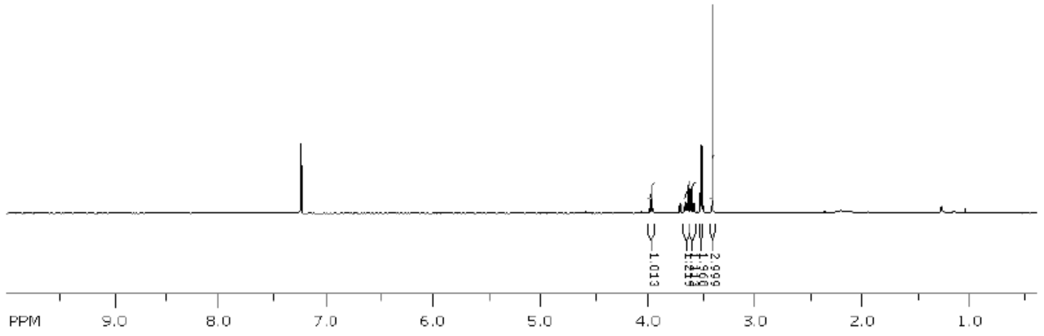

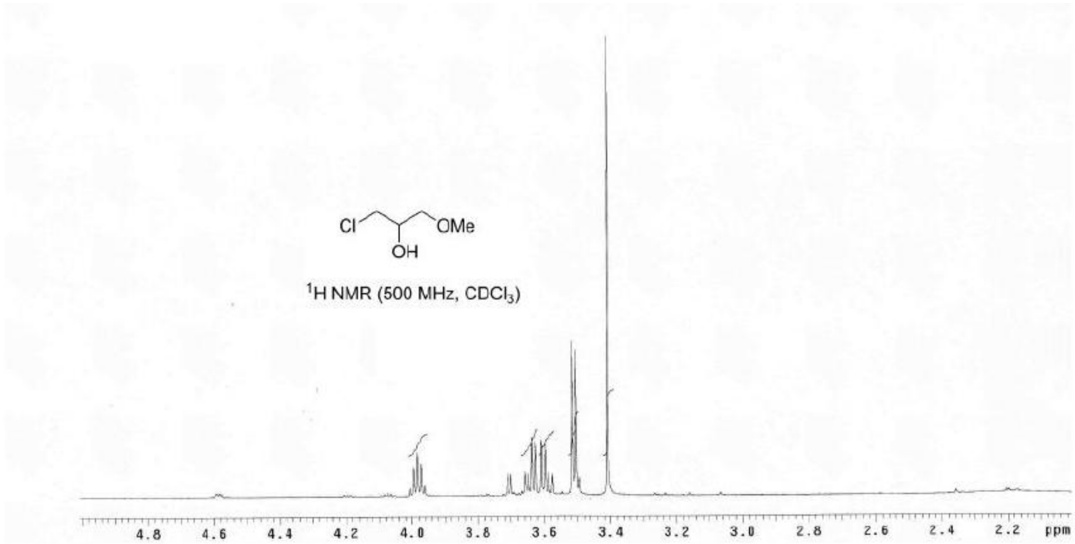

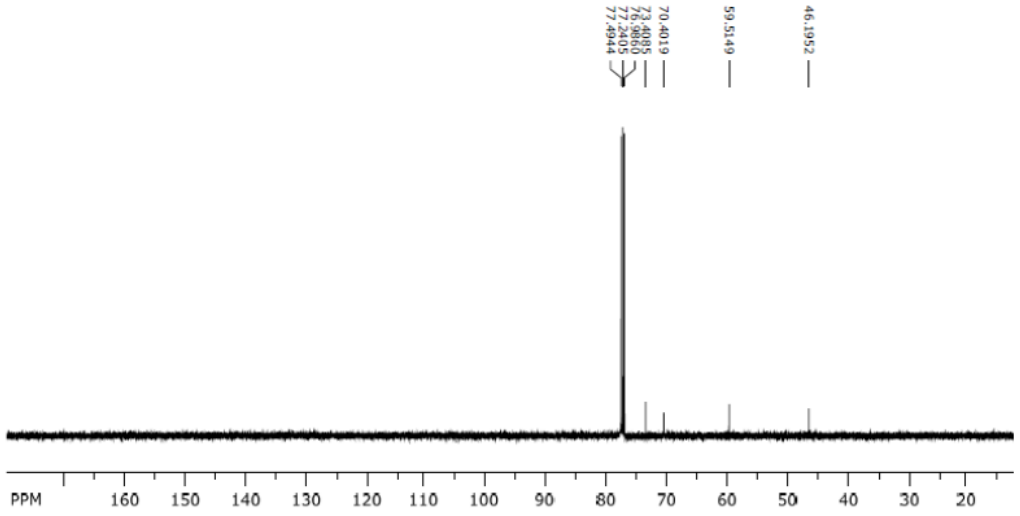

2-methoxy-2-methylpropan-1-ol : ^{1}H NMR (500 MHz, CDCl$_3$) δ 3.47 (s, 2H), 3.22 (s, 3H), 191 (br s, 1H), 1.15 (s, 6H); ^{13}C NMR (125 MHz, CDCl$_3$) δ 77.2, 69.4, 49.6, 21.5.

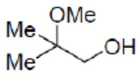

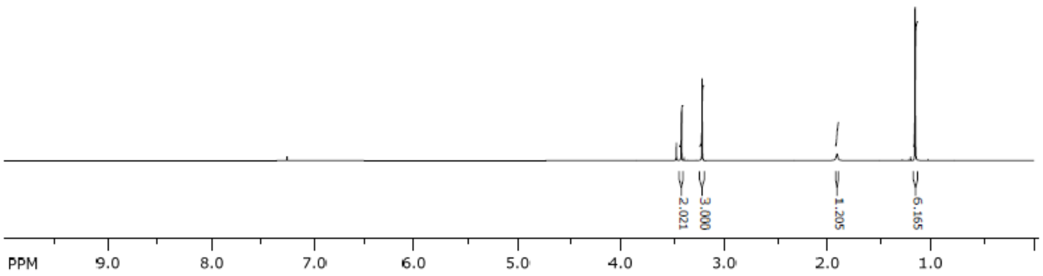

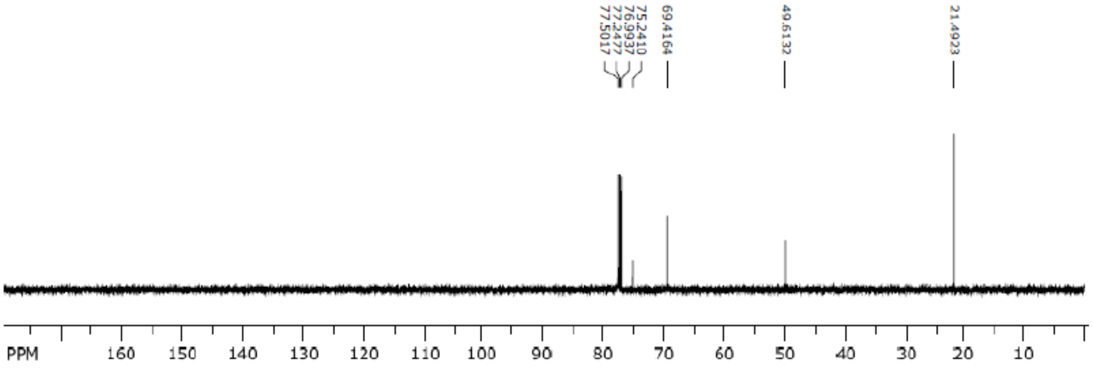

Reference

(1) Yu, K.; Jones, C. W. *Organometallic.s* **2003**, *22*, 2571.

(2) Dalpozzo, R.; Nardi, M.; Oliverio, M.; Paonessa, R.; Procopio, A. *Synthesis* **2009**, 3433.

(3) Yudin, K. A., *Aziridines and Epoxides in Organic Synthesis*. 2006.

(4) Bonini, C.; Righi, G., *Synthesis* **1994**, 225.

(5) Quinn, K. J.; Islamaj, L.; Couvertier, S. M.; Shanley, K. E.; Mackinson, B. L., *Eur. J. Org. Chem.*, 5943.

(6) Kino, T.; Hatanaka, H.; Hashimato, M.; Nishiyama, M.; Goto, T.; Okuhara, M.; Kohsaka, M.; Aoki, H.; Imanaka, H. *J. Antibiot.* **1987**, *40*, 1249.

(7) Henze, O.; Feast, W. J.; Gardebien, F.; Jonkheijm, P.; Lazzaroni, R.; Leclere, P.; Meijer, E. W.; Schenning, A. P. H. J. *J. Am. Chem. Soc.* **2006**, *128*, 5923.

(8) Arrowsmith, J. E.; Campbell, S. F.; Cross, P. E.; Stubbs, J. K.; Burges, R. A.; Gardiner, D. G.; Blackburnt, K. J. *J. Med. Chem.* **1986**, *29*, 1696.

(9) Cao, L.; Lee, J.; Chen, W.; Wood, T. K. *Biotechnol. Bioeng.* **2006**, *94*, 522.

(10) GroÌˆger, H. *Adv. Synth. Catal.* **2001**, *343*, 547.

(11) Drummond, L.; Caldwell, J.; Wilson, H. *Xenobiotoca.* **1990**, *20*, 159.

(12) Lindstad, R. I.; KoÌˆll, P.; McKinley-Mckee, J. S. *Biochem. J.* **1998**, *330*, 479.

(13) Le Bras, J.; Chatterjee, D.; Muzart, J. *Tetrahedron Lett.* **2005**, *46*, 4741.

(14) Olah, G. A.; Fung, A. P.; Meidar, D. *Synthesis* **1981**, 280.

(15) Iranpoor, N.; Shirini, F. *Synth. Commun.* **1994**, *24*, 1959.

(16) Iranpoor, N.; Salechi, P. *Synthesis* **1994**, 1152.

(17) Kolb, H. C.; Finn, M. G.; Sharpless, K. B. *Angew. Chem. Int. Ed.* **2001**, *40*, 2004.

(18) Procopio, A.; Costanzo, P.; Dalpozzo, R.; Maiuolo, L.; Nardi, M.; Oliverio, M. *Tetrahedron Lett.* **2010**, 51, 5150.

(19) Sekar, G.; Singh, V. K., *J. Org. Chem.* **1999**, *64*, 287.

(20) Li, Y.; Tan, Y.; Herdtweck, E.; Cokoja, M.; Kuhn, F. E., *App. Catal., A* **2010**, 384, 171.

(21) Schaus, S. E.; Brandes, B. D.; Larrow, J. F.; Tokunaga, M.; Hansen, K. B.; Gould, A. E.; Furrow, M. E.; Jacobsen, E. N. *J. Am. Chem. Soc.* **2002**, *124*, 1307.

(22) Zhao, P. Q.; Xu, L. W.; Xia, C. G. *Synlet.t* **2004**, *5*, 846.

(23) Tanaka, K.; Otani, K., *New J. Chem.* **2010**, 34, 2389.

(24) Chen, X.; Wu, H.; Wang, S.; Huang, S. *Synth. Commun.* **2012**, 42, 2440.

(25) Barreca, D.; Copley, M. P.; Graham, A. E.; Holmes, J. D.; Morris, M. A.; Seraglia, R.; Spalding, T. R.; Tondello, E. *App. Catal., A.* **2006**, 304, 14.

(26) Salechi, P.; Khodaei, M. M.; Ghareghani, S. B.; Motlagh, A. R. *Russ. J. Org. Chem.* **2003**, 39, 794.

(27) Lee, S. H.; Lee, E. Y.; Yoo, D. W.; Hong, S. J.; Lee, J. H.; Kwak, H.; Lee, Y. M.; Kim, J.; Kim, C.; Lee, J. K. *New. J. Chem.* **2007,** 31, 1579.

(28) Yoo, D. W.; Yoo, S. K.; Kim, C.; Lee, J. K. *J. Chem. Soc., Dalton Trans.* **2002**, 3931.

(29) Dhakshinamoorthy, A.; Alvaro, M.; Garcia, H. *Chem. Eur. J.* **2010**, 16, 8530.

(30) Zettler, M. W.; Paquette, L., *Encyclopedia of Reagents for Organic Synthesis*. **1995**, 2871.

(31) King, B. R. *Encyclopedia of Inorganic Chemistry*. **1994**, 4.

(32) Beller, M.; Bolm, C. *Transition Metals for Organic Synthesis*. **2004**.

(33) Venkatasubbaiah, K.; Zhu, X. J.; Jones, C. W., *Top. Catal.* **2010**, 53, 1063.

(34) Cotton, F. A.; Wilkinson, G. *Advanced Inorganic Chemistry: A Comprehensive Text*. **1982**; 767.

(35) Wezenberg, S. J.; Kleij, A. W. *Adv. Synth. Catal.* **2010**, 352, 85.

(36) Reeve, W.; Christoffel, I. *J. Am. Chem. Soc.* **1950**, 72, 1480.

(37) Olkhovyk, O.; Antochshuk, V.; Jaroniec, M. *Colloids Surf. A* **2006**, 236, 69.

(38) Zhao, D.; Feng, J.; Huo, Q.; Melosh, N.; Fredrickson, G. H.; Chmelka, B. F.; Stucky, G. D. *Science* **2007**, 279, 548.

Chapter IV

Ultrasmall Au Nanoclusters Supported in Mesoporous Channels of SBA-15 as Heterogeneous Catalysts for Selective Styrene Oxidation

4.1 Introduction

Gold has long been considered too inert to catalyze reactions until the discovery by Haruta that small size Au nanoparticles supported on certain metal oxide promoted CO oxidation below room temperature.[1-3] Since then, there has been considerable research activity in the area of gold nanoparticle catalysis, and there is now extensive literature on the use of Au nanoparticles in catalytic chemical transformations of a wide variety of chemical reactions, such as selective hydrogenation,[4,5] selective oxidation,[6,7] carbon–carbon coupling reactions,[8-11] and oxidation reaction of H_2 to H_2O_2.[12,13]

Not surprisingly or just like in many other nanosized metallic catalysts, the catalytic properties of heterogeneous Au catalysts have been widely found to be strongly dependent on the particles' size and stability. In case of supported Au nanoparticles, it was widely documented that particles with sizes close to or less than 5 nm are the most effective catalysts for many types of reactions, although the exact reasons behind this is still under debate.[14,15,16] Furthermore, the effect of sizes in the selectivity of some reactions have been reported in some studies, including our own study recently. [17,18]

In addition to the size of the nanoparticles, the type of support material used for the nanoparticles has been found to strongly affect the catalytic properties of the Au nanoparticles. Supported gold catalysts are often prepared by loading Au nanoparticles onto pristine support materials composed of TiO_2, CeO_2, Fe_2O_3, ZrO_2, Al_2O_3, SiO_2, C, etc. via deposition–precipitation, co-precipitation, or colloidal dispersion synthetic methods.[16] Recently, our group also showed the use of high surface area materials such as mesoporous silica[17] and core-shell-shell metal oxide microspheres[18] as support materials for Au nanoparticle catalysts for oxidation reactions. The synthesis of the materials was achieved by galvanic reaction / electrodeless deposition methods or by in-situ reduction of Au(I) or Au(III) ions on the support materials using pre-placed organic groups as reducing agents. External reducing agents have also been successfully utilized for the synthesis of the supported Au nanoparticles in the latter case.

Oxidation reaction is an important route for the synthesis of many fine chemicals and pharmaceuticals.[19] One of the first examples of oxidation reactions using Au nanoparticles as catalyst was reported by Haruta *et al*.[20] Specifically, direct epoxidation of propylene using molecular oxygen was successfully achieved by using supported Au nanoparticles (AuNPs) as catalyst.[20] Since then, supported Au nanoparticle catalysts have been used for selective epoxidation/oxidation of various alkenes such as styrene, cyclohexene, cis-cyclooctene and *trans*-stilbene.[4,21-25] Despite these reports and some of known facts about the effectiveness of ultrasmall Au nanoparticles in catalysis, the wide range of uses of ultrasmall Au nanoparticles in catalysis has been hampered by the fact that these particles have very strong tendency to aggregate, are unstable and lose their catalytic activities more easily.

4.2 Styrene Oxidation with Ultrasmall Au Nanoparticles as Catalysts

Styrene oxidation has been one of the most commonly used model reactions to test the catalytic activities of Au nanoparticles in presence of molecular oxygen, hydrogen peroxide or organic hydroperoxides. In principle, styrene oxidation can give at least styrene oxide, benzaldehyde, and benzoic acid—three important compounds that can lead to many commercial products. Thus, it is not surprising to find that the few examples reported in the literature on the successful application of supported small gold nanoclusters for styrene oxidation produced mixed products. For example, recently, Lambart *et al.* demonstrated that ultrasmall gold nanoclusters $Au_{55}(PPh_3)_{12}Cl_6$ (1.4 nm) supported on inert materials, like boron nitride, carbon and silica, could be used as catalyst for selective oxidation of styrene with dioxygen.[26] Benzaldehyde was reported to be the main product (82%) of the reaction, although styrene oxide (14%) and acetophenone (4%) byproducts were also observed. In the work by Tsukuda *et al.*[27] with $Au_{25}(SG)_{18}$ (SG = glutathione ligand) nanoclusters supported on hydroxyapatite, the catalytic oxidation of styrene was found to give almost 100% conversion using *tert*-butylhydroperoxide (TBHP) as oxidant in toluene solution at 80 °C. Interestingly, the selectivity of the reaction here was to styrene oxide product (92%), instead of benzaldehyde as in Ref. 26. The catalyst was also shown to be reusable without significant loss of its activity and selectivity. Jin *et al.*[28, 29] also demonstrated that very small size colloidal clusters of gold, such as Au_{25}, Au_{38}, and Au_{144}, that were capped with phenylethanethiolate (*e.g.*, $Au_{25}(SC_2H_4Ph)_{18}$) and supported on hydroxyapatite (HAP) and silica gel could serve as catalysts for styrene oxidation. These materials oxidized styrene and gave benzaldehyde with high selectivity of about 100% with TBHP oxidant and 80% selectivity with dioxygen, with styrene oxide and acetophenone as minor products in the latter case. Furthermore, the catalytic activity was reported to decrease in the order of $Au_{25} > Au_{38} > Au_{144}$ in the presence of O_2 as oxidant.

4.3 General Consideration and Concept

As mentioned above, styrene oxidation can produce styrene oxide, benzaldehyde and even benzoic acid upon extreme oxidation conditions. Although all these possible products can be useful for various processes,[26] getting one of the products in pure form selectively is an important, and yet a very difficult task. Thus, catalytic oxidation of the styrene as well as other alkanes efficiently and selectively still remains important and yet challenging areas of research in catalysis.

In this work, synthetic method to SBA-15 mesoporous silica-supported thiolate-capped ultrasmall Au_n nanoclusters was developed and the use of the resulting materials as heterogeneous catalysts for selective styrene oxidation was investigated. Moreover, the effect of removal of the capping agents from the nanoclusters, after the nanoclusters are supported on the solid material, on the catalytic properties of the materials was investigated. The oxidation reaction was performed in the presence of radical initiator TBHP in toluene as a solvent at 80 °C and by using the SBA-15-supported Au_n nanoclusters as catalyst.

4.3.1 Synthesis and Characterization of Meosporous Silica Supported Au Nanoparticle Catalysts

To synthesize the mesoporous silica-supported ultrasmall Au nanocatalysts, first, SBA-15 mesoporous silica was synthesized by following literature method (Scheme 4.1).[30] Then, 3-mercaptopropyltrimethoxysilane was grafted onto the surface of SBA-15 mesoporous silica, producing mercaptopropyl-functionalized SBA-15. This was achieved simply by stirring SBA-15 with an excess amount of MPTS in toluene at 80 °C for 6 h. The mercaptopropyl-functionalized mesoporous silica sample was labeled as Ext-SBA-15-SH. The mercaptopropyl-functionalized SBA-15 was stirred with dichloromethane solutions of different Au_n nanoclusters. This led to ligand exchange between the thiolate groups on the Au nanoparticles and the mercaptopropyl groups on the SBA-15, producing the SBA-15 mesoporous silica-supported Au nanoparticle catalysts, named Ext-SBA-15-SH-$Au_{n,}$. By changing the reaction conditions and the reagents used during the synthesis, different types of supported Au nanocatalysts were obtained. Two different gold nanoclusters, $Au_{25}[S(CH_2)_2Ph]_{18}$ and $Au_{140}[S(CH_2)_2Ph]_{53}$, which were synthesized in the group of Prof. Flavio Maran at University of Padova, Italy were used as received for the synthesis of these supported Au nanocatalysts. The typical procedure included the stirring of the Ext-SBA-15-SH sample with 2 μM Au_{25} and Au_{140} solutions in dichloromethane (DCM) at room temperature for 3 h. This resulted in the desired SBA-15 mesoporous silica-supported Au nanoparticle catalysts, which were denoted as Ext-SBA-15-SH- Au_{25} and Ext-SBA-15-SH- Au_{140}, respectively (Scheme 4.1).

Furthermore, to investigate the effect of thiolate group around the Au nanoparticles on the catalytic activity of the nanoparticles, the thiolate groups were removed in different degrees from the surface of Au cluster by reducing them with different concentrations of aqueous sodium borohydride solutions and then thoroughly washing the materials with water, via centrifugation and decantation. To perform this, the immobilized Au_n nanoclusters (Ext-SBA-15-SH-Au_n) treated with fresh aqueous solution of sodium borohydride. Two different concentrations of sodium borohydride solutions, 1 mM and 5 mM, were used to yield Ext-SBA-15-SH-Au_n-1 and Ext-SBA-15-SH-Au_n-5 samples, respectively.

Finally, the catalytic properties of all the different Ext-SBA-15-SH-Au_n materials, both with or without some or all of their thiolate groups, were investigated by using styrene oxidation reaction as a model reaction.

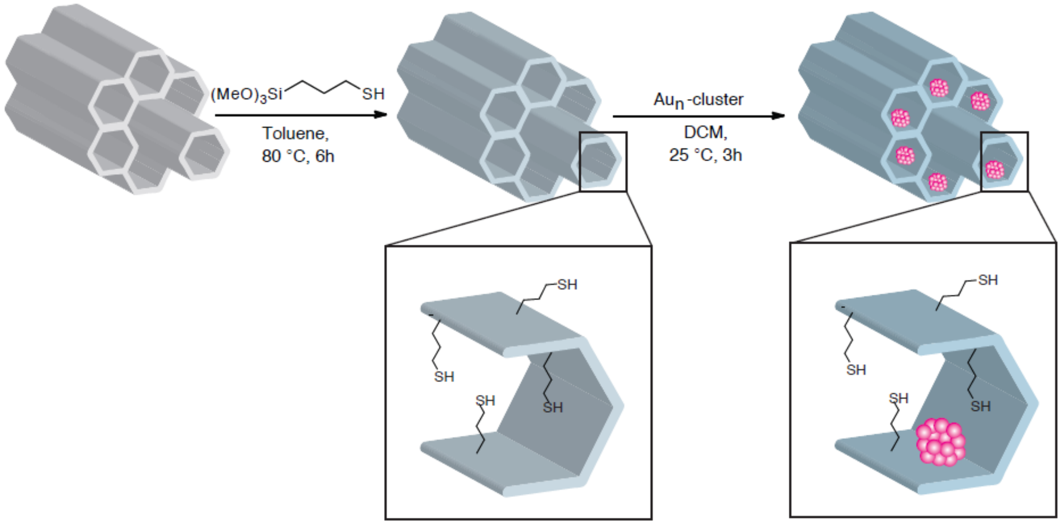

***Scheme 4.1*:** Synthesis of immobilized Au cluster on SBA-15 (Ext-SBA-15-SH-Au$_n$).

The parent materials to the catalysts, i.e., Ext-SBA-15, Ext-SBA-15-SH, and all the different catalysts obtained (Ext-SBA-15-SH-Au$_n$) were then characterized by transmission electron microscopy (TEM). Some representative TEM images are depicted in Figure 4.1. The TEM images of the Ext-SBA-15 samples before and after postgrafting with mercaptopropyl groups revealed the presence of highly ordered mesostructures in the materials (Figure 4.1). Unfortunately, as the gold nanoclusters are so small, they were not detected either by TEM or XRD (XRD pattern not shown). This is not unexpected considering the fact that 1) small nanoclusters give very little XRD reflections, if any, and 2) most of them are encapsulated within the channel pores of the mesoporous materials.[32-35]

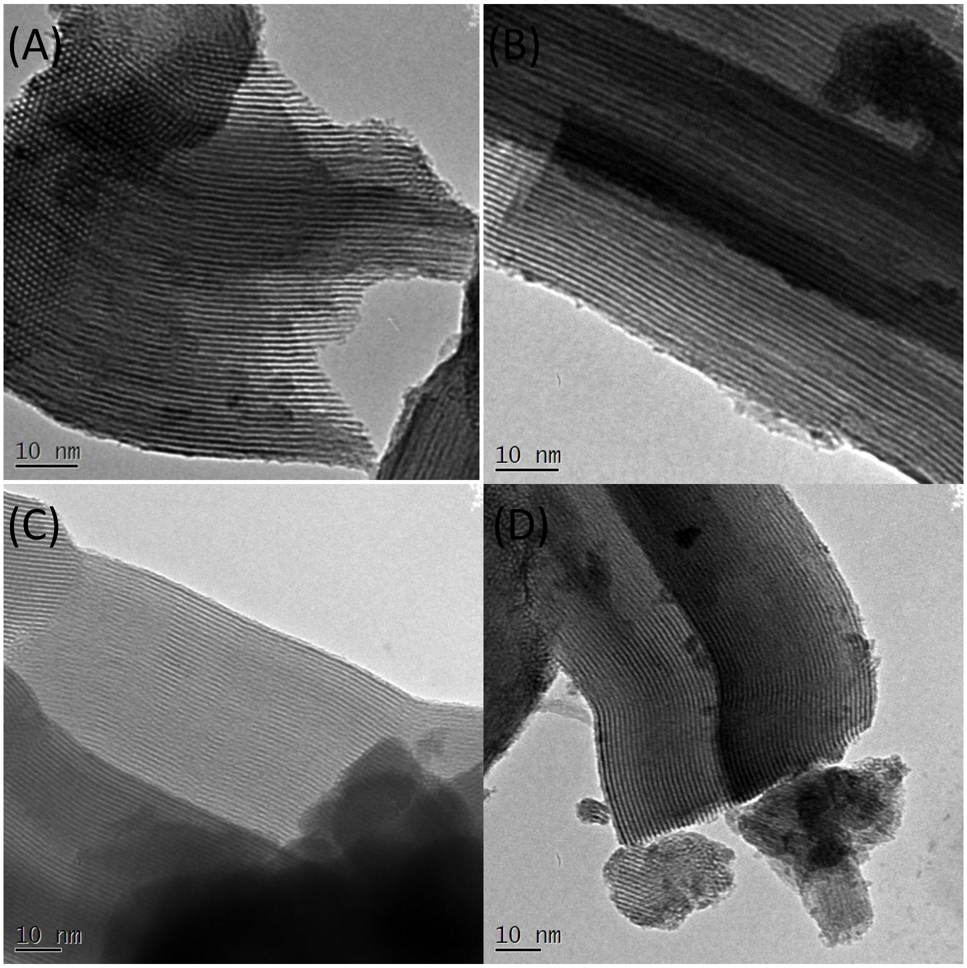

Figure 4.1**:** TEM images of (A, B) Ext SBA-15 and (C, D) Ext-SBA-15-SH.

The removal of the thiolate groups from the gold nanoparticles' surfaces after borohydride treatment was investigated and confirmed successfully by TGA (Figure 4.2). The thermogravimetric traces indicated a slight weight loss below 100 °C for all the samples due to loss of water adsorbed on the materials. The weight loss in the range 100–450 °C, which was associated with the loss of mercaptopropyl groups, was found to be 18.73% and 18.88% for samples Ext-SBA-15-SH and Ext-SBA-15-SH-Au_{25}, respectively. The weight loss from the samples due to mercaptopropyl groups changed after the samples were treated with borohydride. For the Ext-SBA-15-SH-Au$_{25}$ samples treated with 1 mM and 5 mM sodium borohydride solutions, the weight losses in the range 100–450 °C were found to be 12.22% and 10.45%, respectively. This clearly indicates that sodium borohydride solutions successfully removed the thiolate groups from the Au nanoparticles, and the amount of thiolate groups removed from the Au nanoclusters was dependent on the concentration of borohydride solution used.

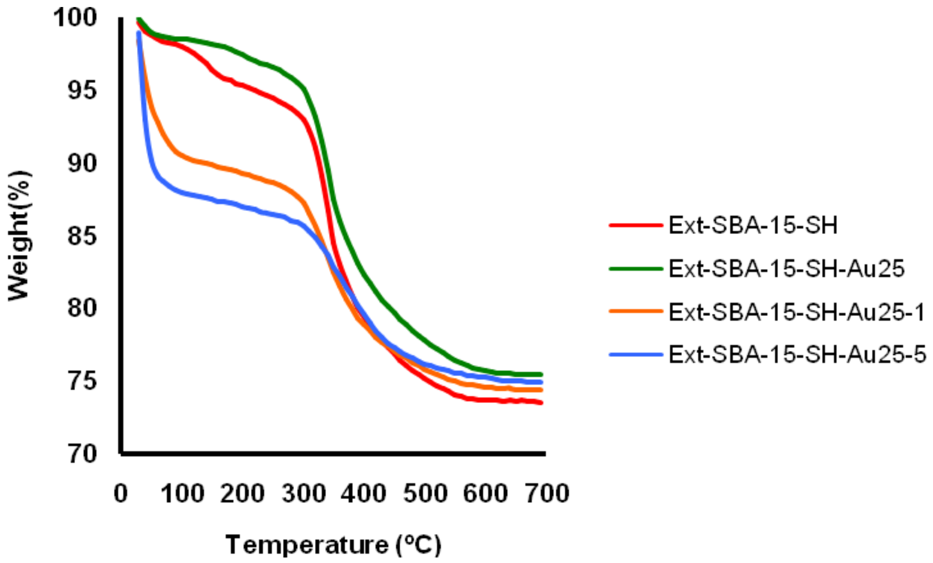

***Figure 4.2*:** Thermogravimetric traces of Ext-SBA-15SH, Ext-SBA-15-SH-Au$_{25}$, Ext-SBA-15-SH-Au$_{25}$-1 and Ext-SBA-15-SH-Au$_{25}$-5.

Furthermore, UV-Vis absorption experiments were performed on the supernantant obtained after sodium borohydride treatment. The UV-vis absorption spectrum of the supernatant showed no absorption maxima unlike the spectrum of the 2 µM Au$_n$ solution, *i.e.*, the solution used for immobilization of the Au nanoclusters into the mercaptopropyl-modified SBA-15 (Figure 4.3). This suggests that Au nanoclusters did not leach or come off the support materials upon or after treatment with the borohydride solution treatment.

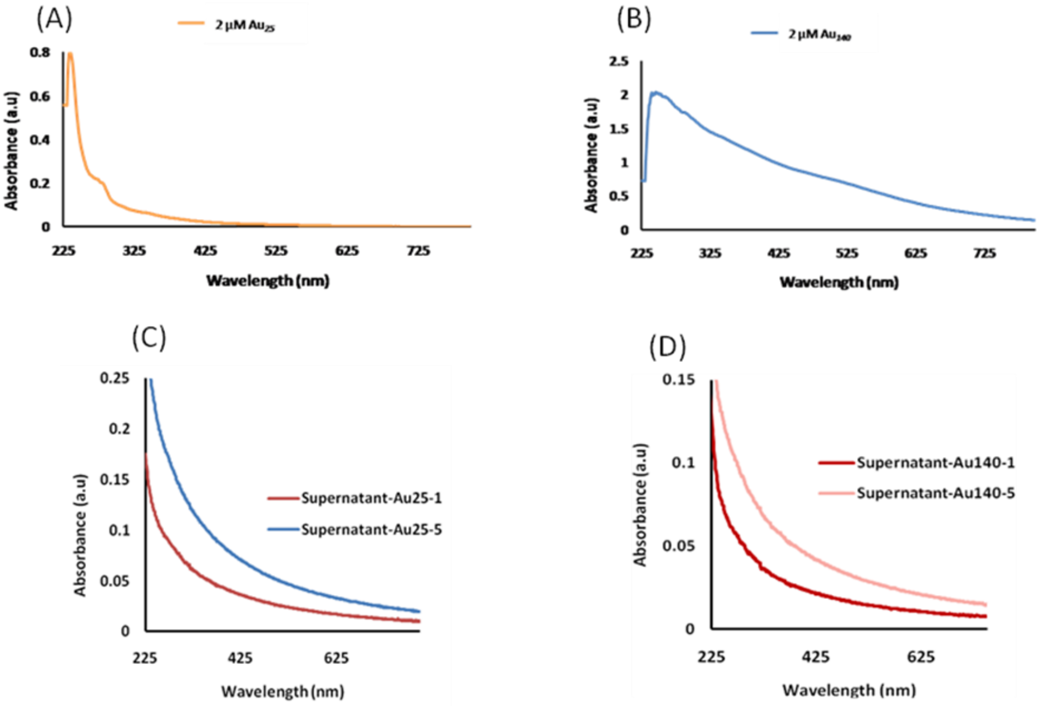

Figure 4.3**:** UV-Vis spectra of (A) 2 µM Au_{25} and (B) 2 µM Au_{140} solutions in dichloromethane, (C) the supernatant collected after treatment of Ext-SBA-15-SH-Au_{25} with 1 mM and 5 mM $NaBH_4$ and centrifugation of the solutions, and (D) the supernatant collected after treatment of Ext-SBA-15-SH-Au_{140} with 1mM and 5 mM $NaBH_4$ and centrifugation of the solutions.

4.3.2 Control Experiments

First, control experiments involving attempted oxidation reactions of styrene in the absence of any material/catalyst or in the presence of Ext-SBA-15 and Ext-SBA-15-SH, which contained no AuNPs, were performed (Scheme 4.2).

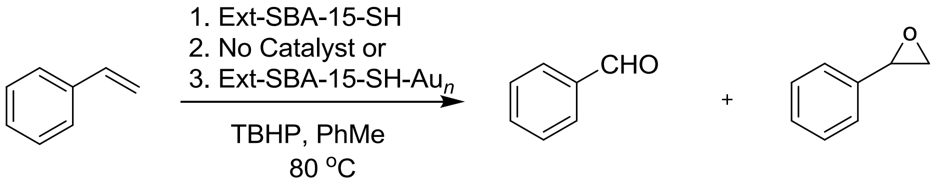

***Scheme 4.2*:** Attempted styrene oxidation without a catalyst or in the presence of various catalysts.

The reaction with Ext-SBA-15 containing no AuNPs gave a low conversion (18%) of styrene in 6 h and 46% conversion of styrene in 24 h at 80 °C. The reaction product contained more benzaldehyde (85%) than styrene oxide (15%). An additional control reaction by using the mercaptopropyl-functionalized SBA-15 (Ext-SBA-15-SH) as catalyst was then performed. This reaction gave even a lower styrene conversion (32%) in 24 h. Moreover, a blank reaction without any material/catalyst was run in anhydrous toluene at 80 °C. The reaction gave 42% conversion of styrene in 24 h, with the reaction products consising of 86% benzaldehyde and 14% styrene oxide. The results of the control reactions are summarized in Table 4.1.

Table 4.1**:** Control experiments of styrene oxidation in the presence of different reference materials or no catalyst.

Catalyst	**Temp (°C)**	**Time (h)**	**Conv. of Styrene (%)**	**Selectivity to Benzaldehyde (%)**	**Selectivity to Styrene Oxide (%)**
Blank	80	24	42	86	14
Ext-SBA-15	80	24	46	85	15
Ext-SBA-15-SH	80	24	32	~100	0

Based on these control experiments and results, it can be concluded that the styrene oxidation reaction is slow, both without a catalyst as well as in the presence of Ext-SBA-15 containing no AuNPs. Since we have chosen to use toluene as solvent because it gave favorable results in alkane oxidation reactions catalyzed by bigger Au nanoparticles in previous studies[17] and since toluene is known to oxidize to benzoic acid with oxygen under severe conditions,[31] the oxidation of toluene with our catalyst under the reaction conditions we have employed here was also studied. The conversion of toluene under the reaction conditions we used was found to be >1 %. Thus, toluene can be safely used as a solvent for our catalytic studies.

4.3.3 Catalytic Activity of Mesoporous Au Nanoclusters (Ext-SBA-15-SH-Au$_n$) in Styrene Oxidation

With the above control experiments in place, the catalytic reactions of styrene oxidation in anhydrous toluene at 80 °C in the presence of the different

Ext-SBA-15-SH-Au_n catalysts synthesized above with TBHP and oxygen as an oxidant were then investigated. First, the catalytic activity of Ext-SBA-15-SH-Au_{25} and Ext-SBA-15-SH-Au_{140} towards the oxidation of styrene was studied. In 24 h, the % conversion of styrene was similar in both cases, giving 30 and 32 % conversion and exclusively benzaldehyde product with Ext-SBA-15-SH-Au_{25} and Ext-SBA-15-SH-Au_{140} catalysts, respectively. Next, the catalytic activity of Ext-SBA-15-SH-Au_n-1 and Ext-SBA-15-SH-Au_n-5, which were obtained by treating the Ext-SBA-15-SH-Au_n, where Au_n is Au_{25} or Au_{140}, with 1 mM and 5 mM $NaBH_4$ solutions, respectively. All the borohydride treated materials exhibited improved catalytic activity compared to their corresponding untreated counterparts. Furthermore, these catalysts also gave benzaldehyde as the major product. Particularly, the ones treated with 5 mM borohydride solution (*i.e.,* Ext-SBA-15-SH-Au_n-5), afforded significantly improved catalytic activity in styrene oxidation (Figure 4.4). For example, whereas Ext-SBA-15-SH-Au_{25} resulted in 30% conversion of styrene in 24 h, Ext-SBA-15-SH-Au_{25}-1 and Ext-SBA-15-SH-Au_{25}-5 gave 38% and 100% conversion of styrene, respectively, in 24 h. A very similar trend was also observed for the bigger nanoparticles, *i.e.,* the mesoporous silica-supported Au_{140} nanoclusters. The conversion of styrene to benzaldehyde was found to be 32%, 68% and 100% in 24 h for Ext-SBA-15-SH-Au_{140}, Ext-SBA-15-SH-Au_{140}-1 and Ext-SBA-15-SH-Au_{140}-5, respectively. In all the cases the reactions selectivity produced benzaldehyde, with barely any styrene oxide byproduct.

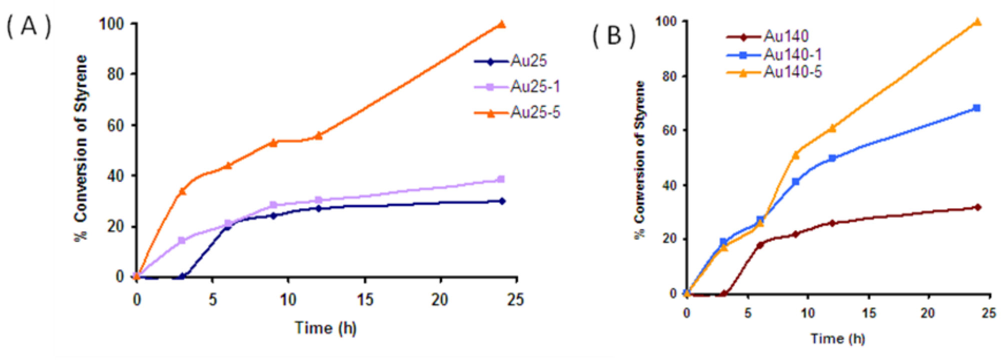

Figure 4.4: Kinetic plot of styrene oxidation catalyzed by (A) Ext-SBA-15-SH-Au$_{25}$, Ext-SBA-15-SH-Au$_{25}$-1 and Ext-SBA-15-SH-Au$_{25}$-5 and (B) Ext-SBA-15-SH-Au$_{140}$, Ext-SBA-15-SH-Au$_{140}$-1 and Ext-SBA-15-SH-Au$_{140}$-5 nanocatalysts.

The styrene oxidation was also studied by using Ext-SBA-15-SH-Au$_{25}$-5 as catalyst and with oxygen as oxidant without TBHP under similar conditions at 80 ºC and using toluene as the solvent. The conversion of styrene to benzaldehyde in the reaction was found to be only 6% in 3 days. Since the reaction was slow in toluene, the same reaction was tried under neat condition (without using solvent) at 80 ºC. The % conversion of styrene in 24 h was 28 %, giving benzaldehyde as the major product (75%) and styrene oxide as a minor product (11%) and other products such as benzoic acid (14%) (Figure 4.5). When the reaction was catalyzed by Ext-SBA-15-SH-Au$_{140}$-5, the conversion of styrene was 14% in 24 h with 71.4% benzaldehyde , 22% styrene oxide and 7% other products.

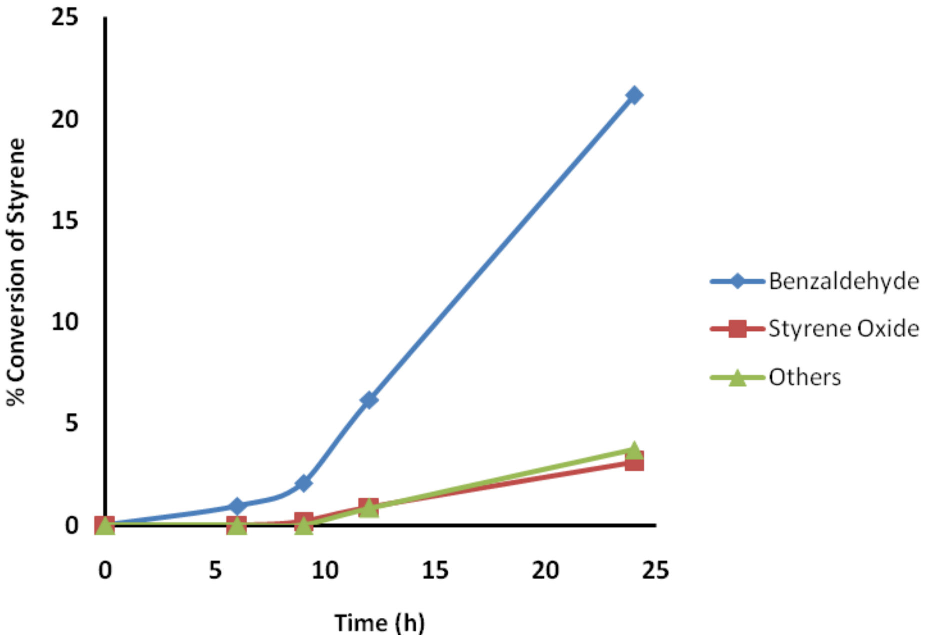

Figure 4.5**:** Product distribution of styrene oxidation catalyzed by Ext-SBA-15-SH-Au_{25}-5 under oxygen at 80 ºC (solvent free condition).

4.3.4 Recyclability

The heterogeneous nature of the the supported Au nanocatalysts and their recyclability were then investigated. The recyclability test was performed by recovering the nanocatalyst, for example, Ext-SBA-15-SH-Au_{140}-5, at the end of a given reaction and reusing it as a catalyst in another catalytic reaction. The material was recovered by centrifugation of the reaction mixture; decanting the supernatant; and washing the solid catalyst with toluene twice, followed by ethanol, and drying it. The nanocatalysts were found to be easily recyclable, at least three times without losing their catalytic activity, as shown in Figure 4.6. However, there was a slight catalytic activity or reduction in the reaction rates observed from the first cycle to the subsequent cycles (for example for the recycled Ext-SBA-15-SH-Au_{140}-5 nanocatalyst), which must be mainly due to loss of the small amount of catalyst during handling and centrifugation.

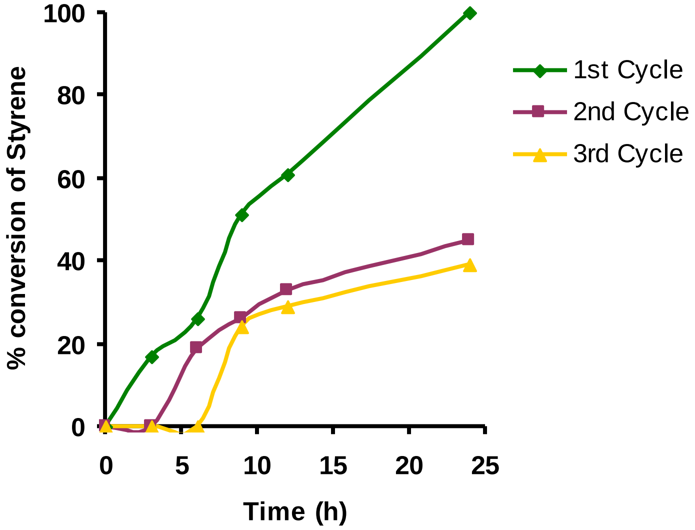

Figure 4.6: % Conversion versus time graphs for styrene oxidation reaction catalyzed by Ext-SBA-15-SH- Au_{140}-5 nanocatalyst.

An experiment was also performed to determine whether or not leaching of Au from the Ext-SBA-15-SH-Au_{140}-5 nanocatalyst into the reaction mixture took place (Figure 4.7). To perform this, the reaction mixture was centrifuged and the catalyst was separated from the reaction mixture after 7 h during the reaction, and the supernatant was then run by itself. The % conversion of styrene in the reaction at 7 h was 20 %. Twenty-four hours after separation of the solid catalyst from the reaction mixture, the conversion of styrene in the reaction was found to be only 31%, which was significantly less than the one obtained in the presence of catalyst in 24 h (*i.e.*, ~100%) or only slightly higher than the one obtained in 7 h with in the presence of the catalyst. Interestingly, this % conversion is similar to what was obtained for the reaction in the presence of mercaptopropyl-functionalized SBA-15 (Ext-SBA-15-SH) (*i.e.,* 32% in 24 h). These results suggest that there was no leached Au in the reaction mixture or the catalytic reaction was not favored by leached Au species, if any.

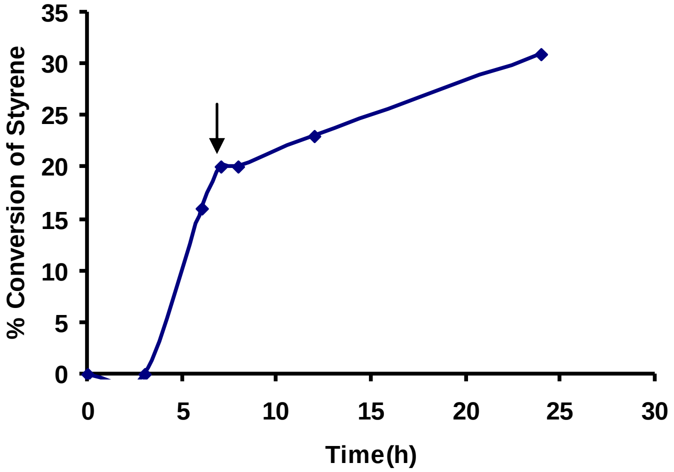

***Figure 4.7*:** Percent conversion versus reaction time in a leaching experiment. The black arrow indicates the time at which the solid Au nanocatalyst was filtered and separated from the reaction mixture and the supernatant was begun to run by itself afterward.

This result was further corroborated by elemental analyses of the reaction mixture. The weight percent of Au analyzed by inductively coupled plasma – atomic emission spectroscopy (ICP-AES) in the fresh catalyst and in the reaction mixture after third cycle was extremely low (Table 4.2). In other words, there was insignificant amount of Au leached from the nanocatalyst or present in the reaction mixture. This clearly indicates the high stability of the Au nanoclusters in Ext-SBA-15-SH-Au$_n$ nanocatalyst towards leaching.

Table 4.2**:** Elemental analysis obtained with ICP-AES of Au in the catalysts as well as in the reaction mixture after 3rd reaction cycle.

Entry	**Au (ppm)**	**Au (%)**	**Au (mmol)**
Catalyst	107	0.01	3.1×10^{-5}
Reaction solution recovered from 3rd cycle	4	0.0004	1.26×10^{-6}

4.4 Summary

A novel heterogeneous catalytic system comprising ultrasmall Au nanocluster immobilized in mercaptopropyl-functionalized mesoporous silica materials was reported. Two types of Au nanoclusters, $Au_{25}[S(CH_2)_2Ph]_{18}$ and $Au_{140}[S(CH_2)_2Ph]_{53}$ with SBA-15 as mesoporous material were employed in the synthesis. This produced materials or nanocatalysts labeled as Ext-SBA-15-SH-Au$_{25}$ and Ext-SBA-15-SH-Au$_{140}$, respectively, which exhibited active catalytic activities toward styrene oxidation. Furthermore, controlled removal of the thiolate capping groups from the supported Au nanoparticles was performed by using borohydride treatment to form ‘naked’ Au nanocatalytic sites with highly exposed surfaces for reactants and to produce Au nanocatalysts with much improved catalytic activities. An increase in reaction rate in styrene oxidation was obtained when the reaction was catalyzed by the resulting borohydride treated samples, denoted as Ext-SBA-15-SH-Au_{25}-1 and Ext-SBA-15-SH-Au_{25}-5 or Ext-SBA-15-SH-Au_{140}-1 and Ext-SBA-15-SH-Au_{140}-5, which were treated by 1 and 5 mM sodium borohydride solutions, respectively. It is also worth mentioning that in all the cases the catalysts gave high selectivity towards benzaldehyde product, with little styrene oxide product. The catalyst was also shown to be easily recoverable and recyclable with barely any leaching of gold and only minor loss of catalytic activity.

Experimental Section

Materials and Reagents. Poly(ethylene glycol)-block-poly(propylene glycol)-block-poly(ethylene glycol) block copolymer (Pluronic® P123, average molecular mass ~5800 g/mol) was obtained from BASF. Tetraethylorthosilicate (TEOS), dichloromethane, toluene, and sodium borohydride were purchased from Sigma-Aldrich. Hydrochloric acid (36.5%) was received from Fischer Scientific. 3-mercaptopropyltrimethoxysilane was obtained from Gelest, Inc.

Synthesis of Mesoporous Silica, SBA-15. SBA-15 was synthesized as reported previously[30] by using Pluronic® P123 as a templating agent in acidic solution. Typically a solution of Pluronincs® P123 : HCl : TEOS : H_2O = 2 : 12 : 4.3 : 26 (mass ratio in g) was stirred at 40 °C for 24 h and then aged at 65 °C for another 24 h. The resulting solution was filtered, and the solid was washed with copious amounts of water resulting in a material labeled as as-synthesized SBA-15. Then 4 g as-synthesized SBA-15 was dispersed in ethanol (400 mL) and diethyl ether (400 mL) and stirred at 50 °C for 5 h to remove the template. The solid material was separated by filtration and was dried in oven at 40 °C for 2 h. This produced surfactant-extracted mesoporous silica, labeled as Ext-SBA-15.

Synthesis of Mercaptopropyl-Functionalized Mesoporous Silica. 500 mg of the dried Ext-SBA-15 sample was stirred with excess 3-mercaptopropyltrimethoxysilane (3.68 mmol) in toluene at 80 °C for 6 h. The solution was filtered and the residue was quickly washed with toluene (3 x 20 mL) and then with ethanol (3 x 20 mL) and air dried. The resulting dried sample was denoted as Ext-SBA-15-SH.

Ligand Exchange of Alkanethiol of Au Cluster (Au$_{25}$) with Mercaptopropyl-Functionalized Mesoporous Silica. Two different gold nanoclusters, $Au_{25}[S(CH_2)_2Ph]_{18}$ and $Au_{140}[S(CH_2)_2Ph]_{53}$, which were synthesized in the group of Prof. Flavio Maran at University of Padova, Italy, were used for the synthesis of the supported Au nanocatalysts. These nanoclusters were labeled as Au_{25} and Au_{140}, respectively. First, 2 μM the Au_{25} and the Au_{140} solutions in dichloromethane (DCM) were prepared. Then, 30 mL of each solution was the dried Ext-SBA-15-SH (300 mg) at room temperature for 3 h. The solution was centrifuged, and the residue was washed with DCM thrice (3 x 10 mL). The resulting pale beige colored solid samples (nanocatalysts) were air dried and labeled as Ext-SBA-15-SH-Au_{25} and Ext-SBA-15-SH-Au_{140}, respectively.

Synthesis of Ext-SBA-15-Au$_{25}$-1. 250 mg of Ext-SBA-15-Au_{25} was dispersed in 25 mL distilled water. One mM sodium borohydride solution (10 mL) was added into the solution at room temperature. After 30 min of stirring, the solid solution was centrifuged, and the precipitate was washed with distilled water thrice (3 x 10 mL). The resulting pale beige colored solid was air dried and denoted as Ext-SBA-15-SH-Au_{25}-1.

Synthesis of Ext-SBA-15-Au$_{25}$-5. 250 mg of Ext-SBA-15- Au$_{25}$ was dispersed in 25 mL distilled water. Then 5 mM sodium borohydride solution (10 mL) solution was added into it. After stirring at room temperature for 30 min, the solution was centrifuged and the precipitate was washed with distilled water thrice (3 x 10 mL). The resulting pale beige colored solid was air dried and denoted as Ext-SBA-15-SH-Au$_{25}$-5.

Ligand Exchange of Alkanethiol of Au Cluster (Au$_{140}$) with Mercaptopropyl-Functionalized Mesoporous Silica. The dried Ext-SBA-15-SH (200 mg) was dispersed in 5 mL of 2 μM Au$_{140}$ solution in DCM and stirred at room temperature for 3 h. The solution was centrifuged and the residue was washed with DCM thrice (3 x 10 mL). The resulting pale beige colored solid was air dried. The resulting sample was labeled as Ext-SBA-15-SH-Au$_{140}$.

Synthesis of Ext-SBA-15-Au$_{140}$-1. 250 mg of Ext-SBA-15-Au$_{140}$ was dispersed in 25 mL distilled water. Into the solution was added 1 mM sodium borohydride solution (10 mL). After stirring at room temperature for 30 min, the solution was centrifuged and the precipitate was washed with distilled water thrice (3 x 10 mL). The resulting pale beige colored solid was air dried and labeled as Ext-SBA-15-SH- Au$_{140}$-1.

Synthesis of Ext-SBA-15-Au$_{140}$-5. 250 mg of Ext-SBA-15-Au$_{140}$ was dispersed in 25 mL distilled water. Then 5 mM sodium borohydride solution (10 mL) was added into it and the solution was stirred at room temperature for 30 min. The solution was centrifuged and the residue was washed with distilled water thrice (3 x 10 mL). The resulting pale beige colored solid was air dried and denoted as Ext-SBA-15-SH-Au_{140}-5.

Catalytic Styrene Oxidation. In a typical styrene oxidation reaction, the catalyst, (25 mg nanocatalyst, *e.g*, with 7.9 x 10^{-2} μmol Au in case of Ext-SBA-15-SH-Au_{25}-5 and 1.27 x 10^{-2} μmol Au in case of Ext-SBA-15-SH-Au_{140}-5), was added into a solution of styrene (0.1 mmol), the radical initiator TBHP (5.5 M in decane, 0.76 μL), and anhydrous toluene (1 mL) in a round-bottom glass reaction vessel. Toluene was used as the solvent for the reaction in this case. The solution was stirred at 80 °C in nitrogen atmosphere and the progress of the reaction was monitored with TLC in 20 : 80 ratio of ethyl acetate / hexane solution. The progress of the reaction was further confirmed by gas chromatography-mass spectrometry (GC-MS). The % conversion of the reactants and the yields of the products were obtained by gas chromatography (GC).

Instrumentation. Analytical thin layer chromatography was performed on EM Reagent, 0.25 mm silica gel 60 F_{254} plates obtained from VWR. Visualization was accomplished with UV light. Mass spectra were obtained on a Finnigan LCQ-DUO mass spectrometer. The nitrogen gas adsorption–desorption measurements were carried out on Micromeritics Tristar 3000 volumetric adsorption analyzer after degassing the samples at 160 °C for 12 h. The powder X-ray diffraction of the material was measured by a Histar diffractometer at 295 K using monochromatized Cu Kα (λ = 1.54 Å) radiation. Thermogravimetric analysis (TGA) or decomposition profiles were acquired for the mesoporous materials and the catalyst with a TGA Q 50 thermogravimetric analyzer. The TGA data were collected under a nitrogen atmosphere (60 cm^3/min) in the temperature range of 25 °C to 700 °C at a rate of 10 °C/min. TEM images were taken with TOPCON-002B electron microscope. The catalytic reaction mixtures were analyzed by GC (HP 6850) equipped with FID detector and an HP-1, 30 m long x 0.25 mm ID column. CHN elemental analyses of the catalyst were carried out at Robertson Microlit Laboratories, NJ. The metal (Au) loading in the fresh catalyst as well as the possible leached Au in the reaction solutions was determined by ICP-AES analysis, also at Robertson Microlit Laboratories, NJ.

Reference

(1) Haruta, M.; Kobayashi, T.; Sano, H.; Yamada, N. *Chem. Lett.* **1987**, *16*, 405.

(2) Haruta, M.; Yamada, N.; Kobayashi, T.; Iijima, S. *J. Catal.* **1989**, *115*, 301.

(3) Haruta, M.; Tsubota, S.; Kobayashi, T.; Kageyama, H.; Genet, M. J.; Delmon, B. *J. Catal.* **1993**, *144*, 175.

(4) Hashmi, A. S. K.; Hutchings, G. J. *Angew. Chem. Int. Ed.* **2006**, *45*, 7896.

(5) Noujima, A.; Mitsudome, T.; Mizugaki, T.; Jitsukawa, K.; Kaneda, K. *Chem. Commun.* **2012**, *48*, 6723.

(6) Choudhary, T. V.; Goodman, D. W. *Top. Catal.* **2002**, *21*, 25.

(7) Tanaka, A.; Hashimoto, K.; Kominami, H. *Chem. Commun*. **2011**, *47*, 10446

(8) González-Arellano, C.; Abad, A.; Corma, A.; García, H.; Iglesias, M.; Sánchez, F. *Angew. Chem. Int. Ed.* **2007**, *46*, 1536.

(9) Carrettin, S.; Guzman, J.; Corma, A. *Angew. Chem. Int. Ed.* **2005**, *44*, 2242.

(10) Tsunoyama, H.; Sakurai, H.; Ichikuni, N.; Negishi, Y.; Tsukuda, T. *Langmuir* **2004**, *20*, 11293.

(11) Karimi, B.; Kabiri Esfahani, F. *Chem. Commun.* **2011**, 47, 10452.

(12) Landon, P.; Collier, P. J.; Papworth, A. J.; Kiely, C. J.; Hutchings, G. J. *Chem. Commun.* **2002**, 2058.

(13) Landon, P.; Collier, P. J.; Carley, A. F.; Chadwick, D.; Papworth, A. J.; Burrows, A.; Kiely, C. J.; Hutchings, G. J. *Phys. Chem. Chem. Phys.* **2003**, *5*, 1917.

(14) Corma, A.; Garcia, H. *Chem. Soc. Rev.* **2008**, *37*, 2096.

(15) Haruta, M. *Chem. Record.* **2003**, *3*, 75.

(16) Ma, Z.; Dai, S. *Nano Res.* **2011**, *4*, 3.

(17) Biradar, A. V.; Asefa, T. *Appl. Catal. A.: Gen.* **2012**, *435*, 19.

(18) Das, S.; Asefa, T. *Top. Catal.* **2012**, *55*, 587.

(19) Caron, S. p.; Dugger, R. W.; Ruggeri, S. G.; Ragan, J. A.; Ripin, D. H. B. *Chem. Rev.* **2006**, *106*,2943.

(20) Hayashi, T.; Tanaka, K.; Haruta, M. *J. Catal.* **1998**, *178*, 566.

(21) Pina, C. D.; Falletta, E.; Rossi, M. *Chem. Soc. Rev.* **2012**, *41*, 350.

(22) Lignier, P.; Morfin, F.; Mangematin, S.; Massin, L.; Rousset, J.-L.; Caps. *Chem. Commun.* **2007**, 186.

(23) Patil, N. S.; Uphade, B. S.; Jana, P.; Bharagava, S. K.; Choudhary, V. R. *J. Catal.* **2004**, *223*, 236.

(24) Gajan, D.; Guillois, K.; DelichÃ¨re, P.; Basset, J.-M.; Candy, J.-P.; Caps, V. R.; Coperet, C.; Lesage, A.; Emsley, L. *J. Am. Chem. Soc.* **2009**, *131*, 14667.

(25) Luo, L.; Yu, N.; Tan, R.; Jin, Y.; Yin, D.; Yin, D. *Catal. Lett.* **2009**, *130*, 489.

(26) Turner, M.; Golovko, V. B.; Vaughan, O. P. H.; Abdulkin, P.; Berenguer-Murcia, A.; Tikhov, M. S.; Johnson, B. F. G.; Lambert, R. M. *Nature.* **2008**, *454*, 981.

(27) Liu, Y.; Tsunoyama, H.; Akita, T.; Tsukuda, T. *Chem. Commun.* **2010**, *46*, 550.

(28) Zhu, Y.; Qian, H.; Jin, R. *Chem. Eur. J.* **2010**, 16, 11455.

(29) Zhu, Y.; Qian, H.; Zhu, M.; Jin, R. *Adv. Mater.* **2010**, *22*, 1915.

(30) Zhao, D.; Feng, J.; Huo, Q.; Melosh, N.; Fredrickson, G. H.; Chmelka, B. F.; Stucky, G. D. *Science.* **2008**, 279, 548.

(31) Weissermel, K.; Arpe, H J. *Industrial Organic Chemistry,VCH, Weinheim*, 3rd edn, **1997**.

(32) Dou, M.; Hou, M.; Zhang, H.; Li, G.; Lu, W.; Wei, Z.; Shao, Z.; Yi, B. *ChemSusChem*. **2012**, *5*, 945.

(33) Yan, W.; Chen, B.; Mahurin, S M.; Hagaman, E W.;Dai, S.; Overbury, S H. *J. Phys. Chem B.***2004**, *108*, 2793.

(34) Wang, L.;Wang, H.; Hapala, P.; Zhu, L.; Ren, L.; Meng, X.; Lewis, J P.; Xiao, F-S. *J. Catal*. **2011**, *281*,30.

(35) Yan, Wenfu.; Petkov, V.; Mahurin, S M.; Overbury, S.; Dai, S. *Catal. Commun*. **2005**, *6*, 404.

Chapter V

Core-Shell-Shell Microsphere Containing Au Nanoparticles: Efficient Heterogeneous Nanocatalysts

5.1 Introduction

The recent intense research activities in the fields of nanoscience and nanotechnology have led to the development of various nanomaterials with high surface area-to volume ratios and tunable nanoscale sizes. Owing to these unique structures and inherent catalytic properties, there has also been a surge in interest in the development of various metallic nanomaterials, particularly those composed of Pd,[1,2] Pt,[3,4] and Au[5,6], for heterogeneous catalysis. Unfortunately however, this very property of high surface area-to-volume ratio in these metallic nanomaterials gives rise to high surface energy and greater tendency of particle aggregation, and thus quick loss of their catalytic activities during catalytic reactions.[7-11]

Among many metal nanoparticle catalysts, Au nanocatalysts have recently attracted much attention due to their unprecedented ability to catalyze a large list of useful chemical reactions,[12-23] including olefin epoxidation.[20-23] However, many of the previously reported metallic (or Au) nanoparticle (AuNP)-based catalysts were synthesized either as supported nanocatalysts with no shells around them, or with strongly bound self-assembled monolayer shells composed of organic groups such as alkanethiols and alkyl amines.[24,25] Whereas in the former case, the AuNPs can undergo aggregation, in the latter case the AuNPs' surfaces are less accessible to reactants. Both these processes, therefore, lead to inefficient or rapid loss of catalytic activities in the metal nanoparticles. Another synthetic strategy that has been commonly used to stabilize metallic nanoparticle involves the encapsulation of the nanoparticles with various materials such as metal oxides[26-29] or polymers.[10,30,31] Unfortunately, here also, the resulting nanomaterials become ineffective catalysts because the shells are either too thick or dense, and thus do not let reactants and products diffuse easily into and out from where the encapsulated metallic nanoparticles catalytic sites are.

5.2 General Consideration and Concept

To overcome the aforementioned problems associated with nanoparticle catalysts, we and others have recently proposed an innovative approach to produce core-shell nanostructured catalysts having nanoporous shells around the metallic nanoparticle catalytic sites.[5,32,33] The nanoporous shells of the resulting nanomaterials allow reactants and products to diffuse in and out of the catalytic sites, while at the same time keep the nanoparticles intact and protect them from aggregation. Such nanocatalysts were previously demonstrated using Pd[5] and Pt[33] nanoparticles; however, the surfaces of these metallic nanoparticles undergo oxidation under the synthetic conditions employed. Our goal was to synthesize stable and robust core-shell-shell microspheres containing AuNPs that are sandwiched between metal oxide cores and nanoporous metal oxide shells and their efficient catalytic activity for epoxidation reaction. The synthesis of the materials was achieved by decorating the surface of silica microsphere cores with citrate-capped AuNPs and then encapsulating the AuNPs with nanoporous silica shells. Controlled etching of the outer silica shell produced nanoporous silica shells. The resulting material, which was labeled as porous SiO_2-AuNPs-SiO_2, was successfully used as an efficient heterogeneous catalyst for epoxidation reaction of styrene.

5.2.1 Synthesis of Porous SiO_2-Au-SiO_2 Core-Shell-Shell Microsphere Catalyst

The porous SiO_2-Au-SiO_2 core-shell-shell microsphere nanocatalysts were synthesized by following the synthetic procedure depicted in Scheme 5.1.

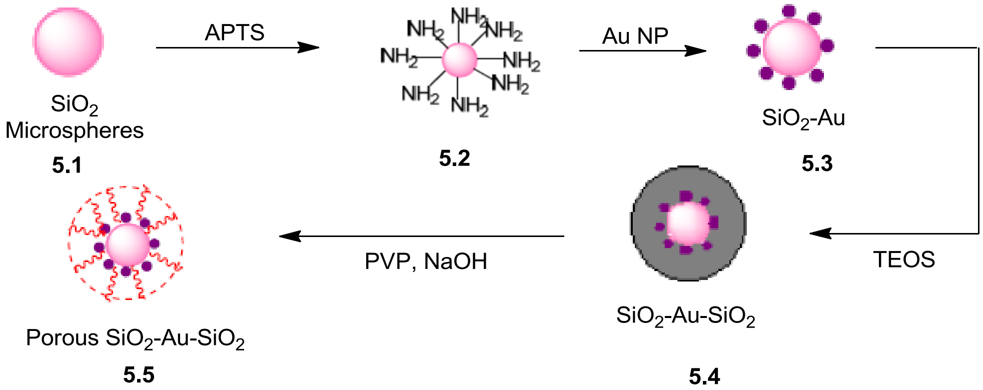

***Scheme 5.1*:** Schematic representation of the synthesis of porous SiO_2-Au-SiO_2 Core-Shell-Shell microsphere nanocatalysts.

First, SiO_2 microspheres were synthesized according to the Stöber method, and their surfaces were functionalized with primary amine groups using APTS.[34] The functionalization of the SiO_2 microspheres with amine groups was confirmed by thermogravimetric analysis (Figure 5.1), FT-IR spectroscopy (Figure 5.2), and elemental analysis.

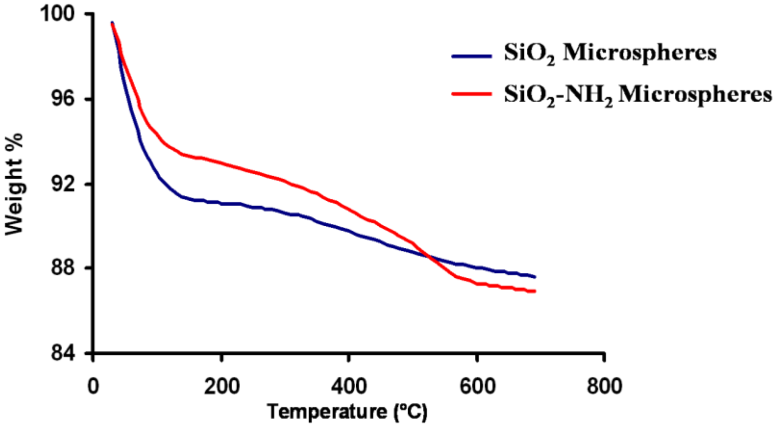

***Figure 5.1*:** Thermogravimetric traces of SiO_2 and amine-functionalized SiO_2 (SiO_2-NH_2) microspheres.

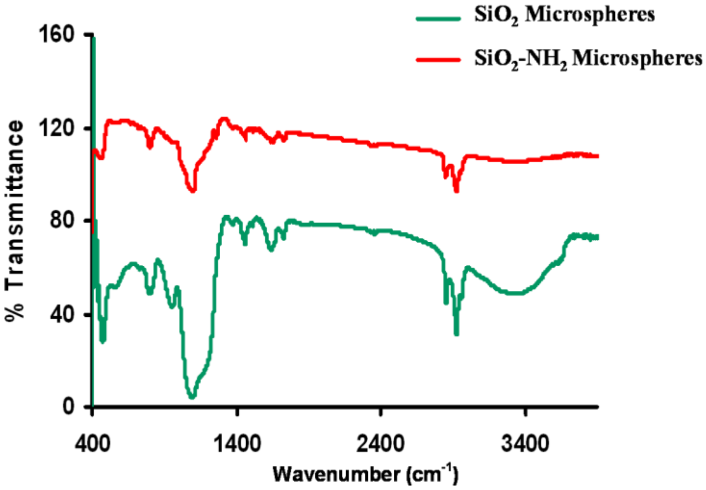

***Figure 5.2*:** FT-IR spectra of SiO_2 and amine-functionalized SiO_2 (SiO_2-NH_2) microspheres.

In both spectra, many similar peaks were observed, as expected. These include a peak at ~1100 cm^{-1} corresponding to Si–O–Si stretching and broad peaks at between 3000 – 3500 cm^{-1} corresponding to O–H and N–H bond stretchings. Furthermore, the spectra show peaks corresponding to N–H or O–H bending at ~1555 cm^{-1}. More importantly however, the spectrum for SiO_2-NH_2 microspheres show a peak at ~900 cm^{-1} that corresponds to N–H wagging, which is not observable in the spectrum for SiO_2. The peaks are consistent with that reported for SiO_2 nanospheres and amine-functionalized silicas reported previously.[35]

Then, AuNPs were synthesized by the Turkevich method,[36] by reducing 250 µM of aqueous $HAuCl_4$•xH_2O solution with dilute sodium borohydride in the presence of sodium citrate. The citrate-capped AuNPs (~16 nm) were mixed with the amine-functionalized SiO_2 microspheres. This led to the chemisorption of the AuNPs onto the surfaces of the amine-functionalized SiO_2 microspheres because the amine groups on the SiO_2 microspheres replaced the citrate ions on the AuNPs when the two contacted. This was a favorable process because of the stronger interaction between the amine groups and AuNPs compared to the weaker interaction between the citrate ions and the AuNPs. The resulting SiO_2-AuNPs core-shell microspheres were further coated with silica shells via the sol-gel chemistry involving TEOS.[37] This produced SiO_2-AuNPs-SiO_2 core-shell-shell microspheres. Finally, controlled etching of the outer silica shells of the SiO_2-AuNPs-SiO_2 core-shell-shell microspheres with an aqueous solution of NaOH resulted in the porous SiO_2-AuNPs-SiO_2 core-shell-shell microspheres (nanocatalysts).

TEM images of the materials obtained after each step of the synthesis are shown in Figure 5.3. The TEM images in Figure 5.3a, b show well-dispersed AuNPs on the surfaces of the amine-functionalized SiO_2 microspheres. The TEM image of SiO_2-AuNPs-SiO_2 (Figure 5.3c) shows the presence of uniform silica shells around the SiO_2-AuNPs core-shell microspheres. From the TEM images, this SiO_2 shell, which was formed from the hydrolysis and condensation of 0.25 mL TEOS in ethanol, was found to be ~50 nm thick. It is worth noting that SiO_2-AuNPs-SiO_2 microspheres with thicker silica shells could be produced by using higher amount of TEOS; however, higher amount of TEOS was also found to lead to the formation of some smaller SiO_2 microspheres by themselves (see Figure 5.4). The highly nanoporous SiO_2 shells around the SiO_2-AuNP-SiO_2 core-shell-shell microspheres (Figure 5.3d–f) were produced by controlled etching of the outer SiO_2 shells of the latter with aqueous NaOH solution in the presence of PVP.[38] PVP's function in the synthesis is to protect the very outer SiO_2 shells from being etched significantly with NaOH solution, by forming strong hydrogen bonding between its carbonyl groups and the surface silanol groups of the SiO_2 shells.[39,40] This allows the NaOH solution to penetrate through the SiO_2 shells, etch the inner parts of the SiO_2 shells that are not protected by PVP, and produce uniform nanoporous SiO_2 shells. The use of appropriate etching times during the synthesis of the microsphere catalysts was also found to be crucial for the formation of intact nanoporous SiO_2 shells. Whereas relatively shorter etching times resulted in only moderate etching of the outer SiO_2 shells of the SiO_2-AuNP-SiO_2 core-shell-shell microspheres, prolonged etching times of >180 min led to complete dissolution of the SiO_2 shells as well as even the inner SiO_2 cores. Thus, by using optimum etching times, which we found to be ~90 min, reasonably intact nanoporous SiO_2 shells with monodisperse pore-sizes were formed around the AuNPs of the SiO_2-AuNP-SiO_2 core-shell-shell microspheres. The nanoporous SiO_2 shells as well as the residual PVP on the SiO_2-AuNP-SiO_2 core-shell-shell microspheres were able to not only protect the AuNPs from aggregation, but also let reactants and products diffuse in and out the catalytic sites during catalytic reactions.

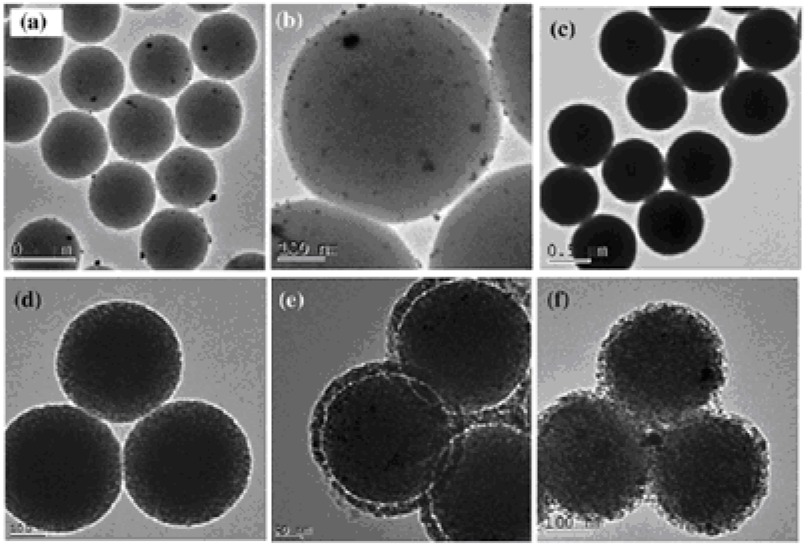

***Figure 5.3*: TEM images of a, b SiO_2-AuNP core-shell microspheres, c SiO_2-AuNPs-SiO_2 core-shell-Shell microspheres, and d–f etched or porous SiO_2-AuNPs-SiO_2 core-shell-shell microspheres (D = etched for 30 min, E = etched for 60 min, and F = etched for 90 min).

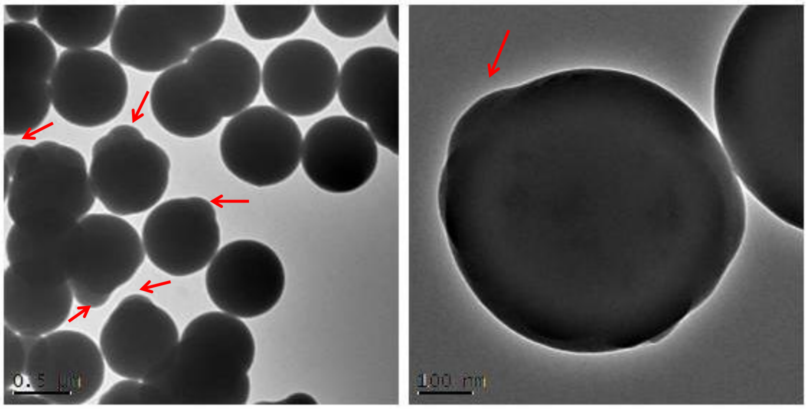

Figure 5.4**:** TEM image showing thick and non-uniform silica shells (indicated by red arrows) when a large amount of TEOS was used for making the silica shells around the SiO_2-AuNP core-shell microspheres.

The presence of AuNPs in the SiO_2-Au, and SiO_2-AuNP-SiO_2, and porous SiO_2-AuNPs-SiO_2 microspheres were confirmed by powder X-ray diffraction (XRD) (Figure 5.5). The XRD patterns showed three well-defined peaks at 2θ values of 38, 44, 65 and 78°, which were indexed as (111), (200), (220) and (311), respectively, of metallic gold.[41] The intensities of these peaks were lower in the XRD patterns of SiO_2-AuNPs-SiO_2 and porous SiO_2-AuNPs-SiO_2, possibly due to the fact that the AuNPs in these materials were coated by SiO_2 shells.

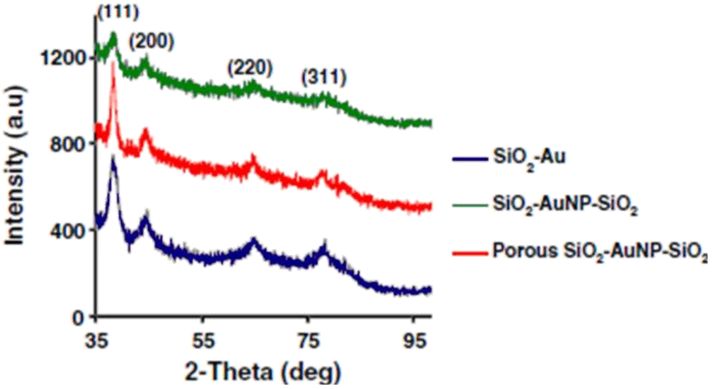

***Figure 5.5*:** Powder XRD patterns of SiO_2-Au core-shell microspheres, and SiO_2-AuNP-SiO_2 and porous SiO_2-AuNP-SiO_2 core-shell-shell microspheres.

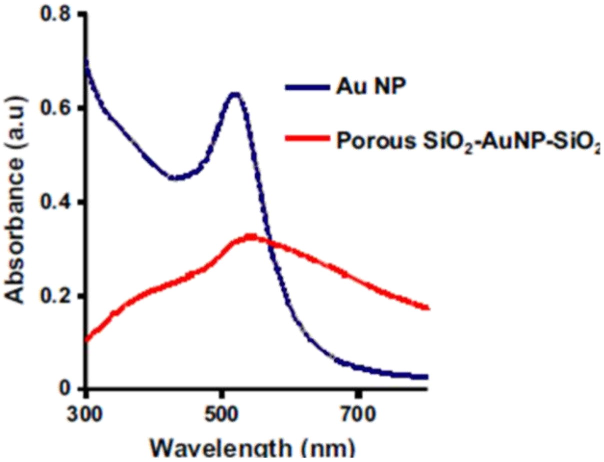

***Figure 5.6*:** UV–Vis spectra of citrate-capped Au nanoparticles (AuNPs) in aqueous solution and porous SiO_2-AuNP-SiO_2 core-shell-shell microspheres.

The AuNPs in the porous SiO_2-AuNPs-SiO_2 nanocatalyst were also characterized by solid-state UV–Vis spectroscopy (Figure 5.6), which showed a broad band at ~534 nm that is characteristic of AuNPs. In contrast the UV–Vis spectrum of the parent citrate-capped AuNPs in solution showed a plasmon band at 510 nm (Figure 5.6). The red shift of the absorption band for the AuNPs in the porous SiO_2-AuNPs-SiO_2 compared to that of citrate-capped AuNPs in solution could be due to the possible optical coupling of the absorption bands of neighboring AuNPs on the surface of the SiO_2-AuNPs-SiO_2 core-shell-shell microspheres.[42]

5.2.2 Control Experiments

A control experiment involving attempted epoxidation reaction of styrene with just SiO_2 microspheres containing no AuNPs was performed (Scheme 5.2).

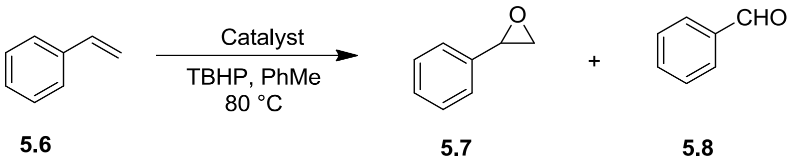

***Scheme 5.2*:** Styrene epoxidation with various catalysts.

The reaction gave a 9% conversion of styrene in 5 h and 22% conversion of styrene in 10 h at 80 °C. The reaction product consisted of more benzaldehyde than styrene oxide. Next up, another control reaction was performed by using as catalyst the etched SiO_2 microspheres, which were prepared by etching SiO_2 microspheres with aqueous NaOH solution. This reaction gave higher styrene conversion of 30% in 5 h and 35% in 10 h at 80 °C. The higher reactant conversions obtained with etched SiO_2 microspheres compared with the ones obtained with unetched SiO_2 microspheres were not unprecedented when considering the fact that: 1) the former possessed higher surface area per unit gram of material, and 2) silica itself was previously implicated to catalyze epoxidation reactions, albeit moderately.[43,44] Not surprisingly, the catalytic activity in epoxidation reaction by silica is often associated with the surface silanol groups on the material. Since higher density of silanol groups exist in the etched/nanoporous SiO_2 microspheres compared to their unetched counterparts, the etched SiO_2 microspheres should indeed exhibit higher catalytic activities than their dense counterparts (Figure 5.7).

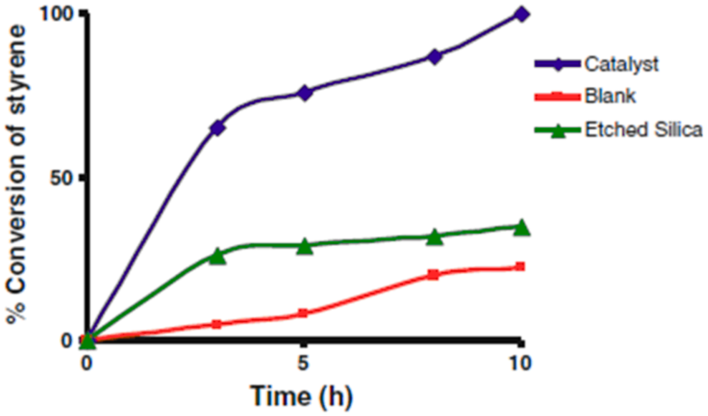

Figure 5.7: Plot of % conversion of styrene versus reaction time of styrene epoxidation reaction using porous SiO_2-AuNPs-SiO_2 core-shell-shell microspheres as catalyst in toluene at 80 °C under nitrogen atmosphere.

An additional control experiments, blank reactions without any material/catalyst were run in anhydrous toluene at different temperatures (RT, 50 °C and 80 °C) (Table 5.1). In 24 h, the reaction gave only 6% conversion of styrene at room temperature and 13% conversion of styrene at 50 °C, but a higher conversion of styrene (66%) at 80 °C. In all cases, again benzaldehyde was found to be the predominant product, with selectivity of 81% at 80 °C in 24 h.

***Table 5.1*:** Control reaction of styrene oxidation in TBHP and toluene at different temperatures without catalyst.

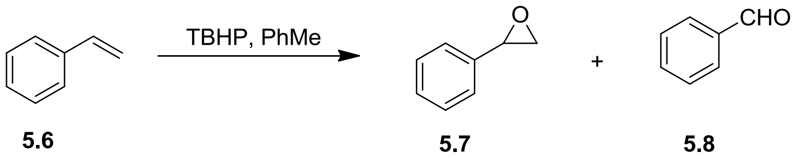

Entry	**Temperature (°C)**	**Time (h)**	**Conv. of Styrene (%)**	**Selectivity to Benzaldehyde (%)**	**Selectivity to Styrene Oxide (%)**
1	RT	24	6	~100	0
2	50	24	13	~100	0
3	80	24	66	53	13

Hence, it can be concluded that the epoxidation reaction is slow both without a catalyst as well as in the presence of SiO_2 microspheres containing no AuNPs, especially at low temperatures. Furthermore, the reaction produces predominantly benzaldehyde (or less epoxide) under these conditions.

5.2.3 Catalytic Activity of Porous SiO_2-AuNP-SiO_2 Core-Shell-Shell Microspheres in Epoxidation of Styrene

The catalytic reaction of styrene epoxidation with the porous SiO_2-AuNPs-SiO_2 core-shell-shell microsphere catalyst in anhydrous toluene at 80 °C in the presence of TBHP under air or nitrogen atmosphere was tested (Figure5.6; Table 5.2). When the reaction was performed under air atmosphere, styrene was found to undergo oxidation almost completely in 12 h, giving benzaldehyde, styrene oxide and traces of benzoic acid, with 54% selectivity towards styrene oxide. However, when the reaction was carried out under nitrogen atmosphere, the oxidation of styrene into benzoic acid was reduced, and only benzaldehyde and styrene oxide were formed (or better reaction selectivity was obtained). Thus, all the subsequent reactions were performed under nitrogen atmosphere. Specifically, the reaction gave 75% conversion of styrene in 5 h and ~100% conversion of styrene in 10 h, with 56% and 61% selectivity towards styrene oxide, respectively, with the porous SiO_2-AuNPs-SiO_2 core-shell-shell microsphere catalyst in nitrogen (Table 5.2).

Table 5.2: Catalytic activity of porous SiO_2-AuNPs-SiO_2 in styrene epoxidation reaction under nitrogen atmosphere.

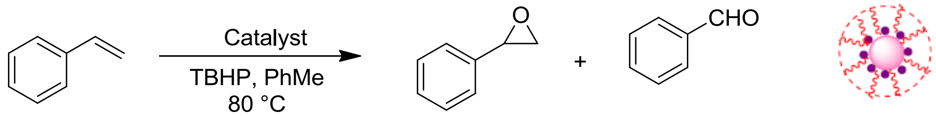

5.6 **5.7** **5.8** Porous SiO_2-Au-SiO_2 Catalyst

Entry	Temperature (°C)	Solvent)	Time (h)	(%) Conv.	Selectivity to Styrene Oxide (%)
1	80	PhMe	5	75	56
2	80	PhMe	10	~100	61
3	80	CH_3CN	5	20	52
4	80	CH_3CN	24	78	58

Hence, the catalytic efficiency of the porous SiO_2-AuNPs-SiO_2 microspheres was clearly much higher than those obtained for the control experiments. Furthermore, the results indicated that the AuNPs in SiO_2-AuNPs-

SiO_2 were responsible for the higher catalytic activities of the materials in the epoxidation reaction.

The catalytic reaction with porous SiO_2-AuNP-SiO_2 microspheres in the polar solvent acetonitrile at 80 °C was also conducted. The results of this catalytic reaction are shown in Table 5.2. The conversion of styrene was only 20% with 52% selectivity towards the epoxide product in 5 h, and the conversion of styrene was 78% with 58% selectivity towards the epoxide product in 24 h. This clearly indicates that the reaction is slow in acetonitrile.

5.2.4 Scope of the Reaction

To study the substrate scope of the porous SiO_2-AuNP-SiO_2 nanocatalyst in epoxidation reaction of olefins, *trans*-stilbene was also used as a substrate for the reaction (Scheme 5.3). The reaction was performed with the catalyst in presence of the radical initiator TBHP in an inert atmosphere at 80 °C using toluene as the solvent. The conversion of trans-stilbene was found to be 52% in 6 h, with 55% selectivity towards *trans*-stilbene oxide.

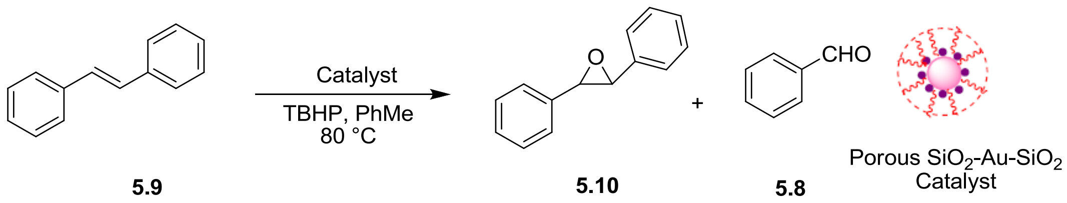

Scheme 5.3**:** Epoxidation of *trans*-stilbene catalyzed by the porous SiO_2-AuNP-SiO_2 nanocatalyst.

5.2.5 Recyclability of the Catalyst

The porous SiO_2-AuNP-SiO_2 core-shell-shell nanocatalyst was shown to be easily recyclable, at least three times without losing its catalytic activity (Table 5.3).

***Table 5.3*: Test of recyclability of the catalyst in epoxidation of styrene.**

Entry	**Time (h)**	**(%) Conv.**	**Selectivity to Styrene Oxide (%)**
1st run	12	~100	63
2nd run	12	100	60
3rd run	12	100	60

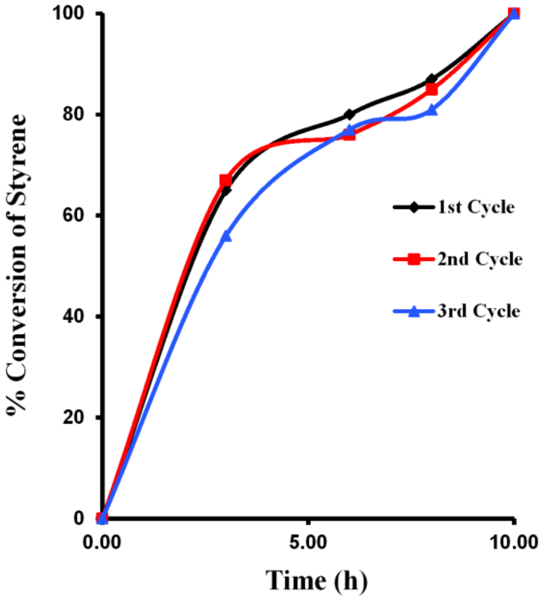

***Figure 5.8*: % Conversion vs time graphs for styrene epoxidation reaction catalyzed by porous SiO_2-AuNPs-SiO_2 microsphere catalysts.**

The recyclability test was performed by recovering the material after a given reaction and reusing the material as a catalyst for another catalytic reaction. The material was recovered by centrifugation of the reaction mixture; decanting the supernatant; and washing the precipitate with toluene twice, followed by ethanol, and drying it. The rate of the reaction barely decreased for the recycled porous SiO_2-AuNP-SiO_2 core-shell-shell nanocatalyst, at least in three cycles (Figure 5.8).

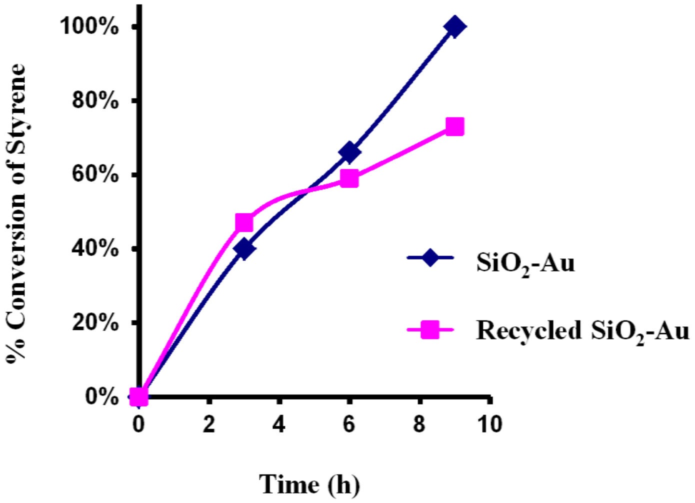

***Figure 5.9*:** % Conversion vs time graphs for styrene epoxidation reaction catalyzed by SiO_2/AuNPs Core-Shell microsphere catalysts.

However, the control nanomaterial containing no porous silica shell (i.e., SiO_2-AuNP core-shell nanocatalyst) showed loss of catalytic activity upon recycling (Figure 5.9) The result shows a decrease in catalytic activity of the catalyst as a result of aggregation of the nanoparticles in this material compared to the porous SiO_2-AuNP-SiO_2 core-shell-shell microspheres. Furthermore, the porous SiO_2-AuNP-SiO_2 core-shell-shell nanocatalyst proved to have intact AuNPs.as shown with the characteristic strong plasmon band at ~530 nm, which is associated with Au nanoparticles, even after three reaction cycles (Figure 5.10). The spectrum shows the characteristic plasmon band of Au nanoparticles at around 530 nm, marked by an arrow. This result indicates the stability of the Au nanoparticles when confined in the core-shell-shell microspheres.

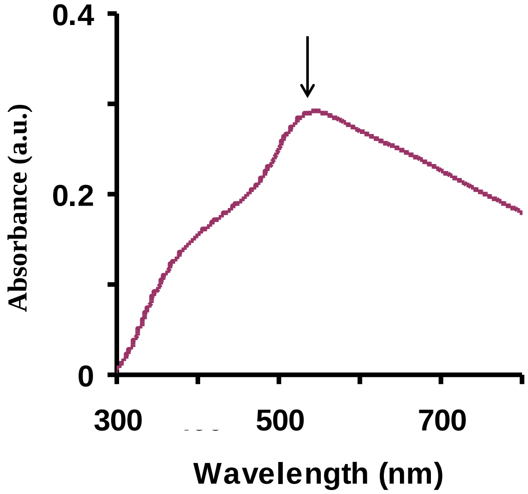

Figure 5.10**:** UV–Vis spectrum of recycled porous SiO_2-AuNP-SiO_2 core-shell-shell microspheres after three reaction cycles.

An experiment was also performed to determine whether or not leaching of Au from the core-shell-shell microspheres into the reaction mixture took place (Figure 5.11). To perform this, the catalyst was centrifuged and separated from the reaction mixture, and the supernatant was then run by itself. There was very little further conversion of styrene even after 3 h reaction time when the supernatant was stirred by itself after the catalyst was removed from it (Figure

5.11). The rate of reaction decreased significantly after separating the solid catalyst and never reached 100 % in 10 h as it did with the catalyst in Figure 5.7.

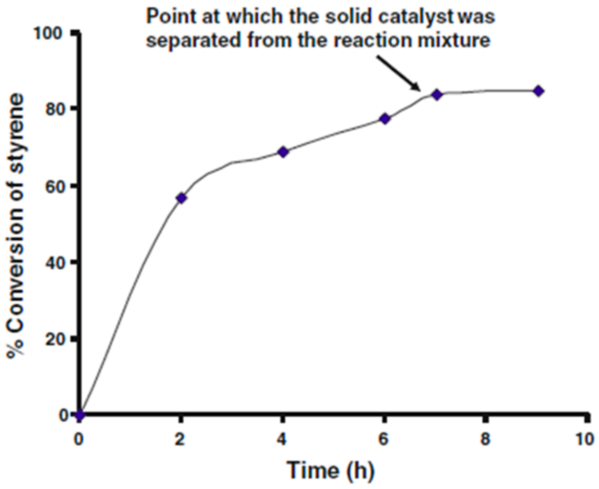

Figure 5.11**:** % Conversion of styrene *vs* time to test possible leaching of Au catalyst.

The result was further corroborated by elemental analyses of the catalyst as well as the reaction mixture. The weight percent of Au analyzed by ICP-AES in the fresh catalyst, in the catalyst after third cycle, and in the reaction mixture after third cycle are given in Table 5.4. The results show that there was insignificant amount of Au leached from the nanocatalyst or insignificant amount of Au present in the reaction mixture. This clearly indicates the high stability of the Au nanoparticles in porous SiO_2-AuNP-SiO_2 nanocatalyst towards leaching.

Table 5.4**:** Elemental analysis obtained with ICP-AES of Au in the recycled catalysts as well as in the reaction mixtures.

Entry	**Au (ppm)**	**Au (%)**	**Au (mmol)**
Catalyst	7632	0.76	2.4×10^{-3}
Catalyst after 3rd cycle	5368	0.54	2.18×10^{-3}
Reaction solution recovered from 3rd cycle	7	0.01	4.05×10^{-5}

5.3 Summary

We have developed a synthetic method to porous SiO_2-AuNP-SiO_2 core-shell-shell microsphere catalysts containing AuNPs and demonstrated their efficient catalytic activities for epoxidation of styrene and *trans*-stilbene with TBHP as an oxidant. The material was synthesized by depositing citrate-capped AuNPs on amine-functionalized silica microspheres, then by coating the AuNPs with silica shells using the sol-gel process, and finally by etching the outer silica shells into nanoporous silica with NaOH solution. The resulting nanoporous silica shells had large enough pore to let reactants and products diffuse in and out of the AuNP catalytic sites, while at the same time they were robust enough to keep the AuNPs stable and intact. The resulting nanocatalyst showed good catalytic activity in styrene and trans-stilbene epoxidation giving moderate selectivity to the corresponding epoxide products. The catalyst was also shown to be recyclable without a substantial loss of its catalytic activity, at least in three cycles.

Experimental Section

Synthesis of Citrate-Capped Au Nanoparticles (AuNPs): The synthesis of citrate-capped AuNPs was adopted from Turkevich method.[36] Typically, to a 250 l M $HAuCl_4$ solution in water (100 mL) was added 0.025 M aqueous sodium citrate solution (1 mL). The solution was stirred for 2 min. Then 2.25 mL of 10 mM sodium borohydride solution was quickly added into the solution under stirring. Within 1 min of stirring, the solution produced a dark red solution containing citrate-capped AuNPs.

Synthesis of Silica Microspheres: Silica microspheres were synthesized by following the Stöber method.[45] Typically 6.2 mL of TEOS was added into a solution containing 6.5 mL of ammonium hydroxide solution (28–30 %), 100 mL of ethanol, and 7 mL of water. After 3 h of stirring at room temperature, a colloidal solution of silica microspheres with 325 nm diameter was obtained. The solution was centrifuged, and the precipitate was washed with ethanol three times via centrifugation, decantation and redispersion. The resulting solid sample was finally dried under ambient conditions, producing silica (SiO_2) microspheres.

Functionalization of Silica Microspheres with Primary Amine Groups: 1 g of SiO_2 microspheres was dispersed in anhydrous toluene (200 mL). This solution was mixed with 3-aminopropyltrimethoxysilane (APTS) (1.5 mL) and stirred at 80 °C for 6 h to functionalize the surfaces of the SiO_2 microspheres with primary amine groups. The solution was centrifuged and the precipitate was washed with toluene, followed by ethanol via centrifugation, decantation, and redispersion. The final precipitate was dispersed in 20 mL distilled water to make a stock solution of amine-functionalized SiO_2 microspheres.

Synthesis of SiO_2-AuNPs Core-Shell Microspheres: The AuNPs prepared above were adsorbed onto the surface of SiO_2 microspheres by stirring the above amine-functionalized SiO_2 microspheres (4.8 mL) with a solution of AuNPs (75 mL) and water (125 mL). The solution was stirred for 10 min and then centrifuged. The resulting precipitate was washed with water twice via centrifugation, decantation, and redispersion. The precipitate was dispersed in 8.6 mL water to give a colloidal solution of SiO_2-AuNPs core-shell microspheres (i.e., SiO_2 microsphere cores decorated with AuNPs shells).

Synthesis of SiO_2-AuNPs-SiO_2 Core-Shell–Shell Microspheres: The solution containing SiO_2-AuNPs core-shell microspheres (2 mL) was dispersed in a mixture of ethanol (100 mL), water (12.5 mL), and ammonium hydroxide solution (5 mL). Then, 0.25 mL of TEOS was added into this solution to encapsulate the SiO_2-AuNPs core-shell microspheres with silica shells (~50 nm-thick). After 12 h of stirring, the solution was centrifuged, and the precipitate was washed with ethanol twice and redispersed in 25 mL of water, giving a colloidal solution of SiO_2-AuNPs-SiO2 core-shell-shell microspheres.

Controlled Etching of the Silica Shell of SiO_2-AuNPs-SiO_2 Core-Shell-Shell Microspheres: To etch the outer silica shells of SiO_2-AuNPs-SiO_2 core-shell-shell microspheres into nanoporous silica shells, first 1 g of PVP–K15 (Polyvinylpyrrolidone) was dissolved in 25 mL solution of SiO_2-Au NPs-SiO_2 under stirring at 100 °C for 3 h.[33] After cooling the solution to room temperature, 0.8 g of NaOH was added into it. The solution was then stirred for different periods of time, that is, 30, 60, or 180 min. This resulted in different degree of etching of the silica shells. After centrifugation and washing the precipitate with water and ethanol three times (3 x 20 mL), porous SiO_2-AuNPs-SiO_2 core-shell-shell microspheres containing nanoporous silica shells around the AuNPs were obtained.

Catalytic Styrene Epoxidation Reaction: In a typical styrene epoxidation reaction, the catalyst, i.e., porous SiO_2-AuNP-SiO_2 microspheres (25 mg, 0.96 μmol Au), was mixed with a solution of styrene (0.1 mmol), the radical initiator TBHP (5.5 M in decane, 0.76 μL), and anhydrous toluene (1 mL), which was used as a solvent, in a round-bottom glass reaction vessel. The solution was stirred at 80 °C in nitrogen (or air), and the progress of the reaction was monitored by thin layer chromatography (TLC) in 20:80 ratio of ethyl acetate/hexane solution. The % conversion of the reactants and the yields of the products were obtained by gas chromatography (GC). The formation of the products was further confirmed by gas chromatography-mass spectrometry (GC–MS). For the catalytic *trans*-stilbene epoxidation reaction, the same reactant:

catalyst ratio and similar reaction conditions as those for styrene epoxidation were used. The TOF values of the reaction were obtained by dividing the mole of reactant converted into products in a given time by the mole of Au in the 25 mg SiO_2-AuNP-SiO_2 microspheres.

Reference

(1) Lee, J.; Park, J. C.; Song, H. *Adv. Mat.* **2008**, *20*, 1523.
(2) Arnal, P. M.; Comotti, M.; Schüth, F. *Angew. Chem. Int. Ed.* **2006**, *118*, 8404.
(3) Lyons, O. D.; Musselwhite, N. E.; Carl, L. M.; Manbeck, K. A.; Marsh, A. L. *Langmuir.* **2010**, *26*, 16481.
(4) Kuhn, J. N.; Huang, W.; Tsung, C.-K.; Zhang, Y.; Somorjai, G. A. *J. Am. Chem. Soc.* **2008**, *130*, 14026.
(5) Wang, Y.; Biradar, A. V.; Duncan, C. T.; Asefa, T. *J. Mater Chem.* **2010**, *20*, 7834.
(6) Galeano, C.; Güttel, R.; Paul, M.; Arnal, P.; Lu, A.-H.; Schüth, F. *Chem. Eur. J.* **2011**, *17*, 8434.
(7) Narayanan, R.; El-Sayed, M. A. *J. Am. Chem. Soc.* **2004**, *126*, 7194.
(8) Budroni, G.; Corma, A. *Angew. Chem. Int. Ed.* **2006**, *45*, 3328.
(9) Yan, W.; Mahurin, S.; Overbury, S.; Dai, S. *Top. Catal.* **2006**, *39*, 199.
(10) Rioux, R. M.; Song, H.; Hoefelmeyer, J. D.; Yang, P.; Somorjai, G. A. *J. Phy. Chem. B.* **2004**, *109*, 2192.
(11) Narayanan, R.; El-Sayed, M. A. *J. Phy. Chem. B.* **2005**, *109*, 12663.
(12) Haruta, M.; Kobayashi, T.; Sano, H.; Yamada, N. *Chem. Lett.* **1987**, *16*, 405.
(13) Hughes, M. D.; Xu, Y.-J.; Jenkins, P.; McMorn, P.; Landon, P.; Enache, D. I.; Carley, A. F.; Attard, G. A.; Hutchings, G. J.; King, F.; Stitt, E. H.; Johnston, P.; Griffin, K.; Kiely, C. J. *Nature* **2005**, *437*, 1132.
(14) Sinha, A. K.; Seelan, S.; Tsubota, S.; Haruta, M. *Angew. Chem. Int. Ed.* **2004**, *43*, 1546.
(15) Wittstock, A.; Zielasek, V.; Biener, J.; Friend, C. M.; Bäumer, M. *Science.* **2010**, *327*, 319.
(16) Beaumont, S. K.; Kyriakou, G.; Lambert, R. M. *J. Am. Chem. Soc.* **2010**, *132*, 12246.
(17) Kyriakou, G.; Beaumont, S. K.; Humphrey, S. M.; Antonetti, C.; Lambert, R. M. *ChemCatChem.* **2010**, *2*, 1444.
(18) Kidwai, M.; Bansal, V.; Kumar, A.; Mozumdar, S. *Green Chem.* **2007**, *9*, 742.
(19) Aguilar, D.; Contel, M.; Urriolabeitia, E. P. *Chem. Eur. J.* **2010**, *16*, 9287.
(20) Choudhary, V. R.; Dumbre, D. K. *Catal.Commun.* **2009**, *10*, 1738.
(21) Patil, N. S.; Uphade, B. S.; Jana, P.; Bharagava, S. K.; Choudhary, V. R. *J. Catal.* **2004**, *223*, 236.
(22) Patil, N. S.; Uphade, B. S.; Jana, P.; Sonawane, R. S.; Bhargava, S. K.; Choudhary, V. R. *Catal. Lett.* **2004**, *94*, 89.
(23) Bawaked, S.; Dummer, N. F.; Bethell, D.; Knight, D. W.; Hutchings, G. J. *Green Chem.* **2011**, *13*, 127.
(24) Turner, M.; Golovko, V. B.; Vaughan, O. P. H.; Abdulkin, P.; Berenguer-Murcia, A.; Tikhov, M. S.; Johnson, B. F. G.; Lambert, R. M. *Nature* **2008**, *454*, 981.
(25) Xing, Y.; Liu, Z.; Suib, S. L. *Chem. Mater.* **2007**, *19*, 4820.

(26) Shi, Y.-L.; Asefa, T. *Langmuir*. **2007**, *23*, 9455.

(27) Shokouhimehr, M.; Piao, Y.; Kim, J.; Jang, Y.; Hyeon, T. *Angew. Chem. Int. Ed.* **2007**, *46*, 7039.

(28) Yin, Y.; Rioux, R. M.; Erdonmez, C. K.; Hughes, S.; Somorjai, G. A.; Alivisatos, A. P. *Science*. **2004**, *304*, 711.

(29) Yu, K.; Wu, Z.; Zhao, Q.; Li, B.; Xie, Y. *J. Phy. Chem. C.* ***2008***, *112*, 2244.

(30) Teranishi, T.; Miyake, M. *Chem. Mater.* **1998**, *10*, 594.

(31) Bianchi, C.; Porta, F.; Prati, L.; Rossi, M. *Top. Catal.* **2000**, *13*, 231.

(32) Joo, S. H.; Park, J. Y.; Tsung, C.-K.; Yamada, Y.; Yang, P.; Somorjai, G. A. *Nat Mater.* **2009**, *8*, 126.

(33) Ge, J.; Zhang, Q.; Zhang, T.; Yin, Y. *Angew. Chem. Int. Ed.* **2008**, *47*, 8924.

(34) Pastoriza-Santos, I.; Gomez, D.; Perez-Juste, J.; Liz-Marzan, L. M.; Mulvaney, P. *Phys. Chem. Chem. Phys.* **2004**, *6*, 5056.

(35) Maria Chong, A. S.; Zhao, X. S. *J. Phys. Chem. B.* **2003**, *107*, 12650.

(36) Turkevich, J.; Stevenson, P. C.; Hillier, J. *Discuss. Faraday. Soc.* **1951**, *11*, 55.

(37) Lu, Y.; Yin, Y.; Li, Z.-Y.; Xia, Y. *Nano. Lett.* **2002**, *2*, 785.

(38) Zhang, Q.; Zhang, T.; Ge, J.; Yin, Y. *Nano. Lett.* **2008**, *8*, 2867.

(39) Gun'ko, V. M.; Zarko, V. I.; Voronin, E. F.; Goncharuk, E. V.; Andriyko, L. S.; Guzenko, N. V.; Nosach, L. V.; Janusz, W. *J. Colloid. Interface. Sci.* **2006**, *300*, 20.

(40) Cohen Stuart, M. A.; Fleer, G. J.; Bijsterbosch, B. H. *J. Colloid. Interface Sci.* **1982**, *90*, 321.

(41) Irzh, A.; Perkas, N.; Gedanken, A. *Langmuir* **2007**, *23*, 9891.

(42) Storhoff, J. J.; Lazarides, A. A.; Mucic, R. C.; Mirkin, C. A.; Letsinger, R. L.; Schatz, G. C. *J. Am. Chem. Soc.* **2000**, *122*, 4640.

(43) Stanger, K. J.; Angelici, R. J. *Energy Fuels.* **2006**, *20*, 1757.

(44) Breton, G. W.; Fields, J. D.; Kropp, P. J. *Tetrahedron Lett.* **1995**, *36*, 3825.

(45) Stöber, W.; Fink, A.; Bohn, E. *J. Colloid. Interface. Sci.* **1968**, *26*, 62.

Chapter-VI

Core-Shell-Shell Microspheres Containing PAMAM Encapsulated Ultrasmall Pd Nanoparticles as Heterogeneous Nanocatalysts

6.1 Introduction

As discussed in the previous chapters, catalysis is indispensable for the production of various fine and commodity chemicals, pharmaceuticals and fossil fuel-based products.[1] At the heart of catalysis are catalysts, which can generally be divided into two major groups: homogeneous catalysts and heterogeneous catalysts. Most of the catalysts used in industries are heterogeneous catalysts, which comprise of solid catalysts in form of highly dispersed metals or metal nanoparticles on metal oxide support materials.[2,3] The incorporation of nanoparticles on heterogeneous catalytic systems has advantage because of the large surface area-to-volume ratio of nanoparticles as well as the inherent unique catalytic activities of many nanomaterials as a result of their surface/electronic properties. The very high surface area-to-volume ratio of nanoparticles can, however, also give rise to high surface energy, and thereby greater tendency of nanoparticle aggregation and quick loss of their catalytic activities during catalytic reactions.[3-5] Furthermore, many catalytic reactions are carried out with stirring under high temperature in the presence of solvents, *i.e.*, conditions that unfortunately assist nanoparticle aggregation. On the other hand, the catalytic activities of many nanomaterials strongly depend on the nanoparticles’ sizes and shapes and the presence/absence of active faceted surfaces on them that promote a given reaction.[6] Collectively, therefore, stabilization of nanoparticles and their sizes are highly important to obtain catalysts with high and stable catalytic activities and desired catalytic properties.

The synthesis of nanomaterials with very stable surfaces or that can accommodate or stabilize a large density of specific catalytic active groups are among the major goals in the development of efficient heterogeneous catalysts.[7] In order to prevent the agglomeration of nanoparticles several stabilizing agents such as organic ligands,[8-11] polymers[12-15]or long chain surfactants[16-18] can be used. For example, many stable polymer stabilized metal nanoparticles have been synthesized via reduction of metal salt solutions with high boiling-point alcohols such as ethylene glycols, in a process commonly known as the polyol process.[19]

6.2 Dendrimer Encapsulated Nanoparticles (DENs)

Dendrimers are monodispersed macromolecules, with well-defined branched three-dimensional architectures. Their structure and chemical properties can be controlled by modifying the core, the type and number of branches, and the terminal functional groups in them.[20] Because of their branched structures with metal complexing groups, many dendrimers have been successfully used to encapsulate metallic nanoparticles and form dendrimer-encapsulated nanoparticles (DENs) that can exhibit catalytic activities in various reactions. However, the nature of dendrimers as stabilizing agent for nanoparticles is fundamentally different from other stabilizers, such as simple organic capping groups such as alkanethiols because dendrimers not only coordinate to the nanoparticle surfaces but also encapsulate them. Thus, the nanoparticles within DENs are sterically confined to the interior region of the dendrimer and are relatively more stable compared with those stabilized by simple organic groups such as alkanethiols.[21]

The basic approach for synthesizing DENs is comprised of two steps (Scheme 6.1). First, appropriate metal ions are mixed with a dendrimer solution. This allows the metal ions to be encapsulated within the dendrimer cores.[22] Then, a chemical reducing agent is added to the solution to reduce the dendrimer entrapped metal ions and form the DENs. Using this approach, a wide range of metal nanoparticles within dendrimers have been synthesized by using solutions containing Pt^{2+}, Pd^{2+}, Au^{3+}, Ag^{+}, Cu^{2+}, Ni^{2+}, Ru^{3+}, Mn^{2+}, and Fe^{3+} as the metal ions.[21,23-26] The resulting DENs were shown to serve as stable nanocatalysts, also known as dendrimer-encapsulated catalysts (DECs).

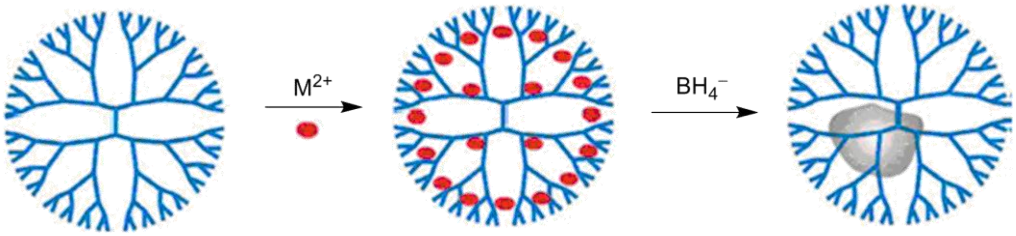

***Scheme 6.1*:** Schematic representation of the synthesis of dendrimer-encapsulated metal nanoparticles (DENs).[71]

6.2.1 Homogeneous Catalysis with DENs

There are many literature reports on the synthesis of various DECs and their use in catalysis. Crooks *et al*.[27] carried out catalytic hydrogenation of allylic alcohol to 1-propanol by using Pd nanoparticles encapsulated within OH-terminated dendrimers in water (Scheme 6.2). For example, the G4OH/Pd(0)40 catalyst catalyzed the hydrogenation of allyl alcohol with the maximum TOF of 480 mol H_2(mol Pd)$^{-1}$h^{-1}. The G4OH(Pd$_{40}$) DECs were also shown to efficiently catalyze the hydrogenation of both linear and branched type alkenes. The authors also showed that steric crowding on the dendrimer periphery, which increased with the dendrimer's generation (i.e., from G4OH to G6OH, and to G8OH), could act as an adjustable-mesh nanofilter. Thus, it was observed that with more steric crowding at the dendrimer periphery (from lower to higher generation dendrimer), the TOF of the DECs decreased. For example, the maximum TOF for the G4OH/Pd(0)40 catalyst for the hydrogenation of allyl alcohol was 480 mol H_2(mol Pd)$^{-1}$h^{-1}, but it decreased to 450 mol H_2(mol Pd)$^{-1}$h^{-1} and 120 mol H_2(mol Pd)$^{-1}$h^{-1} for G6OH/Pd(0)40 and G8OH/Pd(0)40, respectively. Crooks *et al*. also reported on fluorous phase-soluble PAMAM dendrimer-encapsulated Pd nanoparticles catalysts for hydrogenation of alkenes and isomerization of terminal alkenes.[28]

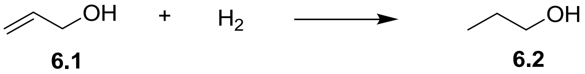

Scheme 6.2**:** Hydrogenation of allyl alcohol to 1-propanol using G4OH/Pd(0)40 DECs.

Ooe *et al.*[29] reported on the synthesis of DECs composed of Pd(0) nanoparticles within poly(propylene imine) (PPI) dendrimers and their catalytic activity for substrate-specific hydrogenation of polar olefins. These dendrimer-encapsulated Pd nanoparticles (PdNPs) with 2–3 nm in diameter were prepared by first immobilizing Pd^{2+} ions inside the dendrimers and subsequently reducing dendrimer-supported Pd^{2+} ions with KBH_4 solution. In another example, Mizugaki *et al.*[30] demonstrated the synthesis and catalytic properties of PAMAM dendron-stabilized PdNPs for hydrogenation of dienes and acetylenes to monoenes (Scheme 6.3).

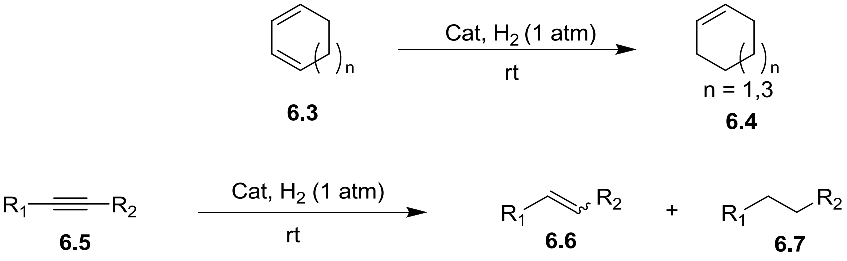

Scheme 6.3**:** Hydrogenation of conjugated dienes and alkynes using dendron encapsulated Pd nanoparticles.

Yeung *et al.*[31] synthesized dendrimer-encapsulated Pd nanoparticles from fluoropolyether modified PPI dendrimers. The resulting DECs catalyzed the Heck reaction between bromo- or iodobenzene and *n*-butyl acrylate in a fluorocarbon/hydrocarbon solvent system (Scheme 6.4). More importantly, the catalyst was found to be catalytically active at relatively low temperature of only 90 °C in the absence of toxic phosphines and gave isolated yields up to 70%, with very high selectivity (almost 100% to *n*-butyl-*trans*formylcinnamate product).

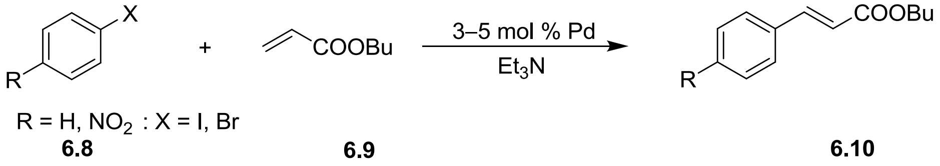

Scheme 6.4**:** C-C coupling reaction between aryl halides and n-butylacrylate catalyzed by Pd nanoparticle containing DEC.

6.2.2 Heterogeneous Catalysis with DENs

Although DECs are proven to be highly effective catalysts for reactions ranging from simple hydrogenation to more sophisticated coupling reactions, they often exhibit the typical properties of homogeneous catalysts, and thus are difficult to separate from the reaction mixtures at the end of reactions. Despite the fact that dendritic catalysts can be recycled from solutions by using the techniques applied for separation of their monomeric analogues such as precipitation,[32] two-phase catalysis,[33, 34] nanofiltration[35] and membrane reactor,[36,37] these methods have been shown to result in some losses of the materials as well as their catalytic activities, which necessitates the immobilization of DECs on insoluble supports to build true heterogeneous systems. Inorganic materials such as silica are particularly suited as heterogeneous catalyst support materials for DECs because of their high physical strength and chemical inertness. In this regard, Alper *et al.*[38] have synthesized silica-PAMAM dendrimers starting from commercial aminopropyl silica gel, in which palladium was complexed to dendritic phosphines, for Heck coupling reaction. Alper *et al.* also reported a solid-phase synthetic approach to obtain dendritic ligands onto polystyrene-based beads to further anchor metallic catalytic groups for regioselective hydroformylation of styrene (Scheme 6.5).[39] To make the catalyst, the authors synthesized dendritic materials having phosphine ligands, and they then used the dendritic phosphine ligands to complex rhodium catalytic groups.

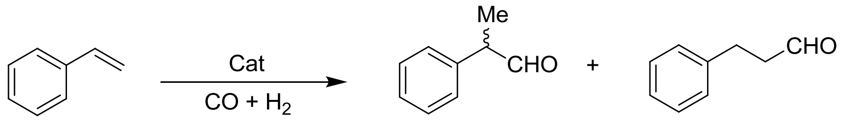

6.11 **6.12** **6.13**

Scheme 6.5**:** Hydroformylation of styrene with rhodium-complexed dendrimers that are anchored onto polystyrene beads.

Hagiwara *et al.*[40] covalently attached PAMAM dendrimers on amorphous silica. Pd(II) ions were then immobilized noncovalently as a supported ionic liquid catalyst (SILC) in the nanosilica dendrimer composite material for Suzuki-Miyuara reaction. The immobilization of the Pd(II) ions on a nanosilica dendrimer as SILC was carried out by stirring a solution of palladium acetate, the nanosilica dendrimer and the ionic liquid butylmethylimidazolinium hexafluorophosphate([bmim]PF_6) in tetrahydrofuran solution. In a related work, Alper, Sayari and co-workers have recently synthesized G4-PAMAM dendrimers using large pore PE-MCM-41(Pore Expanded MCM-41) as support material instead of amorphous silica.[45] Similarly, Somorjai and Toste[41,42] also reported the synthesis of supported Pd_{40}[24] and Pt_{40}[42] nanoparticles encapsulated by the PAMAM dendrimer within the mesoporous channels of SBA-15 for the hydroalkoxylation of 2-phenylethynylphenol (Scheme 6.6). But these types of materials has some limitations as the reactants have difficulty to reach all the metal centers and the DECs entrapped within the cylindrical channels pores of the SBA-15 mesoporous silica support material. Furthermore, as the PAMAMs are noncovalently immobilized on the support material, the DECs are more likely to leach out.[43]

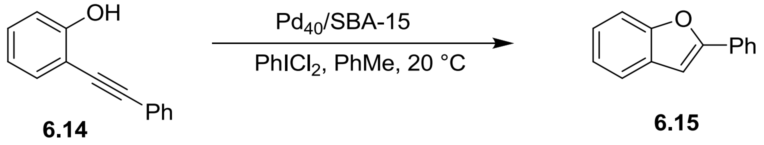

Scheme 6.6: Heterogeneous Pd nanoparticle containing DEC for the hydroalkoxylation of 2-phenylethynylphenol.

Polyamidoamine (PAMAM) dendrimers with up to three generations were grown over amino-functionalized mesoporous silica (MCM-41) via sequential Michael addition of methyl acrylate followed by amidation in the presence of ethylenediamine.[44,45] Although the resulting materials with higher generation dendrimers were expected to contain a higher density of active sites, they were found to exhibit less effective activity than those with lower generation dendrimers.[46] This unexpected result was attributed to steric crowding of the dendrimers within the mesopores of the materials and poor mass transport of reactants to reach the catalytic sites. In fact, the third generation PAMAM was found to almost completely fill the pores of the MCM-41. Using larger pore of mesoporous SBA-15 silica with less-grafted propylamine, Shantz and co-workers synthesized up to G4 melamine-based dendrimers inside the mesoporous channels.[47] Here also the first generation dendrons were found to be the most active for catalyst compared to the larger generation, which limited the mass transport of reactants.

6.3 General Considerations and Concept

In order to overcome some of the limitations associated with dendrimer-based nanocatalysts, our group recently investigated the synthesis of covalently functionalized G4 PAMAM dendrimes on the surface of silica microspheres and their use for stabilization of Pd encapsulated dendrimer nanocatalysts.[48] The synthesis of the nanomaterials was accomplished by synthesizing silica microspheres and functionalizing their surfaces with vinyl groups using vinyltriethoxysilane (VTS). The vinyl groups were then converted into epoxide groups by using m-chloroperoxybenzoic acid. The SiO_2-supported epoxides were treated with amine-terminated G4 poly(amidoamine) (PAMAM) dendrimers and underwent ring-opening to give SiO_2@Pd/PAMAM core-shell microspheres. The resulting materials showed catalytic activity towards hydrogenation reactions of various substrates.

The goal of the work here was 1) to explore the possibility of extending the structures beyond core-shell (SiO_2@Pd/PAMAM core-shell microspheres) and develop stable and robust core-shell-shell type microspheres containing an additional nanoporous metal oxide shell around the supported Pd/PAMAM nanopartices and 2) to investigate the catalytic properties and advantageous features of such nanomaterials for catalytic reactions. The unique structural features of the proposed materials include the presence of a nanoporous silica shell around the Pd/PAMAM nanoparticles that is expected to not only improve the shelf-life of the nanocatalysts but also serve as gate-keeper / selective to reactants.

The synthesis of the nanomaterials was achieved by covalently attaching amine terminated G4 PAMAM dendrimes to carboxylic acid-functionalized silica microsphere cores via EDC coupling (Scheme 6.7). Then Pd nanoparticles within the cores of the SiO_2-supported PAMAM dendrimers were synthesized by complexing the Pd(II) ions with the amine groups in the cores of the dendrimers, followed by reducing them with $NaBH_4$ solution into Pd(0). Finally, the the SiO_2-supported dendrimer encapsulated Pd-NP were coated by silica shells using sol-gel chemistry. Controlled etching of the outer silica shell with dilute NaOH solution produced nanoporous silica shells around the SiO_2-supported Pd/PAMAM nanoparticles. The resulting material was labeled as SiO_2-Pd/PAMAM-pSiO_2. Finally, the material was successfully used as an efficient heterogeneous catalyst for selective hydrogenation reaction of olefin and nitro containing compounds.

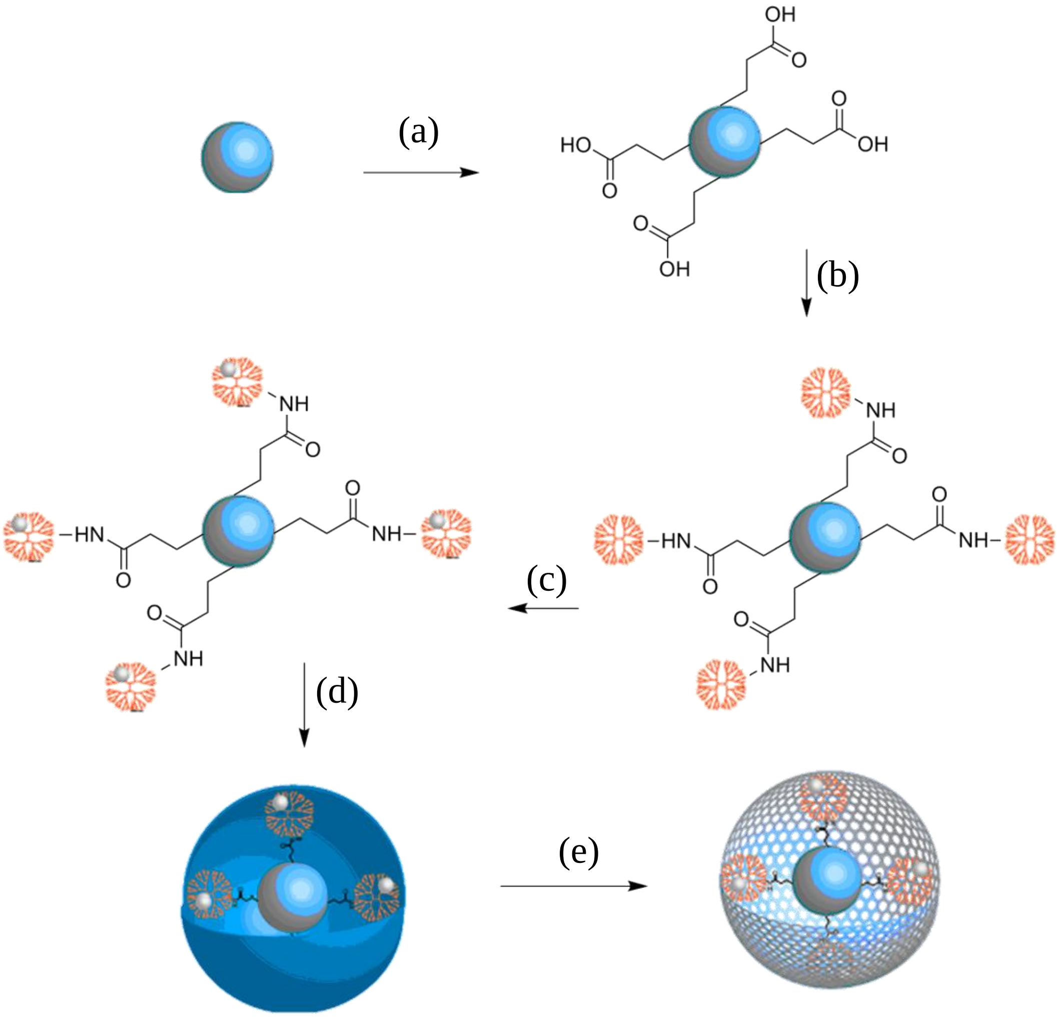

Scheme 6.7: Schematic representation of the synthesis of core-shell-shell microsphere containing SiO_2 microsphere-supported PAMAM-encapsulated Pd nanoparticles that are further coated with nanoporous silica shell. (a) Functionalization of SiO_2 microspheres with carboxylic acid group by grafting the SiO_2 microspheres with carboxyethylsilanetriol, (b) 1-ethyl-3-(3-dimethylaminopropyl)carbodiimide (EDC) coupling of SiO_2-COOH with NH_2 terminated PAMAM dendrimers via EDC coupling, (c) synthesis of PAMAM encapsulated Pd nanoparticles within the SiO_2-COOH supported PAMAM

dendrimers forming SiO_2-Pd/PAMAM microspheres, (d) synthesis of SiO_2 shell around the SiO_2-Pd/PAMAM using TEOS, and (e) controlled etching of SiO_2 shell using aqueous NaOH solution.

6.3.1 Synthesis of Porous SiO_2-Pd/PAMAM-pSiO_2 Core-Shell-Shell Microsphere Catalyst

The SiO_2-Pd/PAMAM-pSiO_2 core-shell-shell microsphere nanocatalyst was synthesized by following the synthetic procedure depicted in Scheme 6.7. First SiO_2 microspheres were synthesized according to the Stöber method,[49] and their surfaces were functionalized with carboxylic acid groups using carboxyethylsilanetriol (CES)[50-52] in anhydrous ethanol at 80 °C for 12 h. The carboxylic acid-functionalized SiO_2 microspheres were mixed with amine terminated G4 PAMAM dendrimers to yield a conjugate of the two molecules via a stable amide bond, resulting in SiO_2-PAMAM core-shell microspheres. Some of the primary amine groups of PAMAM dendrimers form the conjugates onto the SiO_2-COOH microspheres from this coupling reaction; however, but many of the primary amine groups that are not close enough to the carboxylic groups are expected to remain free. As these residual primary amine groups are capable of complexing the metal (Pd(II)) ions in the subsequent steps and leading to the uncontrolled growth or metal (Pd) into bulk materials on the outer surfaces, the primary amine groups have to be passivated in order to prevent this. This was successfully achieved by selective protonation of the residual primary amine groups on the periphery of amine-terminated dendrimers (*i.e.*, the surface primary amines on PAMAM dendrimers, which have has p*K*a = 9.5 are more basic than the interior tertiary amines which have p*K*a = 5.5).[53-55] Alternatively, this could be done by functionalization of the primary amine groups with noncomplexing terminal groups.[56-58] In our case, the residual primary amine groups were converted to quaternary ammonium ions by stirring the SiO_2-PAMAM core-shell microspheres in 2 M aqueous HCl solution. The formation of quaternary ammonium groups prevented the terminal amine groups from anchoring the Pd(II) ions. After the quaternization of the residual amine groups on the peripheriry of the dendrimers, Pd(II) ions from aqueous solution of Na_2PdCl_4 were anchored only within the cores of the dendrimers, resulting in SiO_2-supported PAMAM-Pd(II) complexes. These were then converted into SiO_2-supported Pd/PAMAM by following the method reported in Crooks' work previously.[59] To the PAMAM-Pd(II) complex anchored on SiO_2 microspheres, $NaBH_4$ solution was added to reduce Pd(II) to Pd(0) and yield SiO_2-Pd/PAMAM core-shell microspheres.

The SiO_2-Pd/PAMAM core-shell microspheres were further coated with silica shells via the sol-gel chemistry using tetraethoxysilane (TEOS).[60] This produced SiO_2-Pd/PAMAM-SiO_2 core-shell-shell microspheres. Finally, controlled etching of the outer silica shells with an aqueous solution of NaOH generated the porous SiO_2-Pd/PAMAM-pSiO_2 core-shell-shell microspheres (nanocatalysts) with nanoporous silica shells.

The materials obtained after each step of functionalization above were characterized by FTIR (Figure 6.1) and thermogravimetric analysis (TGA) (Figure 6.2). Most of the peaks on the FT-IR spectra were similar as expected.

The IR spectrum of SiO_2 microspheres showed a broad O–H stretching peak between 3000 and 3500 cm^{-1}, a strong Si–O–Si stretching band centered at 1100 cm^{-1}, and asymmetric vibration of Si-OH is observed at 948 cm^{-1}, as expected.[72]The spectrum for SiO_2-COOH microspheres showed a broad –OH stretch in between 3000 and 3500 cm^{-1} and a carbonyl C=O stretching band at 1657 cm^{-1}. The spectrum for SiO_2-PAMAM depicted a broad band at 3489 cm^{-1} due to free –OH group and a shoulder at 3281 cm^{-1} which is almost merged with the –OH stretch is due to the stretching vibrations of free NH groups. The band corresponding to amide I mode was seen at 1658 cm^{-1} and amide II mode was observed at 1560 cm^{-1}.[73]

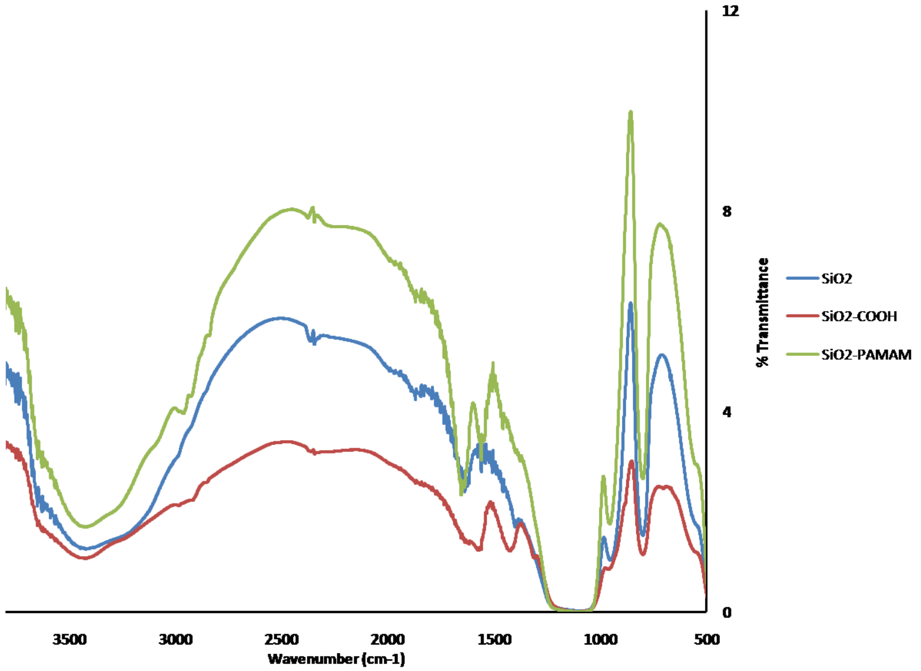

Figure 6.1: FTIR spectra of SiO_2, SiO_2-COOH and SiO_2-PAMAM core-shell microspheres.

The thermogravimetric analysis (TGA) traces (Figure 6.2) showed a slight weight loss below 100 °C for all the samples, which was attributed to the loss of physisorbed water from the samples. The weight loss from the samples in the range 150–700 °C on the TGA traces were attributed mainly to the loss of organic groups. In this temperature range, the weight losses from SiO_2, SiO_2-COOH and SiO_2-PAMAM microspheres were 4.4, 10.8, and 22.7%, respectively. This wt % due to the organic groups increased in the order of SiO_2 < SiO_2-COOH < SiO_2-PAMAM, which clearly confirmed the successful anchoring of ethylcarboxylic acid and PAMAM groups to the SiO_2 microspheres.

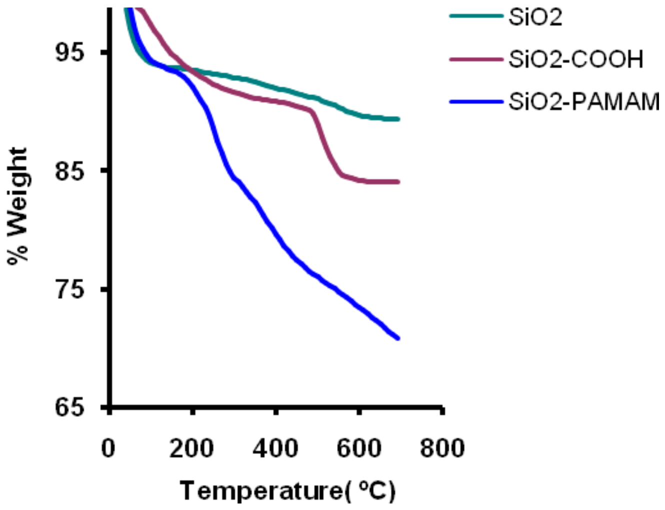

***Figure 6.2*:** Thermogravimetric traces of SiO_2, SiO_2-COOH and SiO_2-PAMAM core-shell microspheres.

Transmission electron microscope (TEM) images of the materials obtained after each step of the synthesis are depicted in Figure 6.3. The TEM image in Figure 6.3A show monodisperse SiO_2 microspheres and those in Figure 6.3B show well-dispersed PdNPs on the surfaces of the dendrimer encapsulated SiO_2 microspheres. The TEM image of SiO_2-Pd/PAMAM-SiO_2 (Figure 6.3C) shows the presence of uniform silica shells around the SiO_2-Pd/PAMAM core-shell microspheres. From careful analysis of the TEM images, the silica shells of SiO_2-Pd/PAMAM-SiO_2 microspheres, which were formed from the hydrolysis and condensation of 0.4 mL TEOS in ethanol, were found to be ~70 nm thick. Higher or lower amount of TEOS than 0.4 mL could result in thicker or thinner silica shells, respectively, around the SiO_2-Pd/PAMAM microspheres.[74]

The nanoporous silica shells around the SiO_2-PAMAM-Pd-SiO_2 core-shell-shell microspheres (Figure 6.3D-F) were produced by controlled etching of their outer silica shells with aqueous NaOH solution in the presence of PVP.[61] PVP forms strong hydrogen bonding between its carbonyl groups and the surface silanol groups of the silica shells; by doing so, the PVP prevents the very outer silica shells from being etched significantly by the NaOH solution.[62,63] Therefore, the NaOH solution penetrates through the silica shells, etches the inner parts of the silica shells that are not protected by the PVP, producing more uniformly etched nanoporous silica shells around the microspheres.

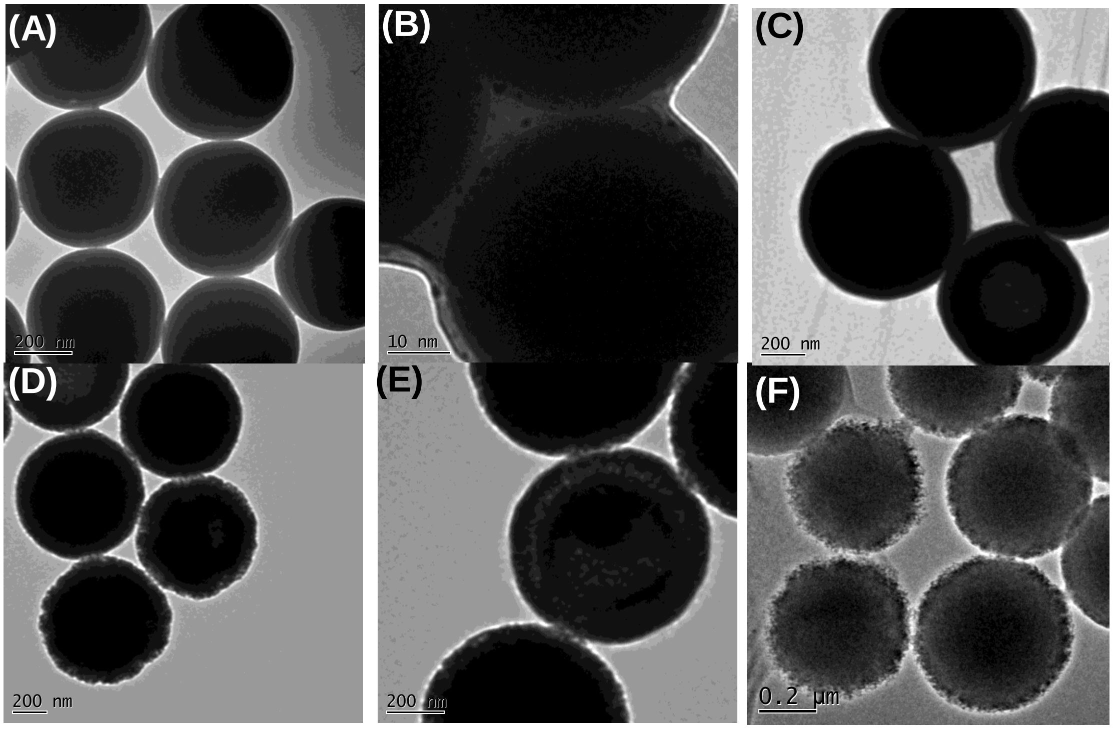

Figure 6.3**:** TEM images of (A) SiO_2 microspheres, (B) SiO_2-Pd/PAMAM core-shell microspheres, (C) SiO_2-Pd/PAMAM-SiO_2 core-shell-shell microspheres, and (D–F) etched SiO_2-Pd/PAMAM-SiO_2 core-shell-shell microspheres with porous silica shell (D = etched for 30 min, E = etched for 60 min, and F = etched for 80 min).

In addition, the etching time had to be optimized in order to obtain microspheres with intact nanoporous silica shells around the Pd/PAMAM nanoparticles. Shorter etching times resulted in only moderate etching and silica shells with no access to Pd nanoparticles, while longer etching times led to complete dissolution of the silica shells.[66,67] By using optimum etching times, which we found to be ~80 min from previous works in our group,[74] reasonably intact nanoporous silica shells around the PdNPs (or SiO_2-Pd/PAMAM-Pd core-shell microspheres) were obtained. These microspheres were finally utilized for catalysis.

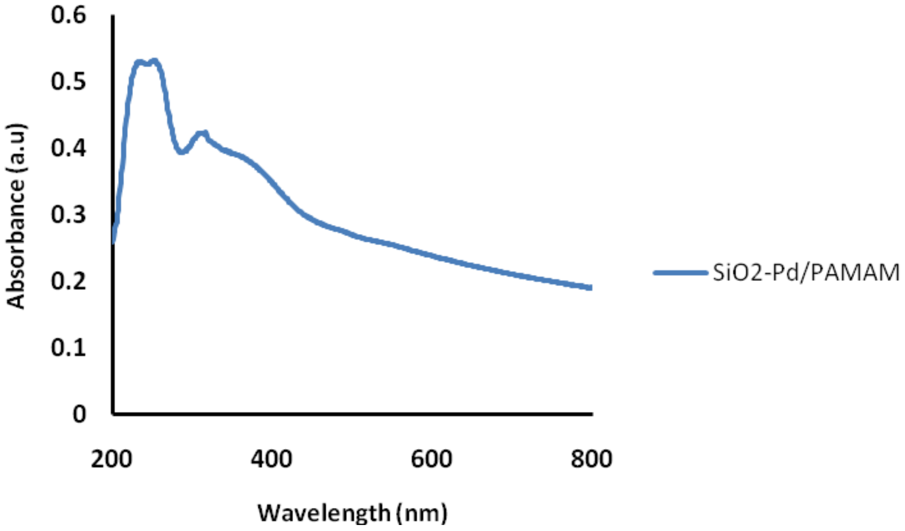

Figure 6.4**:** UV-Vis spectrum of SiO_2-Pd/PAMAM core-shell microspheres.

The presence of Pd nanoparticles in the porous SiO_2-Pd/PAMAM-SiO_2 microspheres was also probed by solid-state UV–Vis spectroscopy (Figure 6.4). Figure 6.4 shows the solid state UV reflectance spectrum of SiO_2-Pd/PAMAM microspheres. In the spectrum, no obvious surface plasmon band (or only a smoothly increasing absorption at increasing energy) was observed, which are in accord with literature reports for ultrasmall Pd nanoparticles.[65,66] The bands in 200–300 nm region arises from a ligand-to-metal charge transfer (LMCT) between the tertiary amines of the dendrimer and Pd^{2+}.[67]

The presence of Pd in SiO_2-Pd/PAMAM-pSiO_2 nanocatalyst was further determined by elemental analysis using inductively coupled plasma atomic absorption spectroscopy (ICP-AES). In addition, ICP-AES helped us to quantify the amount of Pd, which was found to be 2799 ppm or 2.63 x 10^{-4} mmol Pd/g SiO_2-Pd/PAMAM-pSiO_2 core-shell microspheres.

6.3.2 Catalytic Activity of Porous SiO_2-Pd/PAMAM-SiO_2 Core-Shell-Shell Microspheres in Hydrogenation of Olefin

Styrene hydrogenation[68,69] was used as a model reaction to explore the catalytic activity of the encapsulated Pd nanoparticles in the SiO_2-Pd/PAMAM-pSiO_2 core-shell-shell microspheres. In a control experiment where no Pd NPs were present, *i.e.*, without any catalyst or with silica nanospheres containing no Pd NPs, the hydrogenation reaction did not occur, as expected.

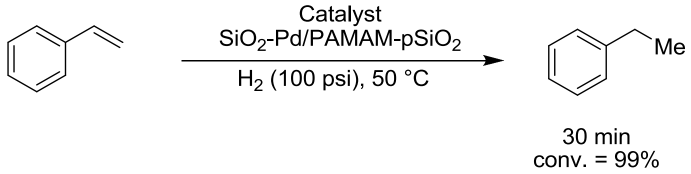

Scheme 6.8: Evaluation of the catalytic activity of the control samples and the catalyst towards hydrogenation reaction.

When the SiO_2-Pd/PAMAM-pSiO_2 core-shell-shell nanospheres etched for 80 min were used as catalyst in the reaction mixture containing styrene and hydrogen, the hydrogenation reaction proceeded at 50 °C and 100 psi H_2 pressure with 100% reactant conversion within 30 min, giving ethylbenzene as the sole product (Scheme 6.8). The turn-over-frequency (TOF) of the reaction was found very high (63371 min^{-1}) which indicates the high catalytic activity the SiO_2-PAMAM-Pd-pSiO_2 core-shell-shell microspheres (Table 6.2).

6.3.3 Scope of the Reaction

The substrate scope of the hydrogenation reaction with SiO_2-Pd/PAMAM-pSiO_2 microsphere catalyst was then studied by using several other different substrates. The results are summarized in Table 6.2. When hydrogenation of phenylacetylene with SiO_2-Pd/PAMAM-pSiO_2 microspheres was performed, 92% of the substrate was converted in 3 h at 50 °C, yielding the two possible products, *i.e.*, styrene and ethylenzene in a ratio of 1.8:1. However, when the reaction mixture was kept under the same condition for prolonged time, it gave ethylbenzene as the major product, as expected. As a part of our further investigation, hydrogenation of 4-nitrostyrene was performed. This idea was indirectly stimulated by our "failed-attempt" to reduce nitrobenzene to aniline using the same catalyst under harsher reaction condition. The hydrogenation of 4-nitrostyrene can form three possible products based on the selectivity and reactivity of the catalyst, *i.e.,* (a) 4-nitroethylbenzene, (b) 4-aminostyrene and (c) 4-aminoethylbenzene. However, under the reaction condition, only product (a) was observed after 30 min. This result is in accordance to our previous study of catalytic hydrogenation of 4-nitrostyrene using SiO_2@Pd/PAMAM core-shell microspheres.[48] However, in the case of SiO_2@Pd/PAMAM core-shell microspheres, the substrate and the intermediate product (b) eventually get converted to product (c) upon longer reaction time (*e.g.*, in 2.5 h, 35% of 4-ethylaniline and 65% 4-nitroethylbenzene were obtained, and in 8 h, 88% 4-ethylaniline and 12% 4-nitroethylbenzene were obtained). On the contrary, in the case of SiO_2-Pd/PAMAM-pSiO_2 core-shell microspheres, after allowing the reaction to go for another 2 h, no significant amount of side products was observed. This result clearly suggests that although the extra porous shell on SiO_2-Pd/PAMAM slows down the catalytic efficiency, it offers better selectivity towards hydrogenation of C=C multiple bonds over other functional groups such as nitro groups.

Table 6.2**:** Scope of the hydrogenation reaction.

Entry	**Substrate**	**Temp (°C)**	**Time (min)**	**Conv. (%)**	**TOF (min^{-1})**	**Product Selectivity**
1	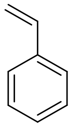	50	30	~99	63371	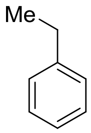
2	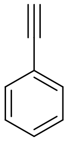	″	180	92	9717	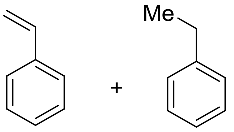 (1.8 : 1)
3	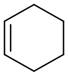	″	30	99	63371	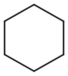
4	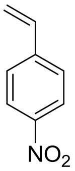	″	30	85	53866	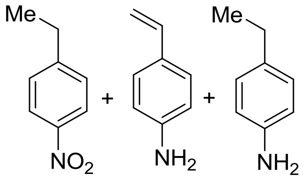 (1: 0: 0)
6	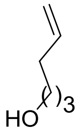	100	120	50	7921	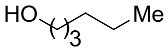
7	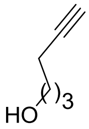	100	60	~99	31685	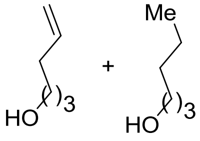 (1 : 4)

Among the other substrates, the simple aliphatic olefin cyclohexene gets converted to cyclohexane within 30 min at 50 °C. The reaction was completed in 3 h, yielding hexane as the sole product. The unsaturated aliphatic alcohols also reacted to form saturated alcohols but required harsher reaction condition. Like phenylacetylene, 5-hexyne-1-ol underwent complete conversion (within 1 h), and it produced its two possible products, *i.e.*, 5-hexene-1-ol and 1-hexanol. However, the product distribution lied more onto saturated alcohol in the case of 5-hexyne-1-ol whereas it lied more onto the unsaturated alcohol in the case of phenylacetylene. This discrepancy might stem from the faster reactivity at elevated temperature in case of 5-hexyn-1-ol, but the inherent preference of the catalyst towards a particular substrate cannot be ruled out. Although these results are not comprehensive and can always be extended for further investigation, they still show the potential of this class of catalyst towards selective hydrogenation.

6.3.4 Recyclability of the Catalyst

The recyclability of the SiO_2-PAMAM-Pd-pSiO_2 nanospheres as heterogeneous catalyst was also demonstrated successfully (Figure. 6.5). The recyclability experiments were performed under the same reaction condition as above, except by using 20 mg instead of 10 mg of the catalyst in order to ensure that enough catalyst was recovered for the second catalytic cycle. Upon completion of the first reaction, the catalyst was recovered from the reaction mixture by simple centrifugation, washed with ethanol three times and used in the next reaction run. The recovered SiO_2-Pd/PAMAM-pSiO_2 core-shell-shell microspheres showed only a very slight decrease in their catalytic activities. The very slight loss of their catalytic activity was actually most likely due to the loss of a small amount of catalyst during and centrifugation and handling of the catalyst during the recycling experiment.

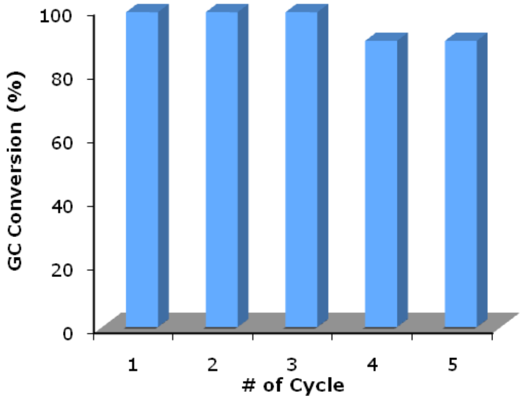

Figure 6.5**:** % Conversion of styrene in 15 min versus catalytic cycles for styrene hydrogenation catalyzed by SiO_2-Pd/PAMAM-pSiO_2 core-shell-shell microspheres.

To determine whether or not the Pd from the core-shell-shell microspheres was leached into the reaction mixture, elemental analyses of the catalyst and the reaction mixture were performed. The weight percent of Pd analyzed by ICP-AES in the fresh catalyst and in the reaction mixture after fifth cycle are given in Table 6.3. The results show that there was no significant loss of Pd from the nanocatalyst or no significant amount of Pd in the reaction mixture. This clearly indicates the high stability of the Pd nanoparticles in the porous SiO_2-PAMAM-Pd-pSiO_2 microspheres towards leaching.

Table 6.3**:** Elemental analysis obtained of Pd with ICP-AES in the recycled catalysts and in the reaction mixtures.

Entry	**Pd (ppm)**	**Pd (%)**	**Pd (mmol)**
Catalyst	2799	0.27	2.63×10^{-4}
Reaction solution recovered from 5th cycle	1	0.0001	9.74×10^{-8}

6.4 Summary

We have developed a synthetic method to porous SiO_2-PAMAM-Pd-SiO_2 core-shell-shell microsphere catalysts containing silica microsphere-supported dendrimer encapsulated ultrasmall PdNPs that are further encapsulated by a porous silica shell and demonstrated their efficient catalytic activities for hydrogenation reactions of various olefins. The microsphere nanocatalyst was synthesized by first supporting PAMAM dendrimers covalently onto silica microspheres. Within the PAMAM dendrimers, Pd ions were anchored and reduced to produce PAMAM encapsulated small and monodisperse palladium nanoparticles (PdNPs). Finally, the PdNPs/PAMAM nanoparticles were then coated with silica shells using the sol-gel process, which were subsequently etched with NaOH solution to produce nanoporous silica shells. The resulting nanoporous silica shells had large enough pores to let reactants and products diffuse in and out of the PdNP catalytic sites, while at the same time they were robust enough to keep the PdNPs stable and intact. The catalyst was also shown to be recyclable without a substantial loss of its catalytic activity, at least in five cycles.

Experimental Section

Synthesis of Silica Microspheres: Silica microspheres were synthesized by following the Stöber method. Typically 6.2 mL of TEOS was added into a solution containing 6.5 mL of ammonium hydroxide solution (28-30%), 100 mL of ethanol, and 7 mL of water. After 3 h of stirring at room temperature, a colloidal solution of silica microspheres with 325 nm diameter was obtained. The solution was centrifuged, and the precipitate was washed with ethanol three times via centrifugation, decantation and redispersion. The resulting solid sample was finally dried under ambient conditions, producing silica (SiO_2) microspheres.

Functionalization of Silica Microspheres with Carboxylic Acid Groups: 800 mg of SiO_2 microspheres was dispersed in anhydrous ethanol (400 mL). This solution was mixed with carboxyethylsilanetriol (CES) (1.0 mL) and stirred at 80 °C for 12 h to functionalize the surfaces of the SiO_2 microspheres with carboxylic acid groups. The solution was centrifuged and the precipitate was washed with ethanol via centrifugation, decantation, and redispersion. The final precipitate was dried in air and was denoted as SiO_2-COOH.

EDC Coupling of Carboxylic Acid Groups on SiO_2 Microspheres with Amine Groups of G4 PAMAM Dendrimer: 600 mg of the above synthesized SiO_2-COOH was dispersed in 40 mL of distilled water and the pH was adjusted to 5. To the solution was added 400 mg EDC followed by 0.8 mL PAMAM and stirred at room temperature for 24 h. The white solid was separated by centrifugation and was washed with water via centrifugation, decantation, and redispersion and the solid was air dried and denoted as SiO_2-PAMAM.

Synthesis of SiO_2-PAMAM-Pd Core-Shell Microspheres: 250 mg of SiO_2-PAMAM microspheres was dispersed in 5 mL water and the pH of the solution was adjusted to 2 by adding 2 M HCl dropwise and stirred at room temperature for 30 min. After this step, 0.05 M Na_2PdCl_4 aqueous solution (250 μL) was slowly added and the solution was stirred again at room temperature for 30 min to let Pd(II) ions anchor within the cores of the PAMAM dendrimers. Then, 1 M $NaBH_4$ aqueous solution (500 μL) was added. As soon as the borohydride solution was added, the solution changed its color from yellow to grey, indicating the transformation of Pd(II) to Pd(0). The solid material was separated by centrifugation; washed thrice with 3 x 10 mL distilled water via sonication, centrifugation, and decantation; and then dispersed in 8.6 mL water. The resulting material was labeled as SiO_2-PAMAM-Pd core-shell microspheres.

Synthesis of SiO_2-Pd/PAMAM-SiO_2 Core-Shell-Shell Microspheres: The solution containing SiO_2-PAMAM-Pd–NP nanospheres from above (4 mL) was dispersed in a mixture of ethanol (200 mL), water (25 mL), and ammonium hydroxide solution (10 mL). Then, 0.5 mL TEOS was added into this solution to encapsulate the SiO_2-Pd/PAMAM-NP with a silica shell. After 12 h of stirring, the solution was centrifuged and the precipitate was washed with ethanol. The final precipitate was dispersed in de-ionized water (50 mL) giving a colloidal solution of SiO_2-PAMAM-Pd-SiO_2 core-shell-shell microspheres.

Controlled Etching of the Silica Shell of SiO_2-PAMAM-Pd-SiO_2 Core-Shell-Shell Microspheres: To etch the outer silica shells of SiO_2-PAMAM-Pd-SiO_2 core-shell-shell microspheres into nanoporous silica shells, first 1.00 g of PVP-K15 was dissolved in 25 mL solution of SiO_2-PAMAM-Pd-SiO_2 under stirring at 100 °C for 3 h. After cooling the solution to room temperature, 0.8 g of NaOH was added into it and stirred for 30, 60, or 80 min. The NaOH solution then slowly etched the silica shells. After centrifugation and washing the precipitate with water and ethanol three times (3x20 mL), porous SiO_2-PAMAM-Pd-pSiO_2 core-shell-shell microspheres containing nanoporous silica shells around the PdNPs/PAMAM nanoparticle shells were obtained.

Catalytic Hydrogenation Reaction: The hydrogenation reactions were carried out in a 50 mL high-pressure reactor (Parr Instrument Co.). The reactor was equipped with a heating arrangement, overhead stirrer, thermowell, and pressure gauge as well as a transducer, a gas inlet, a gas outlet, and a sampling valve. The reactor has controllers to set temperatures, pressure and agitation speeds to maximum values of 350 °C, 4000 psi pressure and 1500 rpm, respectively. In a typical hydrogenation reaction, the reactor was charged with reactant (5mmol), ethanol (30 mL), and porous SiO_2-PAMAM-Pd-pSiO_2 core-shell-shell microspheres catalyst (or control sample) (10 mg) and tightly closed. The reactor was set to a temperature of 50 °C and stirring speed of 500 rpm. After attaining the desired temperature and speed, then hydrogen gas was introduced into the reactor to the desired pressure (150 psi H_2). The absorption of hydrogen gas due to reaction was monitored from the pressure drop in the reactor. The reaction was stopped when the gas absorption ceased. The reactor was cooled, and the reaction mixture was analyzed by gas chromatography (GC).

Reference

(1) Marcilly, C. *J. Catal.* **2003**, *216*, 47.
(2) Roucoux, A.; Schulz, J. R.; Patin, H. *Chem. Rev.* **2002**, *102*, 3757.
(3) Rioux, R.; Song, H.; Grass, M.; Habas, S.; Niesz, K.; Hoefelmeyer, J.; Yang, P.; Somorjai, G. *Top Catal.* **2006**, *39*, 167.
(4) Narayanan, R.; El-Sayed, M. A. *J. Am. Chem. Soc.* **2003**, 125, 8340.
(5) Budroni, G.; Corma, A. *Angew. Chem. Int. Ed.* **2006**, *45*, 3328.
(6) Jia, C.-J.; Schuth, F. *Phys. Chem. Chem. Phys.* **2011**, *13*, 2457.
(7) Lee, I.; Albiter, M. A.; Zhang, Q.; Ge, J.; Yin, Y.; Zaera, F. *Phys. Chem. Chem. Phys.* **2011**, *13*, 2449.
(8) Ganesan, M.; Freemantle, R. G.; Obare, S. O. *Chem. Mater.* **2007**, *19*, 3464.
(9) Schmid, G. *Chem. Rev.* **1992**, *92*, 1709.
(10) Poulin, J. C.; Kagan, H. B.; Vargaftik, M. N.; Stolarov, I. P.; Moiseev, I. I. *J. Mol. Catal.* **1995**, *95*, 109.
(11) Amiens, C.; de Caro, D.; Chaudret, B.; Bradley, J. S.; Mazel, R.; Roucau, C. *J. Am. Chem. Soc.* **1993**, *115*, 11638.
(12) Comotti, M.; Li, W.-C.; Spliethoff, B.; Schüth, F. *J. Am. Chem. Soc.* **2005**, *128*, 917.
(13) Teranishi, T.; Miyake, M. *Chem. Mater.* **1998**, *10*, 594.
(14) Teranishi, T.; Nakata, K.; Miyake, M.; Toshima, N. *Chem. Lett.* **1996**, 277.
(15) Henglein, A. *J. Phys. Chem.* **1993**, *97*, 5457.
(16) Bönnemann, H.; Brijoux, W.; Brinkmann, R.; Joußen, T.; Korall, B.; Dinjus, E. *Angew. Chem. Int. Ed.* **1991**, *30*, 1312.
(17) Esumi, K.; Matsuhisa, K.; Torigoe, K. *Langmuir.* **1995**, *11*, 3285.
(18) Leff, D. V.; Ohara, P. C.; Heath, J. R.; Gelbart, W. M. *J. Phys. Chem.* **1995**, *99*, 7036.
(19) Wiley, B.; Sun, Y.; Mayers, B.; Xia, Y. *Chem. Eur. J.* **2005**, *11*, 454.
(20) Esumi, K.; Antonietti, M. *Colloid Chemistry II. In Springer Berlin / Heidelberg*. **2003**, *227*, 31.
(21) Gröhn, F.; Bauer, B. J.; Akpalu, Y. A.; Jackson, C. L.; Amis, E. J. *Macromolecules.* **2000**, *33*, 6042
(22) Myers, V. S.; Weir, M. G.; Carino, E. V.; Yancey, D. F.; Pande, S.; Crooks, R. M. *Chem. Sci.* **2011**, *2*, 1632.
(23) Crooks, R. M.; Zhao, M.; Sun, L.; Chechik, V.; Yeung, L. K. *Acc. Chem. Res.* **2001**, *34*, 181.
(24) Esumi, K.; Suzuki, A.; Yamahira, A.; Torigoe, K. *Langmuir.* **2000**, *16*, 2604.
(25) Zhao, M.; Crooks, R. M. *Chem. Mater.* **1999**, *11*, 3379.
(26) Ottaviani, M. F.; Montalti, F.; Romanelli, M.; Turro, N. J.; Tomalia, D. A. *J. Phys. Chem.* **1996**, *100*, 11033.
(27) Niu, Y.; Yeung, L. K.; Crooks, R. M. *J. Am. Chem. Soc.* **2001**, *123*, 6840.

(28) Chechik, V.; Crooks, R. M. *J. Am. Chem. Soc.* **2000**, *122*, 1243

(29) Ooe, M.; Murata, M.; Mizugaki, T.; Ebitani, K.; Kaneda, K. *Nano. Lett.* **2002**, *2*, 999.

(30) Mizugaki, T.; Murata, M.; Fukubayashi, S.; Mitsudome, T.; Jitsukawa, K.; Kaneda, K. *Chem. Commun.* **2008**, 241.

(31) Yeung, L. K.; Crooks, R. M. *Nano. Lett.* **2001**, 1, 14.

(32) Mizugaki, T.; Ooe, M.; Ebitani, K.; Kaneda, K. *J. Mol. Catal. A: Chem.* **1999**, *145*, 329.

(33) Deng, G.-J.; Fan, Q.-H.; Chen, X.-M.; Liu, D.-S.; Chan, A. S. C. *Chem. Commun.* **2002**, 1570.

(34) Richter, B.; Spek, A. L.; van Koten, G.; Deelman, B.-J. *J. Am. Chem. Soc.* **2000**, 122, 3945.

(35) Kragl, U.; Dreisbach, C. *Angew. Chem. Int. Ed.* **1996**, *35*, 642.

(36) de Groot, D.; de Waal, B. F. M.; Reek, J. N. H.; Schenning, A. P. H. J.; Kamer, P. C. J.; Meijer, E. W.; vVn Leeuwen, P. W. N. M. *J. Am. Chem. Soc.* **2001**, *123*, 8453.

(37) Eggeling, E. B.; Hovestad, N. J.; Jastrzebski, J. T. B. H.; Vogt, D.; Van Koten, G. *J. Org. Chem.* **2000**, *65*, 8857.

(38) Alper, H.; Arya, P.; Bourque, S. C.; Jefferson, G. R.; Manzer, L. E. *Can. J. Chem.* **2000**, *78*, 920.

(39) Arya, P.; Rao, N. V.; Singkhonrat, J.; Alper, H.; Bourque, S. C.; Manzer, L. E., A Divergent. *J. Org. Chem.* **2000**, *65*, 1881.

(40) Hagiwara, H.; Sasaki, H.; Tsubokawa, N.; Hoshi, T.; Suzuki, T.; Tsuda, T.; Kuwabata, S. *Synlett.* **2010**, 1990.

(41) Huang, W.; Liu, J. H.-C.; Alayoglu, P.; Li, Y.; Witham, C. A.; Tsung, C.-K.; Toste, F. D.; Somorjai, G. A. *J. Am. Chem. Soc.* **2010**, *132*, 16771.

(42) Li, Y.; Liu, J. H.-C.; Witham, C. A.; Huang, W.; Marcus, M. A.; Fakra, S. C.; Alayoglu, P.; Zhu, Z.; Thompson, C. M.; Arjun, A.; Lee, K.; Gross, E.; Toste, F. D.; Somorjai, G. A. *J. Am. Chem. Soc.* **2011**, *133*, 13527.

(43) Andrés, R.; Jesús, E.; Flores, J. C., *New J. Chem.* **2007**, *31*, 1161.

(44) Reynhardt, J. P. K.; Yang, Y.; Sayari, A.; Alper, H. *Chem.Mater.* **2004**, *16*, 4095.

(45) Reynhardt, J. P. K.; Yang, Y.; Sayari, A.; Alper, H. *Adv. Funct. Mater.* **2005**, *15*, 1641.

(46) Soler-Illia, G. J. A. A.; Azzaroni, O. **2011**,*Chem. Soc. Rev.* 40, 1107.

(47) Yoo, S.; Lunn, J. D.; Gonzalez, S.; Ristich, J. A.; Simanek, E. E.; Shantz, D. F. *Chem. Mater.* **2006**, 18, 2935.

(48) Biradar, A. V.; Biradar, A. A.; Asefa, T. *Langmuir.* **2011**, *27*, 14408.

(49) Stöber, W.; Fink, A.; Bohn, E. *J Colloid. Inter. Sci.* **1968**, *26*, 62.

(50) Chen, C.-S.; Chen, C.-C.; Chen, C.-T.; Kao, H.-M. *Chem. Commun.* **2011**, *47*, 2288

(51) Ting, C.-C.; Chung, C.-H.; Kao, H.-M. *Chem. Commun.* **2011**, *47*, 5897.

(52) Tsai, C.-T.; Pan, Y.-C.; Ting, C.-C.; Vetrivel, S.; Chiang, A. S. T.; Fey, G. T. K.; Kao, H.-M. *Chem. Commun.* **2009**,5018.

(53) Zhao, M.; Crooks, R. M.,*J. Am. Chem. Soc.* **1998**, *120*, 4877.

(54) Chechik, V.; Zhao, M.; Crooks, R. M. *J. Am. Chem. Soc* **1999**, *121*, 4910.

(55) Crooks, R.; Lemon, B.; Sun, L.; Yeung, L.; Zhao, M.; Vögtle, F. *Springer Berlin / Heidelberg*. **2001**, *212*, 81.

(56) Zhao, M.; Sun, L.; Crooks, R. M. *J. Am. Chem. Soc.* **1998**, *120*, 4877.

(57) Crooks, R. M.; Zhao, M. *Adv. Mater.* **1999**, *11*, 217.

(58) Zhao, M.; Crooks, R. M. *Angew. Chem. Int. Ed.* **1999**, *38*, 364.

(59) Niu, Y.; Yeung, L. K.; Crooks, R. M. *J. Am. Chem. Soc.* **2001**, *123*, 6840.

(60) Lu, Y.; Yin, Y.; Li, Z.-Y.; Xia, Y. *Nano. Lett.* **2002**, *2*, 785.

(61) Gun'ko, V. M.; Zarko, V. I.; Voronin, E. F.; Goncharuk, E. V.; Andriyko, L. S.; Guzenko, N. V.; Nosach, L. V.; Janusz, W. *J. Colloid. Interface. Sci.* **2006**, *300*, 20.

(62) Irzh, A.; Perkas, N.; Gedanken, A. *Langmuir*. **2007**, *23*, 9891.

(63) Storhoff, J. J.; Lazarides, A. A.; Mucic, R. C.; Mirkin, C. A.; Letsinger, R. L.; Schatz, G. C. *J. Am. Chem. Soc.* **2000**, *122*, 4640.

(64) Kim, S.-W.; Park, J.; Jang, Y.; Chung, Y.; Hwang, S.; Hyeon, T.; Kim, Y. W. *Nano. Lett.* **2003**, 3, 1289.

(65) Gopidas, K. R.; Whitesell, J. K.; Fox, M. A. *Nano. Lett.* **2003**, *3*, 1757.

(66) Kumar, V. K. R.; Krishnakumar, S.; Gopidas, K. R. *Eur. J. Org. Chem.* **2012**, 3447.

(67) Knecht, M. R.; Weir, M. G.; Myers, V. S.; Pyrz, W. D.; Ye, H.; Petkov, V.; Buttrey, D. J.; Frenkel, A. I.; Crooks, R. M. *Chem Mater.* **2008**, *20*, 5218.

(68) Deshmukh, R. R.; Lee, J. W.; Shin, U. S.; Lee, J. Y.; Song, C. E. *Angew. Chem. Int. Ed.* **2008**, *47*, 8615.

(69) Huang, J.; Jiang, T.; Gao, H.; Han, B.; Liu, Z.; Wu, W.; Chang, Y.; Zhao, G. *Angew. Chem. Int. Ed.* **2004**, *43*, 1397.

(70) Ranu, B. C.; Chattopadhyay, K.; Adak, L.; Saha, A.; Bhadra, S.; Dey, R.; Saha, D. *Pure Appl. Chem.* **2009**, *81*, 2337.

(71) Niu, Y.; Crooks, R M. *C. R. Chimie*. **2003**, *6*, 1049.

(72) Beganskienė, A.; Sirutkaitis, V.; Kurtinaitienė, M.; Juškėnas, K.; Kareiva, A. *Mater. Sci.* **2004**, *10*, 287.

(73) Popescu, M-C.; Filip, D.; Vasile, C.; Cruz, C.; Rueff, J M.; Marcos, M.; Serrano, J L.; Singurel, G. *J. Phys. Chem. B.* **2006**, *110*, 14198.

(74) Wang, Y.; Biradar, V A.; Duncan, T C.; Asefa, T. *J. Mater. Chem.* **2010**, *20*, 7834.

Chapter-VII

Concluding Remarks

The present investigation employed simple and inexpensive methods to synthesize mesoporous silica and silica microsphere based nanocatalysts for various reactions. The mesoporous silica catalysts were synthesized by starting with mesoporous silica (SBA-15), which was prepared by using triblock copolymer pluronic P123 as structure directing agent. The mesoporous silica was then functionalized with different functional groups by postgrafting. First, SBA-15 was functionalized with tertiary amine groups and many residual silanols in it was synthesized and employed as a bifunctional acid/base cooperative catalyst for Michael addition reaction. It was observed that the catalysts with tertiary amine and significant number of silanol (weak acid) groups in them exhibited cooperative catalytic properties, and thereby more efficient catalytic activities than the ones without enough silanol groups in them. Furthermore, the scope of the catalytic reaction properties of the material was investigated by using different active methylene compounds as nucleophiles. Then SBA-15 mesoporous silica was functionalized with ethylenediamine groups and subsequently letting Fe(III) groups onto the ethylenediamine groups, which acted as a ligand in this case. The Fe(III)-containing mesoporous silica was then employed as a catalyst successfully for epoxide ring-opening reactions of various epoxides with water and a variety of alcohols. This synthetic method has advantages because it involves easily available, less costly and nontoxic reagents and produces an easily recyclable catalyst that shows no leaching and generates high yields of the products. Next, a novel heterogeneous catalytic system comprising ultrasmall Au nanocluster immobilized in the mercaptopropyl-functionalized mesoporous silica materials was reported. Two types of Au nanoclusters, $Au_{25}[S(CH_2)_2Ph]_{18}$ and $Au_{140}[S(CH_2)_2Ph]_{53}$ as the Au nanocluster were employed in the synthesis. Furthermore, controlled removal of the thiolate groups from the supported Au nanoparticles was performed by using borohydride treatment to form even more efficient Au nanocatalysts with naked surfaces. Styrene oxidation was used as a model reaction to study the catalytic activity of these materials. An increase in reaction rate in styrene oxidation was obtained when the reaction was catalyzed by the materials. It is interesting to note that in both the cases there the catalysts gave high selectivity towards benzaldehyde product. When the reaction was done under oxygen, benzaldehyde was the major product with little styrene oxide product. The catalyst was also easily recovered and recycled with little leaching of gold and little loss of catalytic activity. All the mesoporous materials were characterized using analytical techniques such as N_2 gas adsorption, TEM, TGA, XRD, FTIR, UV-Vis and elemental analysis.

In the next part of the dissertation, core-shell-shell microspheres were synthesized and employed as catalyst. One of the material was synthesized by depositing citrate-capped AuNPs on amine-functionalized silica microspheres, then by coating the AuNPs with silica shells using the sol-gel process, and finally by etching the outer silica shells into nanoporous silica with NaOH solution. The catalyst was successfully employed in the epoxidation of styrene and *trans*-stilbene. Next the core-shell-shell material was further extended to dendrimer encapsulated nanoparticles. The material was synthesized by supporting PAMAM dendrimers covalently onto silica microspheres and then encapsulating small and monodisperse palladium nanoparticles (PdNPs) within the supported PAMAM dendrimers, then by coating the PdNPs with silica shells using the sol-gel process, and finally by etching the outer silica shells into nanoporous silica with NaOH solution. The material demonstrated efficient catalytic activities for hydrogenation of various olefins. The resulting nanoporous silica shells in both the cases had large enough pore to let reactants and products diffuse in and out of the metal-NP catalytic sites, while at the same time they were robust enough to keep the metal-NPs stable and intact.

In terms of future work, first investigation would rest on using the tertiary amine based mesoporous silica for Aza-Henry reaction. Aza-Henry reaction is also a base catalyzed C-C bond formation reaction like Henry reaction where alkyl nitronates anions attack the protected imines derived from aldehydes (Scheme 7.1). The catalyst can be synthesized by postgrafting tertiary amine onto the surface of SBA-15.

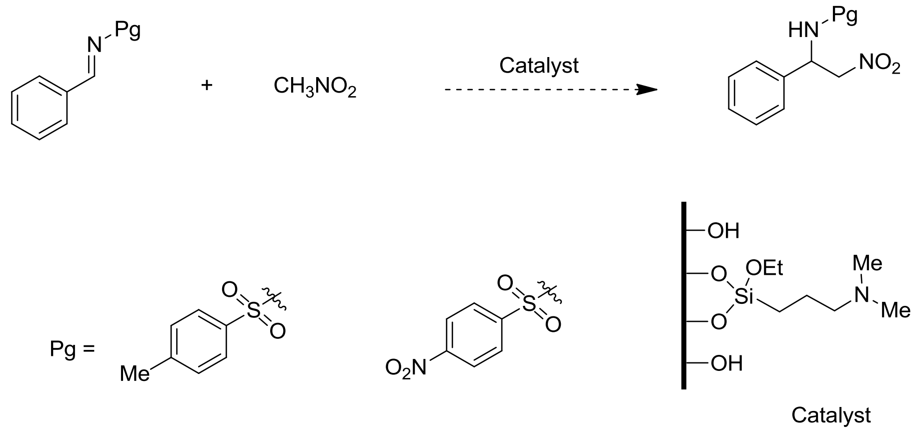
Pg
Catalyst
CH_3NO_2
HN
NO_2
Pg =
Me
O_2N
OH
OEt
Si
Me
N
Catalyst

Scheme 7.1**:** Aza-Henry reaction using tertiary-amine based mesoporous silica catalyst.

Like iron, there are other Lewis acids (Zn or Cu) which can be supported on mesoporous silica for various Lewis catalyzed reactions. A new solid supported Zn can be synthesized by coordination of the Zn salt to the mesoporous silica by using ethylenediamine as the ligand. The synthesized catalyst can be used in the Freidel-Craft alkylation of indole (Scheme 7.2).[1]

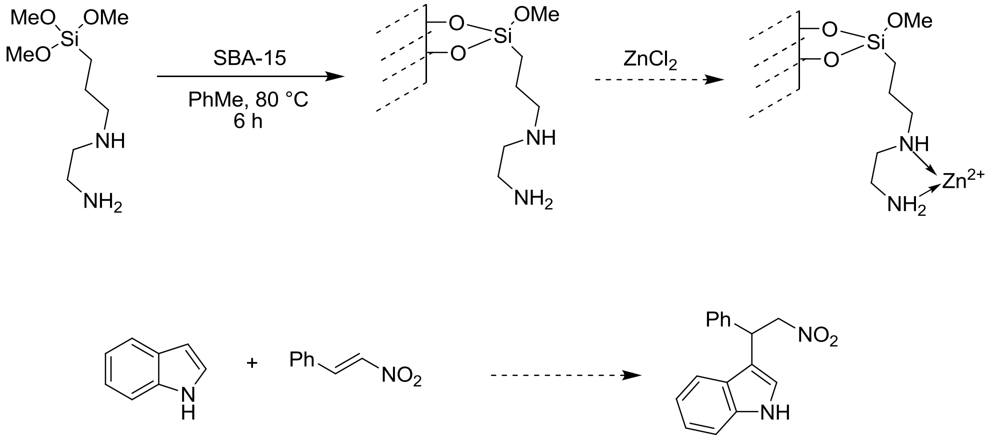
MeO
OMe
Si
NH
NH_2
SBA-15
PhMe, 80 °C
6 h
$ZnCl_2$
Zn^{2+}
Ph
NO_2
NH
H

Scheme 7.2: Synthesis of new mesoporous silica supported Zn catalyst for Friedal-Craft alkylation of indole.

Copper can also be supported on the mesoporous silica using the same methodology like iron and zinc and can be used in various reactions like oxidative coupling of 2-napthol[2,3] (Scheme 7.3)and amination reaction (Scheme 7.4).[4,] All the new solid catalysts would be characterized by N_2 gas adsorption, TEM, TGA, XRD, FTIR, UV-Vis and elemental analysis.

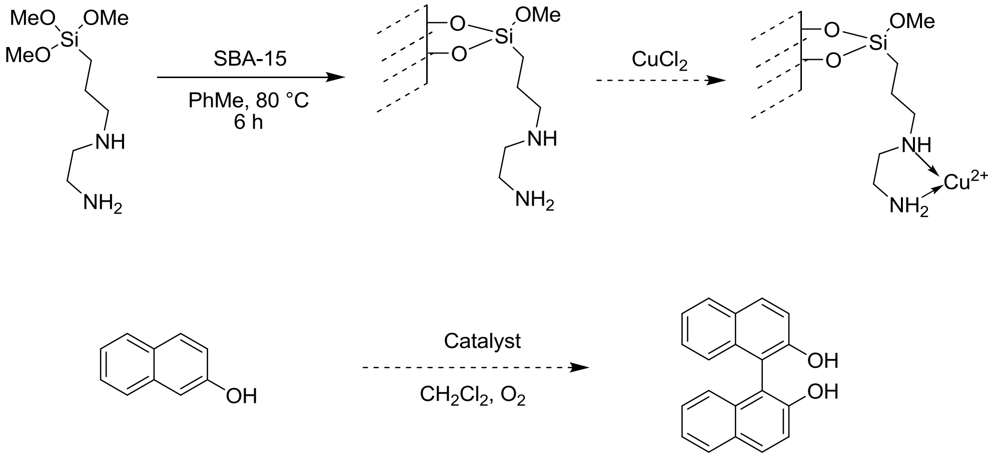
MeO
OMe
Si
MeO
NH
NH2
SBA-15
PhMe, 80 °C
6 h
O
O
Si
OMe
NH
NH2
CuCl2
Cu2+
OH
Catalyst
CH2Cl2, O2
OH
OH

Scheme 7.3**:** Synthesis of new mesoporous silica supported Cu catalyst and application to oxidative coupling of 2-naphthol.

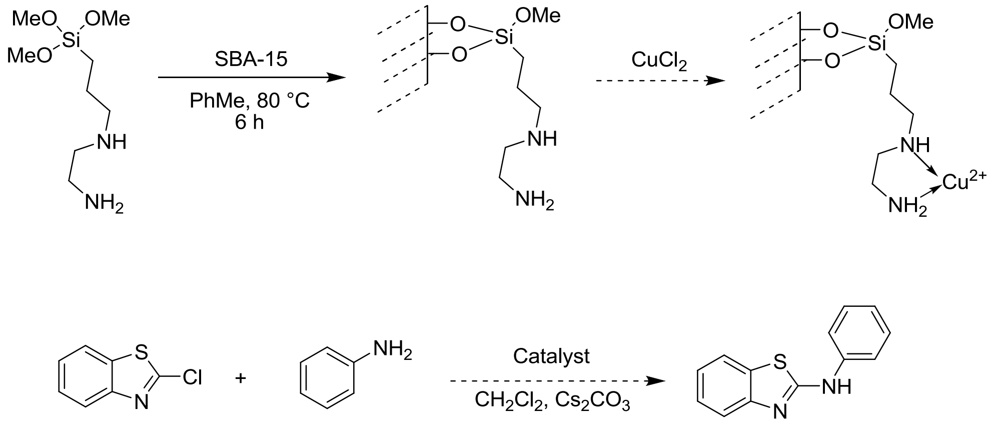
MeO
OMe
Si
MeO
NH
NH2
SBA-15
PhMe, 80 °C
6 h
O
O
Si
OMe
NH
NH2
CuCl2
Cu2+
S
N
Cl
+
NH2
Catalyst
CH2Cl2, Cs2CO3
S
N
NH

Scheme 7.4**:** Synthesis of new mesoporous silica supported Cu catalyst and application to amination reaction.

A potential area of possible research can rest on extension of our silica based core-shell-shell material to other materials like grapheme oxide (GO). GO is a compound of carbon, oxygen and hydrogen and is obtained by oxidizing graphite using strong oxidizing agents. GO possess many functional groups like aldehydes, phenols, epoxides, carboxylic acids as a result they can be functionalized with different functional groups and can be used as a support material for heterogeneous catalysis. GO can functionalized with matal nanoparticle, e.g., Pd and then it can be evcapsulated with a porous silica shell (Figure 1). The resulting material would be Pd nanoparticle sandwiched between GO core and silica shell and can be used as catalyst for several Pd catalyzed C-C bond formation reaction.

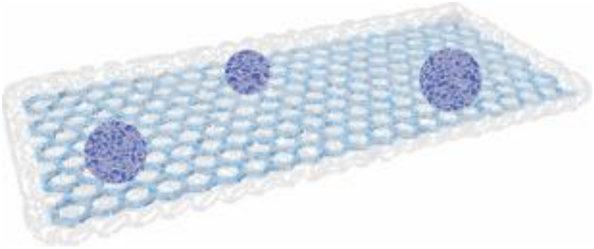

Figure 7.1: Core-shell-shell nanocatalysts containing Pd nanoparticle sandwiched between GO core and porous SiO_2 shell.

Reference

1. Ganesh, M.; Seidel, D. *J. Am. Chem. Soc*. **2008**, *130*, 16464.
2. Li, X.; Hewgley, B J.; Mulrooney, C A.; Yang, J.; Kozlowski, M C. *J. Org. Chem*. **2003**, *68*, 5500.
3. For general reviews, see: (a) Whiting, D A.; Oxidative Coupling of Phenols and Phenol Ethers In Comprehensive Organic Synthesis, Trost, B M.; Fleming, I.; Pattenden, G. Oxford, **1991**, *3*, 659.
4. Shen, G.; Lv, X.; Bao, W. *Eur. J. Org. Chem*. **2009**, *34*, 5897.